THE APPLICATION OF PHASED ARRAYS TO THE ANALYSIS OF SEISMIC BODY WAVES

By J. W. BIRTILL and F. E. WHITEWAY

United Kingdom Atomic Energy Authority, Blacknest, Brimpton, Berkshire

(*Communicated by Sir William Penney, F.R.S.—Received* 29 *September* 1964—*Revised* 16 *December* 1964)

CONTENTS

Vol. 258. A. 1091. (Price £2. 4*s*.; U.S. $6.60) 53 [Published 25 November 1965

(Two charts are contained in a pocket attached to the back cover.)

Arrays of seismometers, spaced over a distance comparable to the longest apparent wavelength of the signal, have been used to facilitate the separation and identification of seismic phases by a process of *velocity filtering*. Individual seismometers in the array are recorded on separate tracks of magnetic tape, and summed on playback with the insertion of time delays to cancel the propagation delays of the required signal. The inserted delays have the effect of *tuning* the array to a required velocity and azimuth, thereby discriminating against signals or noise of different velocity or azimuth. The improvement in signal/noise ratio of weak signal onsets enables a more accurate estimate to be made of epicentre location.

Correlation methods, presenting the correlator output as a function of velocity or azimuth, are an objective aid to identifying seismic phases. Velocity filtered records of the Gnome nuclear event, recorded by an experimental array at a distance of 1000 km, enabled at least ten seismic phases to be identified, many of them being multiple reflexions from the Mohorovičić discontinuity. The travel times of the reflexions enabled the mean thickness of the crust along the propagation path to be deduced. Examples are given to show the application of array techniques to teleseismic events, including the detection and identification of core phases, and reduction of noise generated by the signal in the vicinity of the recording station.

The theoretical responses of arrays of several configurations are presented, and their relative merits discussed. The theoretical performance of cross arrays is given in detail, including the application of correlation methods and a discussion of errors in velocity or azimuth determination. Theoretical expressions are derived for correlator signal/noise ratios in the case of random noise. Details are given of the experimental arrays, including siting criteria. The present analogue processing facility, and a special purpose computer under construction, are also described.

List of symbols (in order of introduction)

n	number of seismometers in complete array
σ_s	standard deviation of signal
σ_n	standard deviation of noise
φ_{12}	cross correlation integral between detector outputs 1 and 2
τ	delay inserted in one detector output during cross correlation
t	time
T_1	averaging time of cross correlation

S	amplitude of signal
N	amplitude of noise
σ_0	standard deviation of correlator output
Δf	frequency bandwidth
f : $\omega/2\pi$	frequency
β_r	phase shift of rth seismometer relative to fixed point in array (figure 2(*a*))
d_r	distance of rth seismometer to fixed point in array (figure 2(*a*))
λ	apparent wavelength of signal or noise
V	apparent ground velocity of signal or noise
θ	azimuth of signal or noise
α_r	angle subtended by rth seismometer (figure 2(*a*))
a_r	amplitude of vector representing output of rth seismometer
A_n	amplitude of vector representing summed output of array of n seismometers
γ_n	phase angle of vector representing summed output of array of n seismometers
E_n	normalized amplitude of summed output of array of n seismometers
D_A, D_B	distance of centre point of lines A, B, to point of intersection of lines
D	dimension of array to which wavelength is normalized for contoured responses (figure 2)

Additional symbols in appendix B

m	number of seismometers in line A of cross array
Δ	phase difference between adjacent seismometers in uniform line array after insertion of delays (if any)
Δ_A, Δ_B	values of Δ for lines A, B
E_A, E_B	normalized output amplitudes of summed line arrays A, B
d	spacing between adjacent seismometers in lines A and B
γ_A, γ_B	phase angles of vectors representing summed outputs of lines A, B
$T_r(x)$	rth order Tchebyscheff polynomial
R	ratio between maximum primary and subsidiary peak levels of response of line array
φ_{AB}	cross correlation integral between summed outputs of lines A and B
τ_A, τ_B	delays inserted between adjacent seismometer outputs in lines A, B
$\delta\tau_B$	systematic error in τ_B
$\delta\theta_1$	error in estimated value of θ_1 due to $\delta\tau_B$
δV_1	error in estimated value of V_1 due to $\delta\tau_B$
t_s	sampling time interval in digital system
a_{S_1}, a_{S_2}	amplitude of signal components S_1, S_2 at each seismometer
E_{AS_1}, E_{BS_1}	normalized amplitudes of summed lines A, B, for signal component S_1
E_{AS_2}, E_{BS_2}	normalized amplitudes of summed lines A, B, for signal component S_2
ϕ_1, ϕ_2	phase angle of signal components S_1, S_2, at centre point of symmetrical cross array at time ($t = 0$)

Glossary of terms

Signal component

A signal wavetrain which has travelled along a single propagation path with a single mode of propagation. Normally the term 'seismic phase' is used in seismology; it is not used in this paper because of possible confusion with the phase angle of the signal.

Noise component

A noise wavetrain which has travelled along a single propagation path with a single mode of propagation.

Three component set of instruments

A set of three instruments measuring ground movement in three mutually perpendicular directions.

Apparent wavelength

The wavelength of a signal measured in the horizontal plane at the earth's surface in the direction of propagation.

Apparent ground velocity, phase velocity

The product of frequency and apparent wavelength.

Teleseismic signal

Signals from events at ranges greater than 30°.

Coherent signal or noise components

Signal components which have the same waveform at all parts of the array.

Cross correlation integral

The cross correlation integral of a single pair of detectors refers to the output obtained when a fixed delay is inserted in one signal channel, the two signals multiplied together and integrated over a period of time. Normally, this process is carried out continuously giving the correlator output as a function of time.

Cross correlation function

The cross correlation function refers to the correlator output at a fixed time as a function of inserted delay. Normally, the delays are chosen so that the correlation function corresponds to a range of velocity or azimuth.

Window of integration

This refers to the characteristics of integration in the correlation process, namely the averaging time and the time dependent weighting function (if any) applied to the unsmoothed product.

Square window integration

This refers to integration between two finite time limits, without using a time dependent weighting function.

Exponential window of integration

This refers to the use of an exponential weighting function in the correlation process, changing one of the time limits to $-\infty$. This form of integration is obtained with a simple C.R. integrator.

Noise whitening

A term in common use in filter theory, meaning to operate on the noise so as to produce a frequency spectrum of constant amplitude over the frequency range of interest.

1. Introduction

The purpose of most seismological studies is to determine the internal structure of the Earth. Travel time curves are constructed for the various signal components observed, records being used from a number of independent stations. From these curves, Earth models are deduced to fit the observed arrivals. These models represent an average over a large area. For a given signal path, the actual structure, and hence the arrival times of individual signal components, may differ. Arrivals which do not fit the average model, particularly those which cannot be identified at all observing stations, tend to be discarded. Identification is often difficult for a number of reasons. A seismic signal recorded by a single seismometer is the summation of a number of signal components which have travelled along different paths and which may have different modes of propagation. It also includes noise generated locally by the signal from mode conversions and multiple reflexions. The nature of the resultant seismogram is therefore dependent upon the relative phase of the individual signal components at the seismometer emplacement. Any one component may be either reinforced or reduced by the presence of a second component. Usually this renders the identification of the onset time of later components difficult, particularly for signals received at relatively short distances. Such arrivals can only be identified on a single seismogram by noting a change of amplitude or frequency. A three component set of instruments is sometimes used to assist in separating signal components, but local signal generated noise could still be confused with true signal components. In addition to the problem of interference between components of the same signal, the seismogram may be affected by signals from other sources, or by noise (microseisms). These may obscure the signal onset, or even the whole of the required signal for low signal/noise ratios. It is therefore usual in seismological studies to select events of magnitude $m6$ and above where the signal/noise ratio is high. The authors, however, are concerned with the study of events of magnitude $m3\frac{1}{2}$ to $m5$ which produce maximum ground displacements of 2 to 100 Å at teleseismic ranges.

A considerable improvement in signal identification can be achieved by the use of arrays of seismometers spaced over a distance comparable to the longest signal wavelength. In order to process the array data, each seismometer output is recorded separately. A single array can separate signal components of differing apparent ground velocity or azimuth, and discriminate against ambient and signal generated noise. Arrays of detectors are in common use in other branches of science, such as radio astronomy, radar and underwater acoustics. Use has been made, where possible, of the published work on these applications, and a bibliography is given in appendix C. The applications all differ to some extent from

the seismological case. Some, such as radar, use active systems in which the character of the transmitted signal is known, and repeated echoes observed. Others, such as radio astronomy, deal with continuous signals, whereas seismic signals are transient in character. Furthermore, in most non-seismic cases the propagation velocity is substantially constant, and is known. No comprehensive study on the application of arrays to earthquake seismology has been published. The theoretical performance of seismometer arrays, including the application of correlation techniques, is therefore given in detail.

An array of seismometers was installed on Salisbury Plain in February 1961 to test the effectiveness of a practical array. Recordings were made of signals from depth charges exploded at distances of 100 to 200 km (Operation Seagull, Phase I). Some of the results obtained by the authors from these early experiments were used as illustrations by Willmore (1962). Another array was installed at Pole Mountain, Wyoming, U.S.A. in early December 1961, and recordings made of the 3·5 kT Gnome nuclear explosion near Carlsbad, New Mexico, at a distance of 1000 km. This array was discontinued in September 1963. Continuous recordings from a third array at Eskdalemuir, Dumfriesshire, were begun in June 1962. This array has been described by Truscott (1964). A calibration exercise (Operation Seagull, Phase II) was carried out in July 1962, to determine the crustal structure in the vicinity of the station (Agger & Carpenter 1964). Another array was installed near Yellowknife, Northwest Territories, Canada, in collaboration with the Canadian Department of Mines and Technical Surveys. This began operation in December 1962. The lines, now complete, are $22\frac{1}{2}$ km long, which is comparable to the apparent wavelength of P arrivals at an epicentral distance of 90°.

The data from these arrays are processed by means of a Pace 231 R analogue computer. Time shifts, frequency filtering, summation and correlation methods are applied to the signals on playback. Details are given of these methods and also of a proposed on-line system for sweeping the array through a range of velocity and azimuth.

The probability of identifying the onset of a signal as a function of signal/noise ratio was determined experimentally using noise recorded by the Eskdalemuir array and a simulated signal. Results from these experiments are presented, and different correlation methods compared. The application of velocity filtering to the separation and identification of signal components is illustrated by results obtained from combining the Gnome data. These results are then applied to the determination of the local crustal structure. Processed data from teleseismic events are also presented and their significance discussed.

2. General principles

2·1. *Signal characteristics*

Each signal component arrives at the seismometer array with an apparent ground velocity which is dependent upon the path and mode of propagation. Figure 1 shows the apparent ground velocity, derived from the Jeffreys–Bullen tables, for a number of signal components as a function of range. The velocity of the first P arrival increases from about 8 km/s at 2° to 24 km/s at 90°, while the corresponding S wave velocities increase from 4·5 to 12·3 km/s. These apparent ground velocities are modified by variations of crustal thickness and constitution, and therefore an evaluation of crustal delays by a local shot programme is desirable.

The individual signal components will each be coherent across the array, provided that the distance to the source is large compared to the dimensions of the array, and that the geological structure under the recording site is uniform. These ideal conditions will be assumed to apply.

The frequency spectrum of the signal varies with the nature of, and distance to, the source. Body waves from events at distances of about 100 km have significant energy up to 20 c/s, whereas P waves from teleseismic events undergo high attenuation at frequencies above 2 c/s.

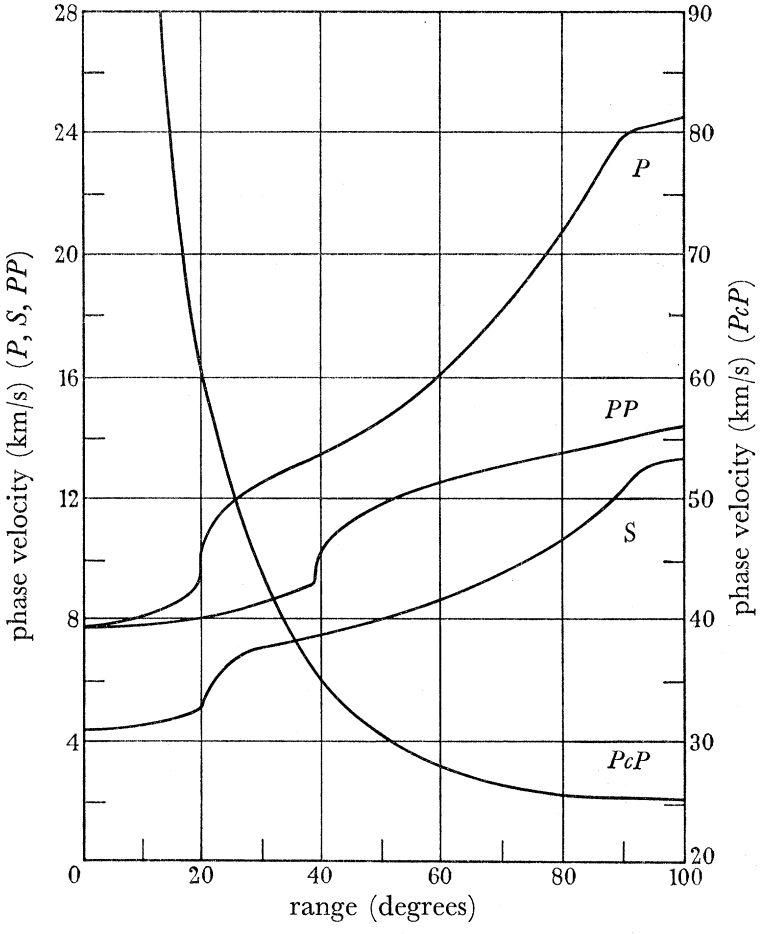

FIGURE 1. Phase velocities of P, S, PP and PcP.

2·2. *Noise characteristics*

Seismic noise consists of the sum of a large number of wavetrains originating from a variety of sources. In the frequency band 0·1 to 10 c/s the following types of seismic noise are significant:

(*a*) *Ocean microseisms.* These are mainly Rayleigh waves with a velocity of about 3·5 km/s. The amplitude can be as high as 20 μm in regions within 200 km of the coast. The spectrum is sharply peaked at a period of about 6 s. The amplitude falls off rapidly with decreasing period. This reduction in amplitude is caused by the nature of the source spectrum and also by increased attenuation in the propagation path for shorter period waves. Harmonics caused by non-linear propagation of the main ocean microseismic noise may contribute at shorter periods.

(*b*) *Cultural noise.* Industrial machinery, transport and other forms of human activity produce seismic noise, particularly at frequencies higher than 1 c/s. This noise is very variable, and can have very high amplitudes. It is necessary to select sites which are far from industrial areas, main roads and railways.

(*c*) *Wind noise.* Seismic noise is generated by the action of wind, either directly on the ground, or on obstacles such as trees. The amplitude of this noise is also very variable, and depends upon wind velocity and local geology, including surface weathering and topography. Experience at Pole Mountain has shown that a 10:1 variation in amplitude of wind generated noise can be encountered between seismometers spaced a few kilometres apart.

(*d*) *Low magnitude events.* At frequencies greater than 1 c/s, numerous unidentified low magnitude events may predominate over the total seismic noise from causes (*a*) to (*c*) for a substantial part of the time at carefully selected mid-continental sites such as Yellowknife. An average of 11 events per day, excluding local quarry blasts, were observed on a single seismometer trace at this site. Their amplitudes exceeded those of other forms of noise for an average of 32 min/day. The number of earthquakes increases by a factor of approximately 8 for every reduction of one order of earthquake magnitude. These events will therefore be significant for a much greater time if lower noise sites can be found, or if other forms of noise are reduced by signal processing. This affects the choice of array dimensions, as discussed in appendix B.

(*e*) *Local signal generated noise.* Another form of noise is that generated by the signal itself in the vicinity of the recording station. This can take the form of multiple reflexions and mode conversions. *P* wave reflexions, in a uniform, horizontally layered, homogeneous medium, are delayed relative to *P*, but have the same apparent velocity. A simple inclined discontinuity causes a difference in apparent velocity between the incident *P* wave and reflected signals. The boundaries may be discontinuous, or appreciably folded, causing partially coherent and random noise. Furthermore, side reflexions from vertical faults can occur, and such arrivals differ in azimuth from the incident *P* wave. Thus signal generated noise may contain coherent components with a wide range of apparent ground velocity, as well as random components.

(*f*) *Instrumentation noise.* Another important source of noise is that produced by the recording system, particularly if this includes amplifiers and magnetic tape recording. Electronic noise is introduced at the input of the recording amplifier, but with careful design it is possible to make this contribution small compared to the seismic noise, even at sites as quiet as Yellowknife. A magnetic tape recording system can also be designed such that the average noise contributed is low relative to the seismic noise. However, tape defects cause transient noise of large amplitude, and the number of these transients increases with tape wear, and transcription of data. Care is therefore needed in the design, operation and maintenance of magnetic tape recording and playback systems to minimize this defect.

The total noise varies considerably from site to site and from day to day in amplitude and characteristics (Frantti, Willis & Wilson 1962). Sites with noise amplitudes of the order of 1 nm in the frequency band 1 to 2 c/s have been found in the middle of large continents. The amplitude probability distribution has been found to be approximately Gaussian. However, the noise is not entirely stationary, and contains transients arising

from disturbances such as gusts of wind, animal activity, lightning induced surges and magnetic tape defects.

The frequency spectrum of the noise below 1 c/s is mainly governed by ocean microseisms. Above 1 c/s, other forms of noise, particularly wind generated and cultural noise, may predominate.

The coherence of ocean microseismic noise is high at periods of about 6 s. Little work has been published on the coherence of noise at much shorter periods. In general it may be expected that distant sources will create coherent noise, while noise from local sources, such as wind, will be mainly unrelated between seismometers.

2·3. *Discrimination against noise by processing array data*

The data may be processed by linear or non-linear methods. The former includes frequency filtering and array summation, and has the advantage that no information is destroyed. Non-linear methods, such as cross correlation, distort the signal, and may destroy information such as frequency and phase. Nevertheless, correlation methods have certain advantages, as described later.

At any given site there will be present both random and coherent noise, originating from sources described in §2·2. The frequency spectrum of the noise and the relative amplitudes of the random and coherent components differ from site to site, and it is necessary to conduct a comprehensive noise survey in order to determine the model of the noise for each site. Frequency filtering to improve signal/noise ratio applies equally to random and coherent components. Summation and correlation methods for random noise are considered separately from coherent noise. The latter can be treated as interfering signals, and discriminated against by the methods described in §2·4.

2·3·1. *Frequency filtering*

Frequency filtering is often used to improve signal/noise ratio. However, this can result in distortion of the signal waveform, and is not necessary for large amplitude events. For this reason it is desirable to design the complete recording system with a level frequency response over the complete signal frequency range. Frequency filters can then be selected on playback to enhance the signal/noise ratio for a given signal. In practice, some reduction in gain is usually necessary below 1 c/s to avoid overloading the recording system with ocean microseismic noise. Most of this attenuation is provided mechanically, by setting the natural period of the seismometer to about 1 c/s.

The optimum filtering method on playback is first to pass the signal and noise through a filter having the inverse response of the noise spectrum. This process *whitens* the noise, i.e. results in a noise spectrum of constant amplitude. The modified signal and noise are then passed through a filter having a response corresponding to the spectrum of the required signal. However, the exact spectrum of the signal is not known, whilst the mean spectrum of the noise may not apply exactly to the noise which is present with the signal. Good signal/noise improvements for teleseismic *P* wave signals have been achieved with fixed frequency filters having a passband between 1 and 2 c/s, and a high rate of attenuation outside the passband. Filters currently in use in the playback system by the authors have attenuation rates of 30 dB/octave in addition to the attenuation produced by the seismometer and

recording system. Similar filters are in use at the recording sites in series with amplifiers supplying paper recorders. These recorders are used as monitors for detecting the presence of teleseismic events, and operate in parallel with the tape recording system.

2·3·2. *Array summation for random noise*

Consider an array which is perturbed by random noise. A coherent signal component travelling across the array incurs delays between seismometers. Such delays may be cancelled on playback without affecting the character of the noise, since this is unrelated between seismometers. The signal component is then in phase at each output. When the outputs are added, the amplitude of the signal component is equal to the sum of the signal amplitudes at the individual outputs. The mean signal power is thus proportional to n^2 where n is the number of seismometers, if the signal component has the same amplitude at each output. The mean noise power is equal to the sum of the noise powers of the individual outputs, and increases by the factor n if these are equal. The resultant signal/noise power ratio is therefore increased by the factor n.

It is unlikely in the practical array that the above conditions will be satisfied. Differences occur in noise level and signal coupling at the individual pits, resulting in a variation in signal/noise ratio. The frequency spectrum of the noise will also differ between seismometer locations. Ideally, optimum frequency filtering should be applied to the individual outputs prior to summation. In practice, the normalized noise frequency spectrum does not change appreciably between seismometers at a well chosen site, and frequency filtering may be applied after summation, or identical filters inserted into each of the individual output channels. Variations in signal/noise ratio may still exist between individual outputs. The best signal/noise improvement is obtained when the amplitude sensitivity of each seismometer channel is weighted in proportion to the signal/noise power ratio, after normalizing for equal signal amplitude (see appendix A). The resultant signal/noise power ratio after summation is equal to the sum of the signal/noise power ratios of the individual seismometers. For instance, if two seismometers have signal/noise power ratios equal to

$$\sigma_s^2/4\sigma_n^2, \quad \sigma_s^2/\sigma_n^2,$$

then the second should be weighted by a factor of 4 compared to the first. The resultant signal/noise power ratio is then

$$1{\cdot}25\sigma_s^2/\sigma_n^2.$$

If the outputs are not weighted, the resultant signal/noise power ratio is

$$0{\cdot}80\sigma_s^2/\sigma_n^2.$$

In the latter case the signal/noise ratio of the combination is lower than that of the best seismometer output.

2·3·3. *Correlation methods for random noise*

Correlation techniques have been used extensively for the detection of very weak periodic signals in noise (Jacobson 1957; Wainstein & Zubakov 1962; Symposium on Sonar Systems 1962). A very great signal/noise improvement may be achieved with only two detectors for continuous signals. The cross correlation integral $\varphi_{12}(\tau)$, of two signals $f_1(t)$, $f_2(t)$, at

time t_1 is obtained by delaying $f_2(t)$ by an amount τ, multiplying by $f_1(t)$ and averaging the product over a period T_1, i.e.

$$\varphi_{12}(\tau) = \frac{1}{T_1}\int_{t_1-T_1}^{t_1} f_1(t)f_2(t-\tau)\,\mathrm{d}t. \tag{1}$$

The form of this expression differs from that normally adopted, but it is a truer representation of the actual correlation process performed on data which are being received continuously. The above cross correlation integral may be presented as a function of τ at discrete values of t_1, or as continuous functions of time t_1 for fixed values of τ. There are many variations of the cross correlation integral given by equation (1), and the method adopted will depend upon the nature of the information required. The main factors are:

(*a*) *The window of integration.* The form of correlation integral shown above represents a *square window* of integration, since the product of the function is averaged between two finite limits without a time dependent weighting factor. In analogue systems a simple resistance capacitance type of integrator is more convenient. This may be regarded as an *exponential window*, the product of the functions being multiplied by an exponential weighting factor, and the time limits of integration changed to $-\infty$ and t_1. The correlation integral in this case is given by

$$\varphi_{12}(\tau) = \frac{1}{T_1}\int_{-\infty}^{t_1} \exp\left[(t-t_1)/T_1\right] f_1(t)f_2(t-\tau)\,\mathrm{d}t.$$

This method has the advantage that it gives greatest weight to the most recent information, and is therefore useful for the determination of onset times. However, it is sometimes difficult to detect small correlated signals occurring during the exponential decay following a signal of large amplitude. Other forms of window are possible, but only these two have been used in this application.

(*b*) *The averaging time* T_1. The value chosen for T_1 depends upon the nature of the information required. It should be high for maximum detection capability of very weak signals in noise, although there is no advantage to be gained in exceeding the duration of the signal component. This may only be equal to a few periods of the dominant frequency, and limits the signal/noise improvement which may be obtained. For information on accurate onset time it is advantageous to limit the averaging time to about 3 periods of the dominant frequency.

(*c*) *The dynamic range of the correlator.* The cross correlation integral is proportional to the square of the amplitude and is very sensitive to changes in amplitude. In order to reduce the wide dynamic range of the output of the correlator for visual presentation, a number of methods may be used. The square root of the product of $f_1(t)$ and $f_2(t-\tau)$ may be taken before or after integration, or the correlator output normalized by dividing by the square root of the product of the mean square values of $f_1(t)$ and $f_2(t-\tau)$. This yields the correlation coefficient, which is a function of coherence and independent of amplitude.

The cross correlation integral for a single pair of seismometers may be represented by

$$\varphi_{12} = \overline{(S_1+N_1)\,(S_2+N_2)}.$$

The bar denotes the time averaging process.

If S_1 and S_2 are identical, in phase, and equal to S, then

$$\varphi_{12} = \overline{S^2}+\overline{S(N_1+N_2)}+\overline{N_1N_2}.$$

If there is no correlation between S and N_1 or N_2, and between N_1 and N_2, then the amplitude of $\overline{S(N_1+N_2)}$ and $\overline{N_1N_2}$ will fluctuate about zero. These fluctuations represent the noise of the correlator output, which before integration has a variance about the mean level σ_s^2 given by

$$\sigma_0^2 = \sigma_s^2(\sigma_{n1}^2+\sigma_{n2}^2)+\sigma_{n1}^2\sigma_{n2}^2.$$

On integration, the variance is reduced by the number of degrees of freedom (Bendat 1958). If the spectrum of the signal and noise is flat over a common bandwidth Δf, and zero at all other frequencies, then for a square window of integration of duration T_1 there are $2\Delta fT_1$ equivalent independent samples, and

$$\sigma_0^2 = [\sigma_s^2(\sigma_{n1}^2+\sigma_{n2}^2)+\sigma_{n1}^2\sigma_{n2}^2]/2\Delta fT_1. \tag{2}$$

Before the arrival of the signal, the variance is given by

$$\sigma_0^2 = \sigma_{n1}^2\sigma_{n2}^2/2\Delta fT_1. \tag{3}$$

The correlator noise tends to mask the mean level, and the ratio of mean level to the standard deviation σ_0 is therefore a measure of the correlator signal/noise amplitude ratio. Defined in terms of the correlator noise which exists before the arrival of the signal, the correlator signal/noise amplitude ratio is given by

$$\sigma_s^2/\sigma_0 = (2\Delta fT_1)^{\frac{1}{2}}\sigma_s^2/\sigma_{n1}\sigma_{n2}.$$

If $\sigma_{n1} = \sigma_{n2} = \sigma_n$, then

$$\sigma_s^2/\sigma_0 = (2\Delta fT_1)^{\frac{1}{2}}\sigma_s^2/\sigma_n^2. \tag{4}$$

This means that the correlator signal/noise amplitude ratio is equal to the input signal power ratio increased by the factor $(2\Delta fT_1)^{\frac{1}{2}}$. Defined in terms of the correlator noise which exists after the arrival of the signal, the correlator signal/noise amplitude ratio is given by

$$\frac{\sigma_s^2}{\sigma_0} = (2\Delta fT_1)^{\frac{1}{2}}\frac{\sigma_s^2}{\sigma_n^2}\frac{1}{(1+2\sigma_s^2/\sigma_n^2)^{\frac{1}{2}}}. \tag{5}$$

For very low input signal/noise ratios equations (4) and (5) are virtually the same. Equation (4) is the appropriate one for determining the detection threshold for a transient signal. For higher input signal/noise ratios, the correlator noise increases considerably on arrival of the signal. The signal/noise ratio given by equation (5) is therefore more appropriate when attempting to measure the mean level. If $2\sigma_s^2/\sigma_n^2 \gg 1$, the equation becomes

$$\sigma_s^2/\sigma_0 = (\Delta fT_1)^{\frac{1}{2}}\sigma_s/\sigma_n. \tag{6}$$

Equations (4) to (6) show the importance of retaining the full bandwidth of the noise over the range corresponding to the signal. It is important to avoid either a rising characteristic at the low frequency end, or sharp peaks common to both channels.

The correlator signal/noise ratio may be further improved by summing the cross correlation integrals of a number of pairs of seismometers. If the output of two summed groups of $\frac{1}{2}n$ seismometers are cross correlated, the output corresponds to $\frac{1}{4}n^2$ cross product pairs, and is given by

$$\varphi = \tfrac{1}{4}n^2\overline{S^2}+\sum_{i=1}^{\frac{1}{2}n}\overline{\tfrac{1}{2}nSN_i}+\sum_{j=\frac{1}{2}n+1}^{n}\overline{\tfrac{1}{2}nSN_j}+\sum_{i=1}^{\frac{1}{2}n}\sum_{j=\frac{1}{2}n+1}^{n}\overline{N_iN_j}.$$

The variance of the noise after the arrival of the signal is given by

$$\sigma_0^2 = (n^3\sigma_s^2\sigma_n^2+n^2\sigma_n^4)/8\Delta fT_1.$$

The correlator signal/noise amplitude ratio is therefore

$$n^2\sigma_s^2/4\sigma_0 = (2\Delta f T_1)^{\frac{1}{2}} \frac{\sigma_s^2}{\sigma_n^2} \frac{\frac{1}{2}n}{(1+n\sigma_s^2/\sigma_n^2)^{\frac{1}{2}}}. \tag{7}$$

If $n\sigma_s^2/\sigma_n^2 \gg 1$, equation (7) simplifies to

$$n^2\sigma_s^2/4\sigma_0 = (\Delta f T_1)^{\frac{1}{2}} (\sigma_s/\sigma_n) (\tfrac{1}{2}n)^{\frac{1}{2}}. \tag{8}$$

Comparing this with equation (6), it is seen that the signal/noise ratio is increased by the factor $(\frac{1}{2}n)^{\frac{1}{2}}$ compared to a single pair.

For an array of n seismometers, there are $\frac{1}{2}n(n-1)$ possible cross product pairs, which on summation result in a greater signal/noise improvement than that given by equation (8). In this case

$$\begin{aligned}\varphi &= \sum_{\substack{i=1\\ i\neq j}}^{n} \sum_{j=1}^{n} \overline{(S+N_i)(S+N_j)} \\ &= \tfrac{1}{2}n(n-1)\overline{S^2} + \sum_{i=1}^{n} \overline{(n-1)SN_i} + \sum_{\substack{i=1\\ i\neq j}}^{n} \sum_{j=1}^{n} \overline{N_iN_j}.\end{aligned} \tag{9}$$

The variance of the noise after the arrival of the signal is given by

$$\sigma_0^2 = [n(n-1)^2\sigma_s^2\sigma_n^2 + n(n-1)\sigma_n^4/2]/2\Delta f T_1.$$

The correlator signal/noise amplitude ratio is given by

$$\frac{n(n-1)\sigma_s^2}{2\sigma_0} = (2\Delta f T_1)^{\frac{1}{2}} \frac{\sigma_s^2}{\sigma_n^2} \left[\frac{\frac{1}{2}n(n-1)}{1+2(n-1)\sigma_s^2/\sigma_n^2}\right]^{\frac{1}{2}}. \tag{10}$$

If $2(n-1)\sigma_s^2/\sigma_n^2 \gg 1$, equation (10) simplifies to

$$\frac{n(n-1)\sigma_s^2}{2\sigma_0} = (\Delta f T_1)^{\frac{1}{2}} \frac{\sigma_s}{\sigma_n} (\tfrac{1}{2}n)^{\frac{1}{2}}. \tag{11}$$

This is the same as that given by equation (8), and there is only an advantage in using all possible pairs if the input signal/noise power ratio is less than $1/n$. This is important, since there are 210 possible pairs for an array consisting of 21 seismometers, and it is not practical to compute these individually in an analogue computer. One solution is to cross correlate the output of seismometer 1 with the summed outputs of seismometers 2 to 21, then cross correlate the output of seismometer 2 with the summed output of seismometers 3 to 21, and so on. In this way, the number of multipliers required is reduced to 20. Alternatively, the array may be summed into, say, 3 groups of 3 seismometers, and 3 groups of 4 seismometers, and the cross correlation integral of all possible pairs of groups summed. The correlator output then corresponds to the sum of 183 pairs out of the 210 possible pairs, and uses only 5 multipliers. A further possibility is to subtract the sum of the mean square values of the individual seismometer outputs from the mean square value of the summed array (Tullos & Cummings 1961). This may be represented by

$$\varphi = \overline{\left[\sum_{i=1}^{n} (S_i+N_i)\right]^2} - \sum_{i=1}^{n} [\overline{(S_i+N_i)^2}].$$

This expression reduces to twice the sum of the correlation integrals of all possible pairs.

The mean square value of the summed array is given by

$$\varphi = n^2\overline{S^2} + \sum_{i=1}^{n} \overline{2nSN_i} + \sum_{\substack{i=1 \\ i\neq j}}^{n} \sum_{j=1}^{n} \overline{2N_iN_j} + \sum_{i=1}^{n} \overline{N_i^2}. \tag{12}$$

This is very similar to equation (9) for high values of n, allowing for a common factor of 2 in each term. There is an additional term in equation (12), i.e. $\sum_{i=1}^{n} \overline{N_i^2}$. For stationary noise, and large values of $\Delta f T_1$, this only affects the mean level of the correlator. However, if bursts of noise occur at one or more seismometers, the level of the correlator output due to this term will change, and could be mistaken for a signal.

2·4. *Separation of signal components by azimuth and velocity filtering*

2·4·1. *Summed arrays*

A coherent seismic signal component is propagated across a horizontal array at its apparent ground velocity. As it does so, phase shifts exist between the seismometer outputs. For any given array the phase shifts may conveniently be related to an arbitrary point in the plane of the array, preferably near the centre. Referring to figure 2 (*a*), the phase shift relative to P for the rth seismometer is given by

$$\beta_r = 2\pi(d_r/\lambda)\cos(\theta - \alpha_r). \tag{13}$$

The output of the rth seismometer may be represented by a vector of amplitude a_r, angle β_r. The summed output of the array is then given by the vector sum of the individual outputs. Thus if the amplitude of the summed array of n seismometers is A_n and the phase shift γ_n, then

$$A_n\cos\gamma_n = \sum_{r=1}^{n} a_r\cos\beta_r; \quad A_n\sin\gamma_n = \sum_{r=1}^{n} a_r\sin\beta_r,$$

whence

$$A_n = \left[\left(\sum_{r=1}^{n} a_r\cos\beta_r\right)^2 + \left(\sum_{r=1}^{n} a_r\sin\beta_r\right)^2\right]^{\frac{1}{2}}, \tag{14}$$

$$\gamma_n = \tan^{-1}\left[\left(\sum_{r=1}^{n} a_r\sin\beta_r\right)\Big/\left(\sum_{r=1}^{n} a_r\cos\beta_r\right)\right]. \tag{15}$$

If the outputs of all seismometers are equal in amplitude, the amplitude E_n of the summed output normalized to unity for the in-phase condition is given by

$$E_n^2 = \left[\left(\sum_{r=1}^{n} \cos\beta_r\right)^2 + \left(\sum_{r=1}^{n} \sin\beta_r\right)^2\right]\Big/n, \tag{16}$$

$$\gamma_n = \tan^{-1}\left[\left(\sum_{r=1}^{n} \sin\beta_r\right)\Big/\left(\sum_{r=1}^{n} \cos\beta_r\right)\right]. \tag{17}$$

The response E_n^2 given above may be shown as contours of equal attenuation on a polar diagram, the radial distance being equal to the wavenumber $1/\lambda$, and the angle θ being the azimuth relative to a chosen line through P. It is often more convenient to normalize the radial distance in terms of one dimension of the array, so that the response is dependent only upon the array configuration and not upon its size. Figure 4 shows the contoured response for a summed, circular, 20 element array in terms of $(D/\lambda, \theta)$, the configuration

being given by figure 2(*b*). Figure 5 shows the corresponding response for the 18 element, solid pattern array shown in figure 2(*c*). These figures give the responses when all the seismometer outputs are summed without change of phase. The centre point corresponds

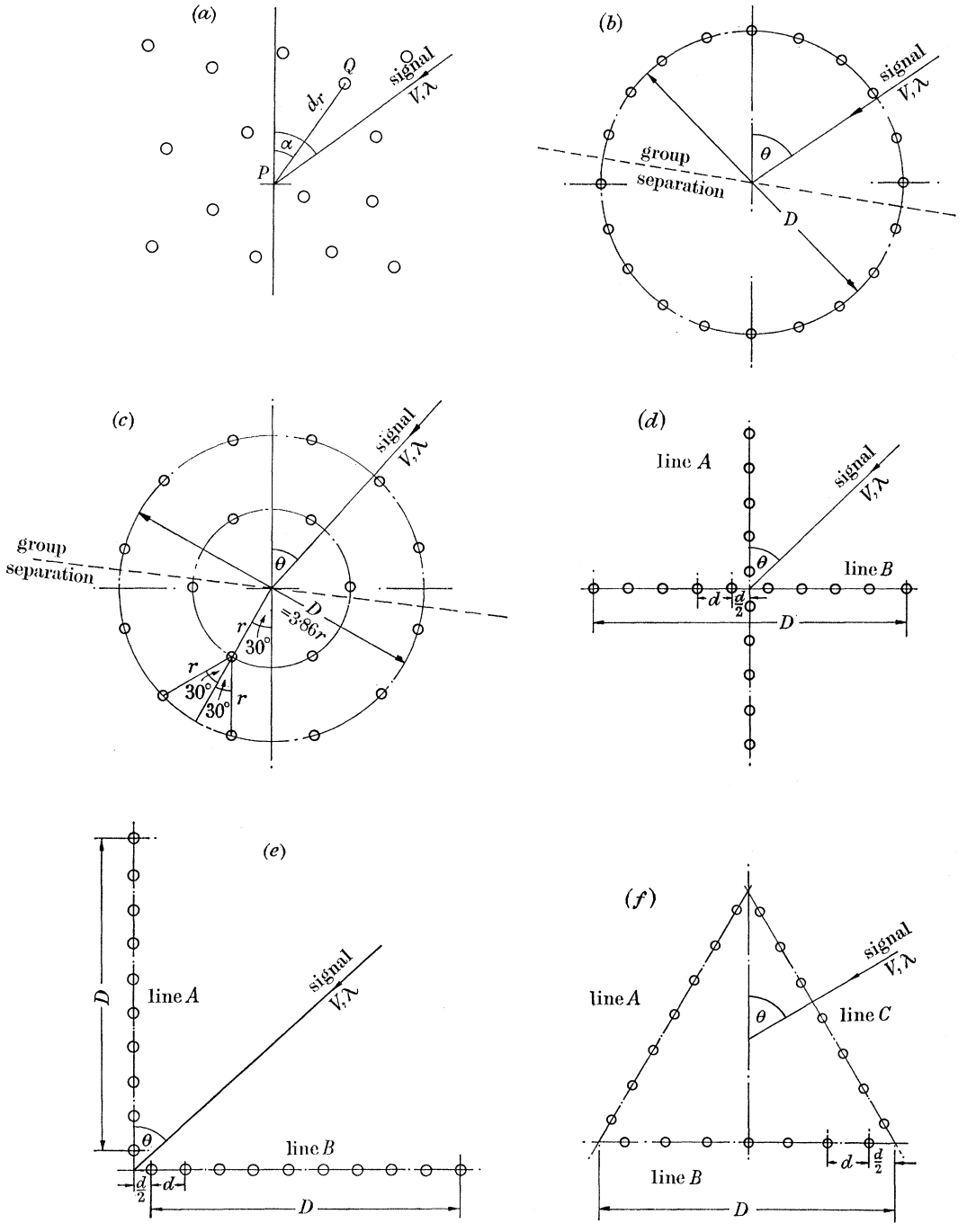

FIGURE 2. (*a*) General seismometer array; (*b*) 20 element circular array; (*c*) 18 element cluster; (*d*) 20 element symmetrical cross array; (*e*) 20 element L-shaped array; (*f*) 21 element triangular array.

to infinite signal wavelength measured on the horizontal ground surface and, therefore, to waves arriving vertically from below. The seismometer outputs are thus all in phase, and the response is unity. The contours about the centre point show how the summed

output is attenuated for finite apparent wavelengths, due to phase differences between seismometer outputs. The radius of the innermost half level contour is a measure of the discriminating power of the array in terms of D/λ. As D/λ is increased, there is a range of values of D/λ for which the attenuation is high. Beyond this range, higher level contours occur corresponding to 'side-lobes' of the array response.

Equations (16) and (17) can be simplified in the case of uniform line arrays. The simplified expressions are given in appendix B, which also considers the application of Dolph–Tchebyscheff optimum weighting to obtain a more uniform response. The contoured responses for the individual summed 10 element lines A and B of the linear cross arrays, illustrated by figures 2(d) and 2(e), are simply straight lines at right angles to the axis of the line array concerned. Figures 6 and 7 show the contoured responses for the two summed 20 element cross arrays, one being a symmetrical cross ($D_A = D_B = 0$), and the other being L-shaped ($D_A = D_B = 5d$). Figure 8 shows the contoured response for a summed 21 element array with the equilateral triangle configuration of figure 2(f). The application of these contoured responses, when delays are inserted to phase the array to receive signals of finite apparent wavelength, is considered in §2·4·3.

2·4·2. *Correlator responses*

The summed response of a linear cross array contains many undesirable half level contours for azimuths at right angles to the direction of either line. This is because one of the two line arrays is always in phase in these directions, and although the signal may be attenuated in the other line, the normalized total summed response fluctuates about the level $\frac{1}{2}$. A greatly improved response can be achieved by cross correlating the summed outputs of the two lines. It is shown in appendix B that the amplitude of the correlator output is proportional to the product of the individual responses of the two lines, and the cosine of the phase difference between the centre points of the two lines. Figures 9 and 10 show the normalized correlator responses for the symmetrical and L-shaped arrays already considered. These should be compared with the corresponding sum squared responses given by figures 6 and 7, since the correlator response is proportional to the square of the signal amplitude. The correlator responses are considerably better than the sum squared responses, although the directions at right angles to the line arrays still result in contours of least attenuation. Figure 11 shows the correlator response for lines A and B of the triangular array previously considered.

Correlation techniques can also be applied to the circular and solid pattern arrays. Figure 12 shows the normalized correlator response for the circular array previously considered, the seismometers being separated into two equal groups as shown by figure 2(b). Figure 13 shows the normalized correlator response for the 18 element, solid pattern array, with the division shown by figure 2(c). These should be compared with the corresponding sum all squared responses of figures 4 and 5 respectively. Many other forms of seismometer groupings are possible, and merit further investigation.

2·4·3. *Application of contoured responses to azimuth and velocity filtering*

The contoured responses given represent the condition of zero inserted delay. This is not the normal condition, since delays will have been inserted to tune the array to a required

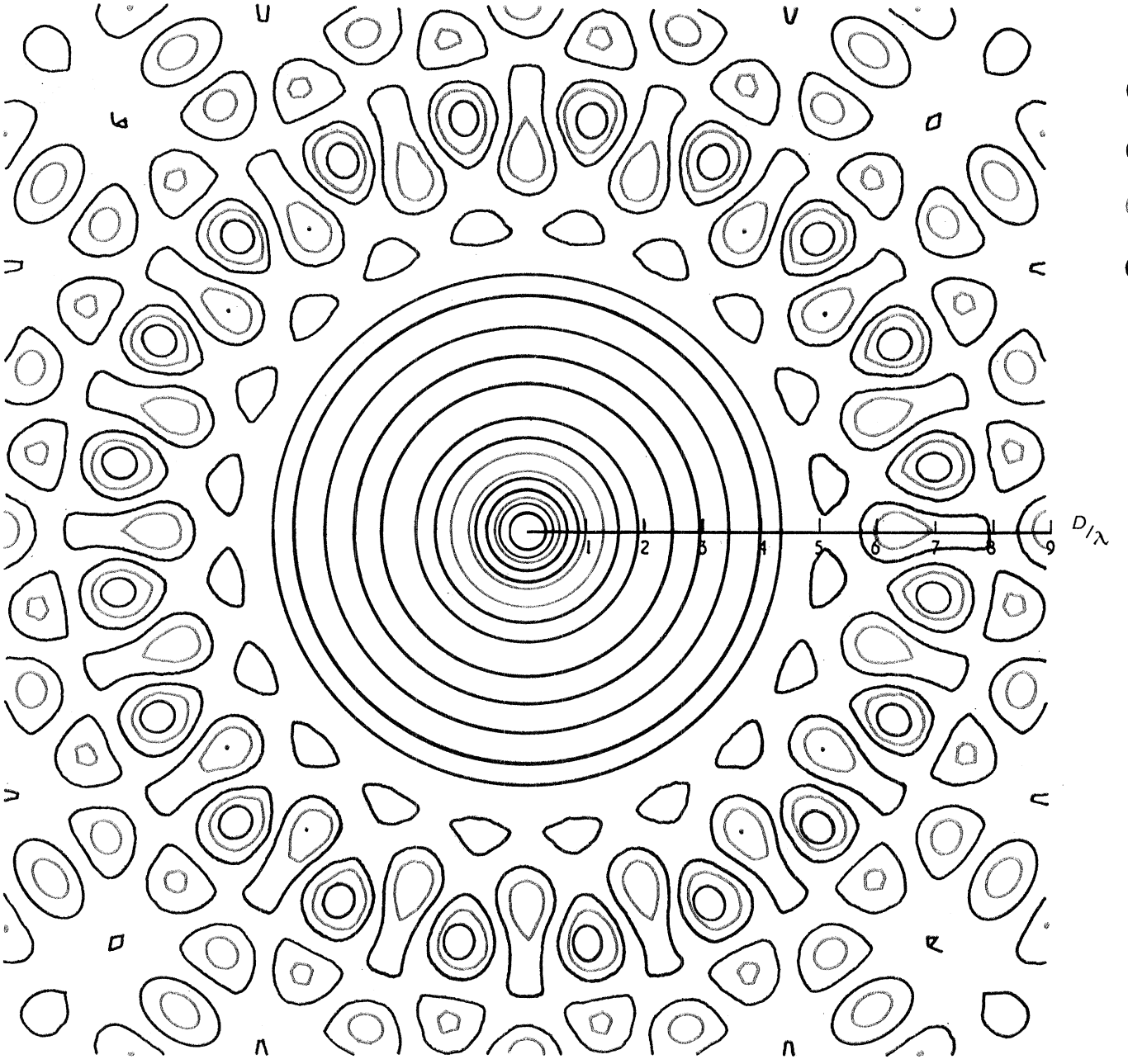

FIGURE 4. Sum squared response of 20 element circular array.

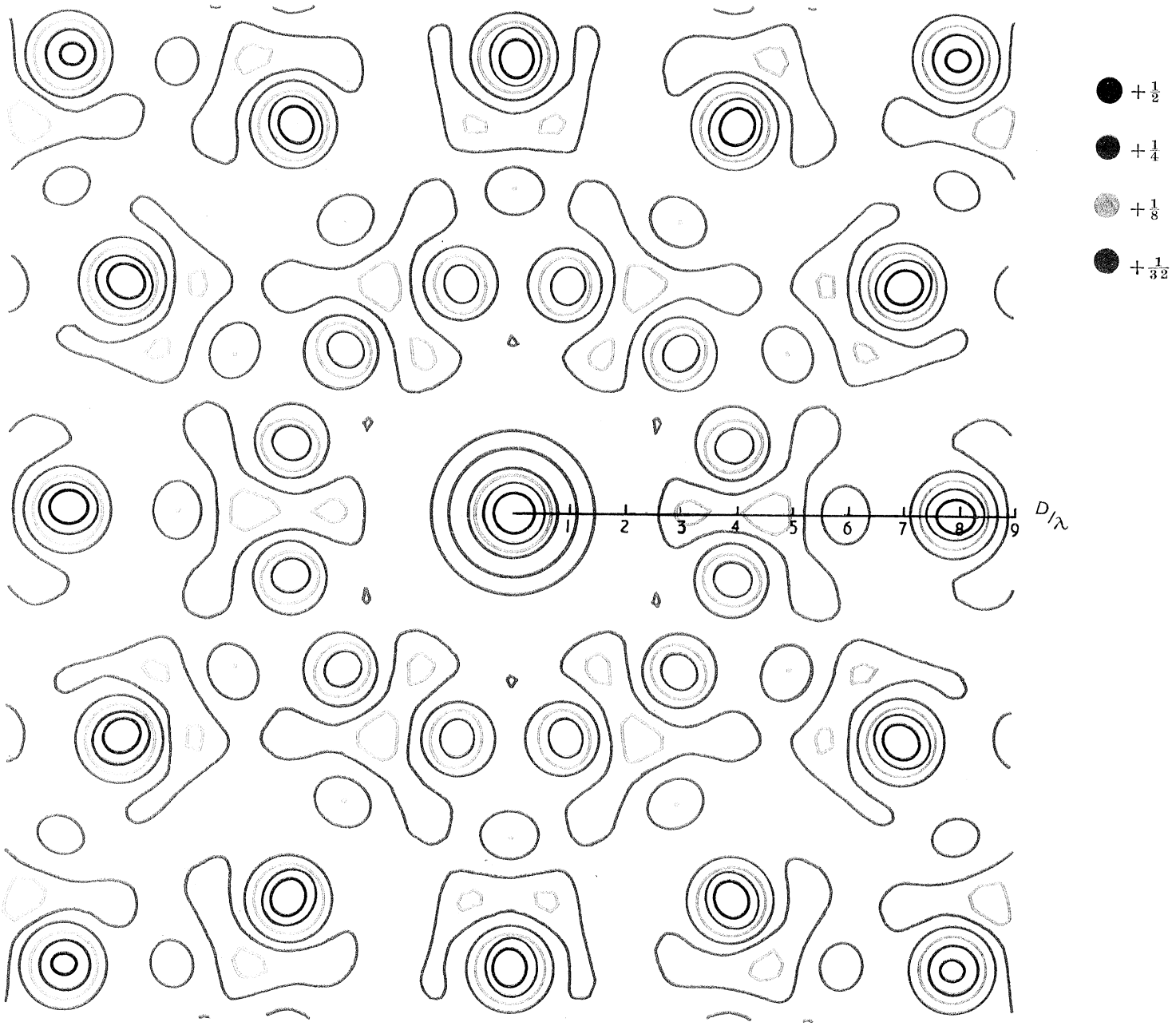

FIGURE 5. Sum squared response of 18 element cluster.

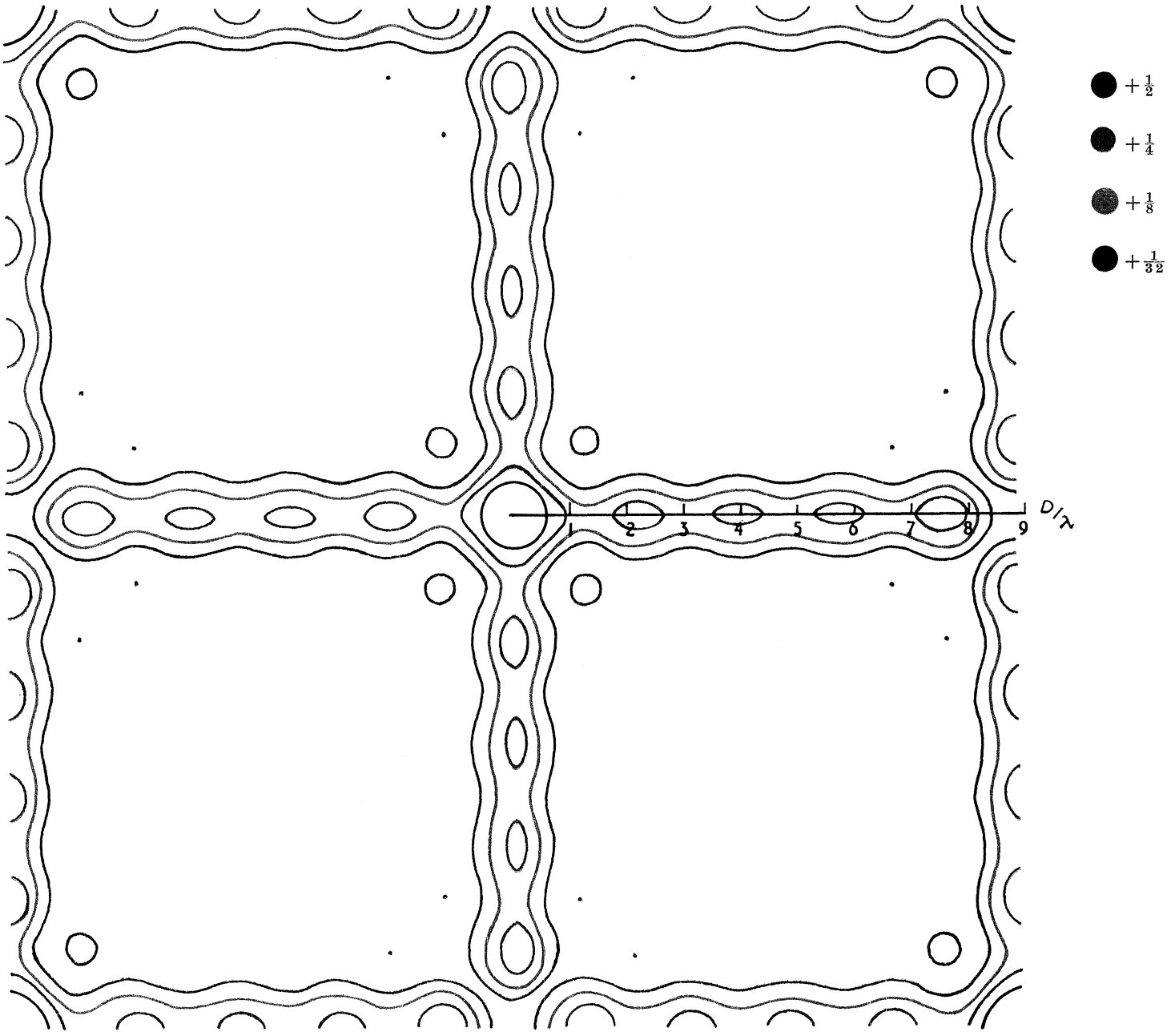

FIGURE 6. Sum squared response of 20 element symmetrical cross array.

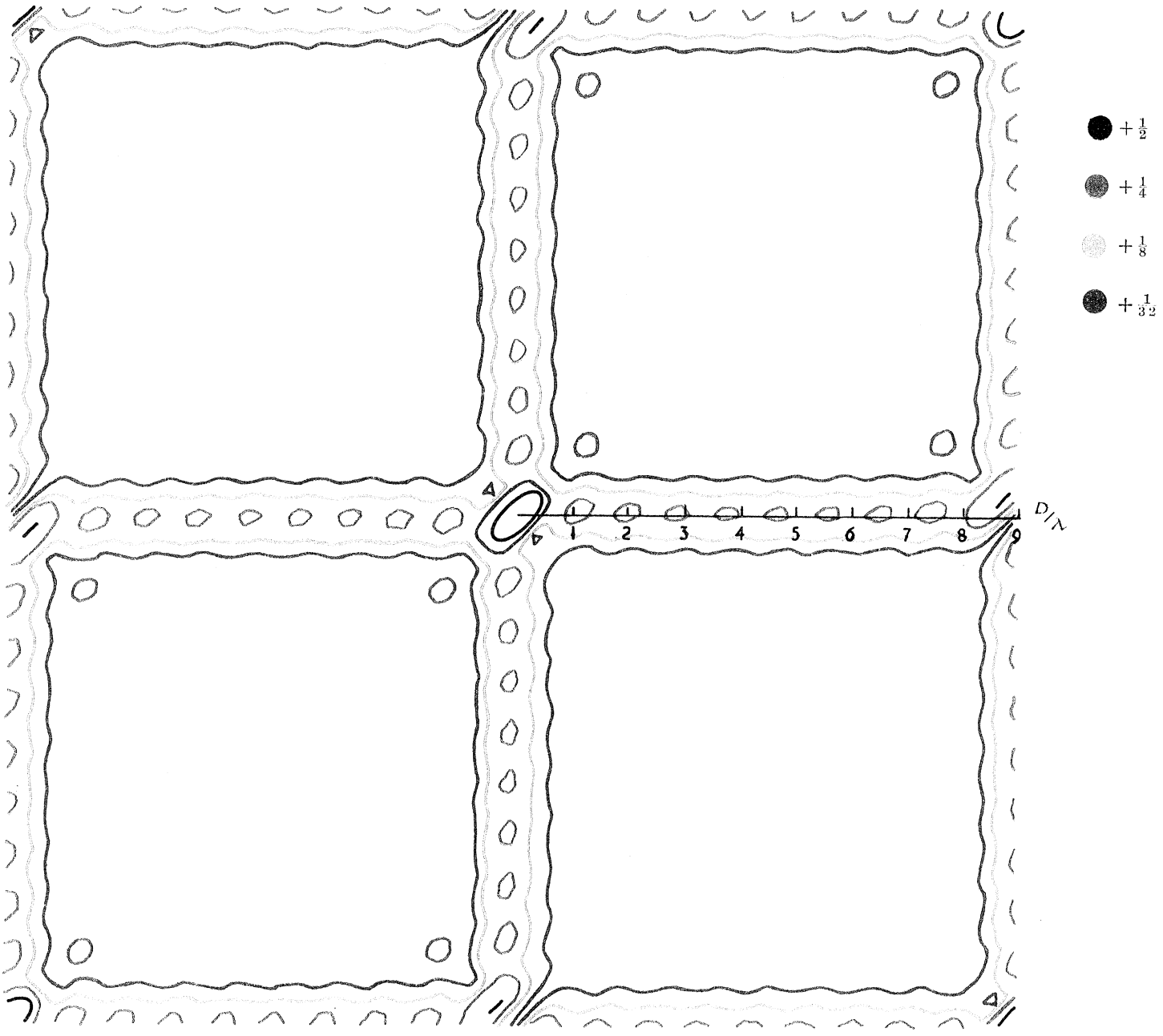

FIGURE 7. Sum squared response of 20 element L-shaped array.

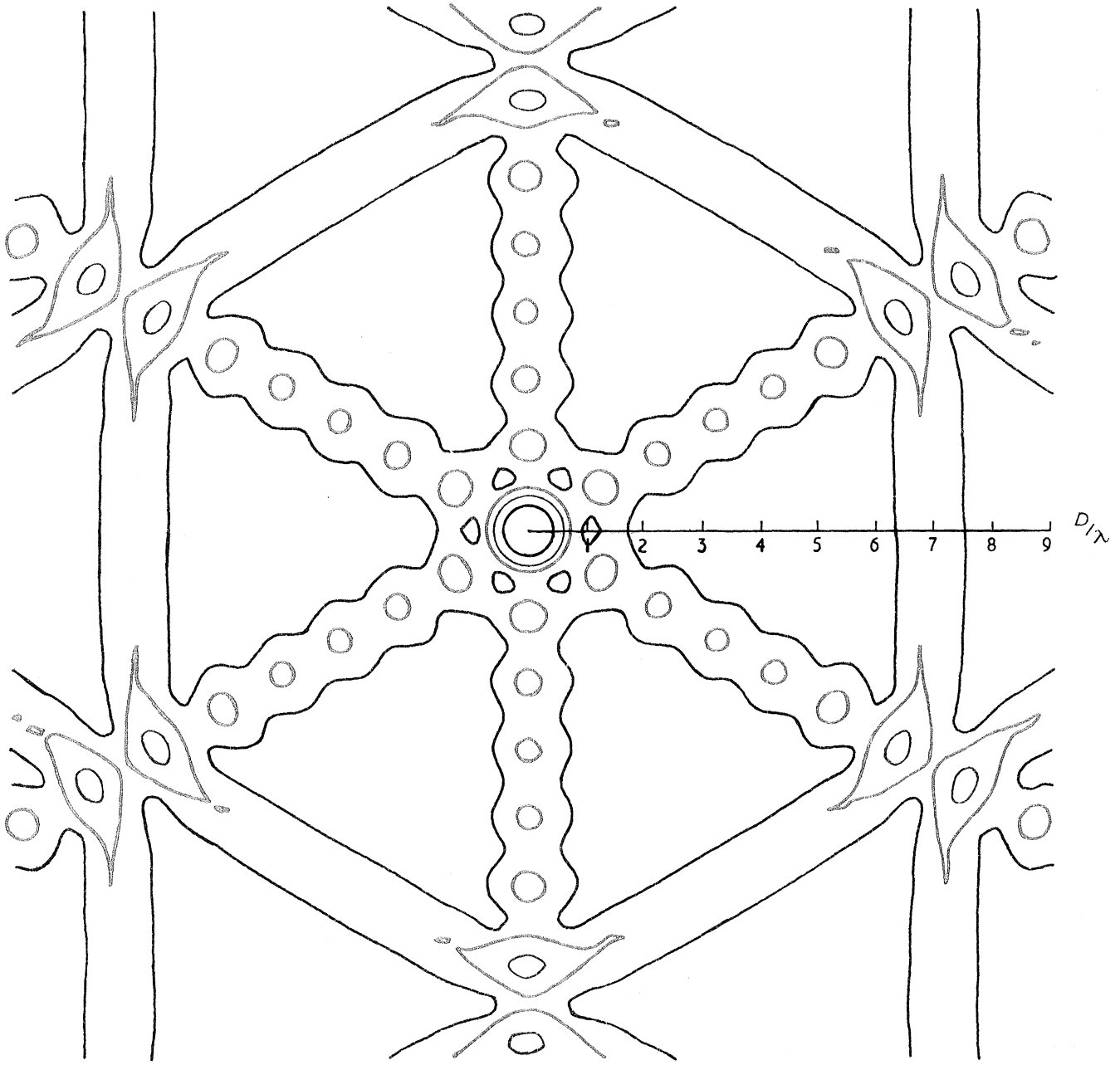

FIGURE 8. Sum squared response of 21 element triangular array.

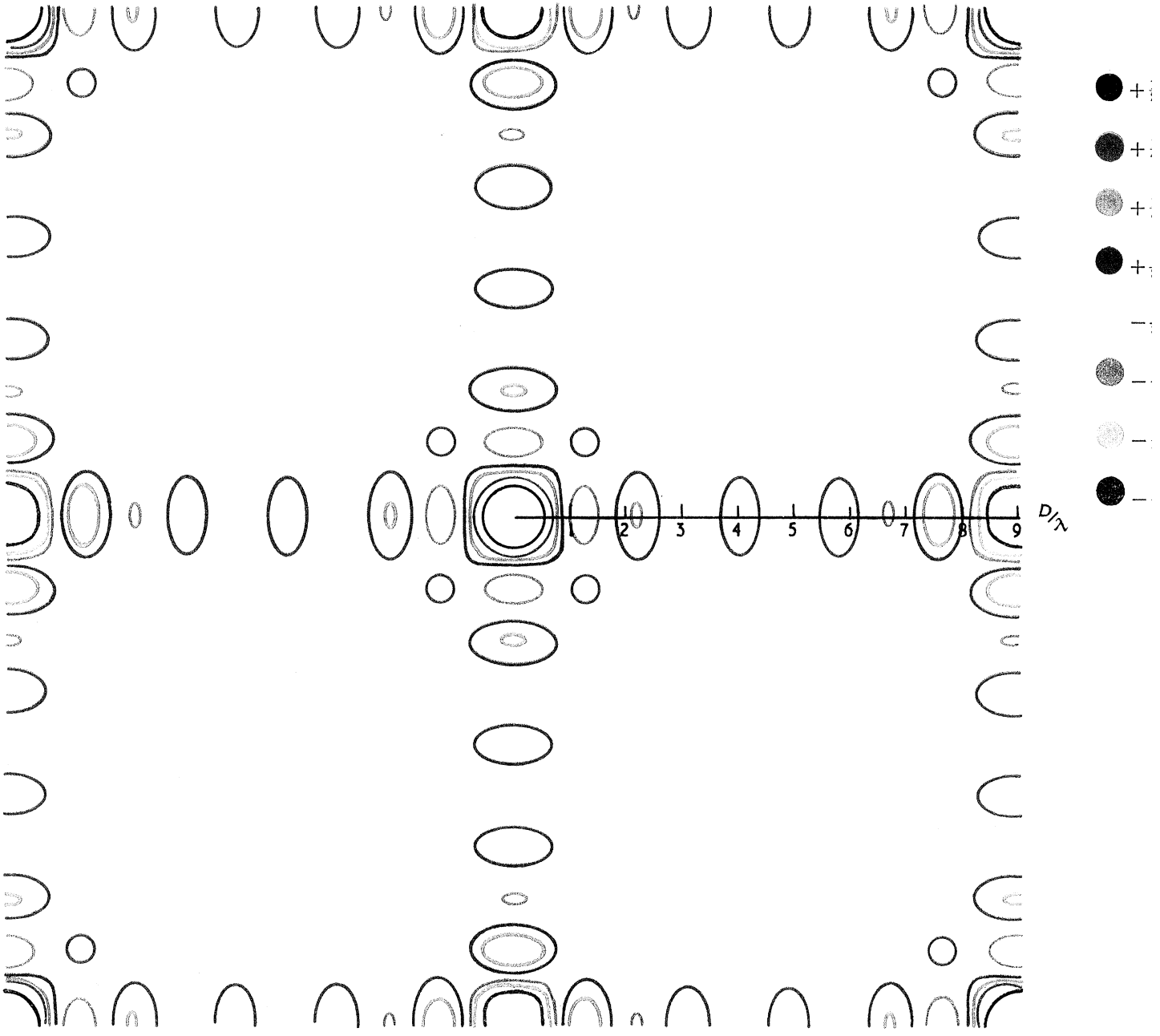

FIGURE 9. Correlator response of 20 element symmetrical cross array.

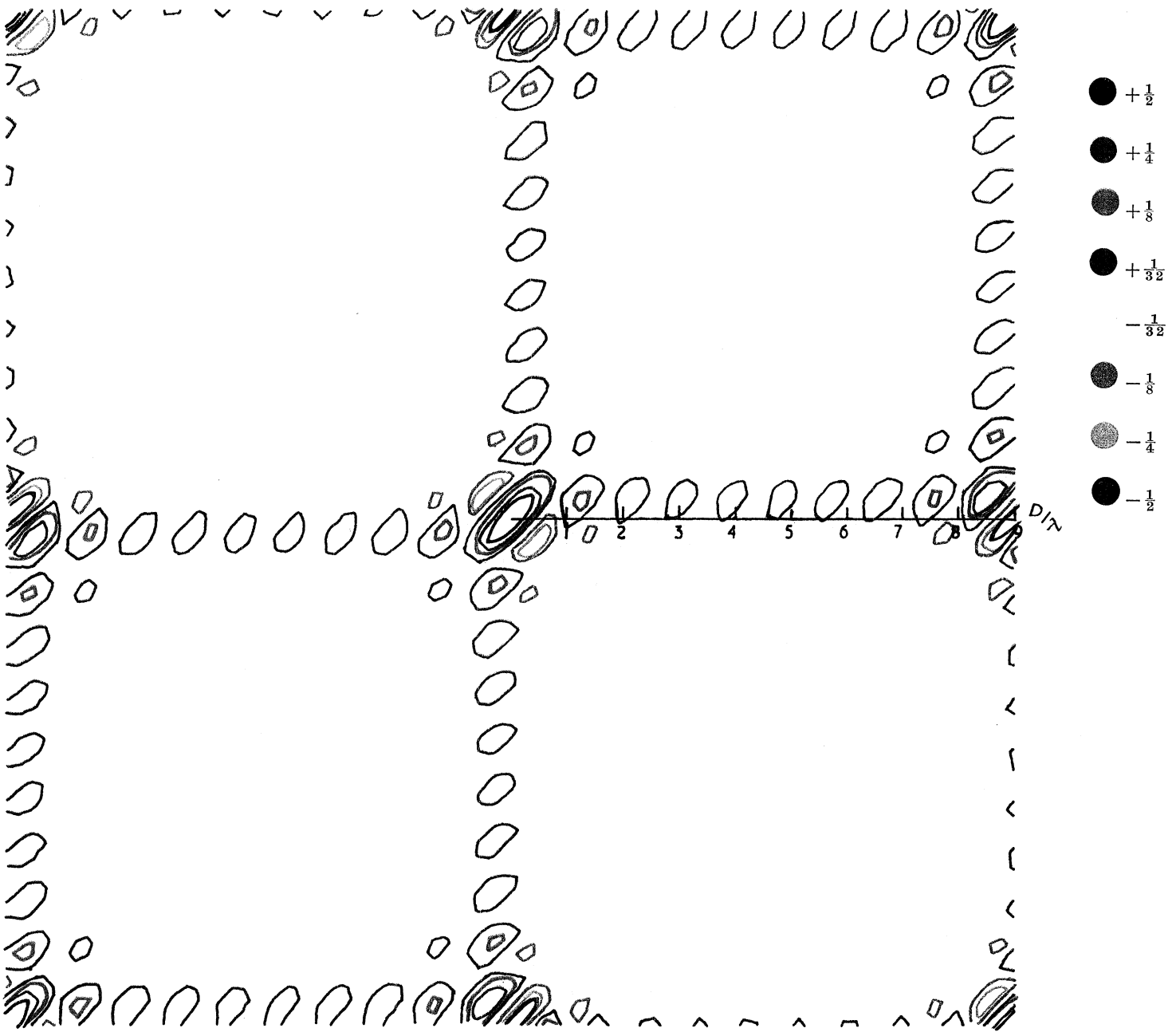

FIGURE 10. Correlator response of 20 element L-shaped array.

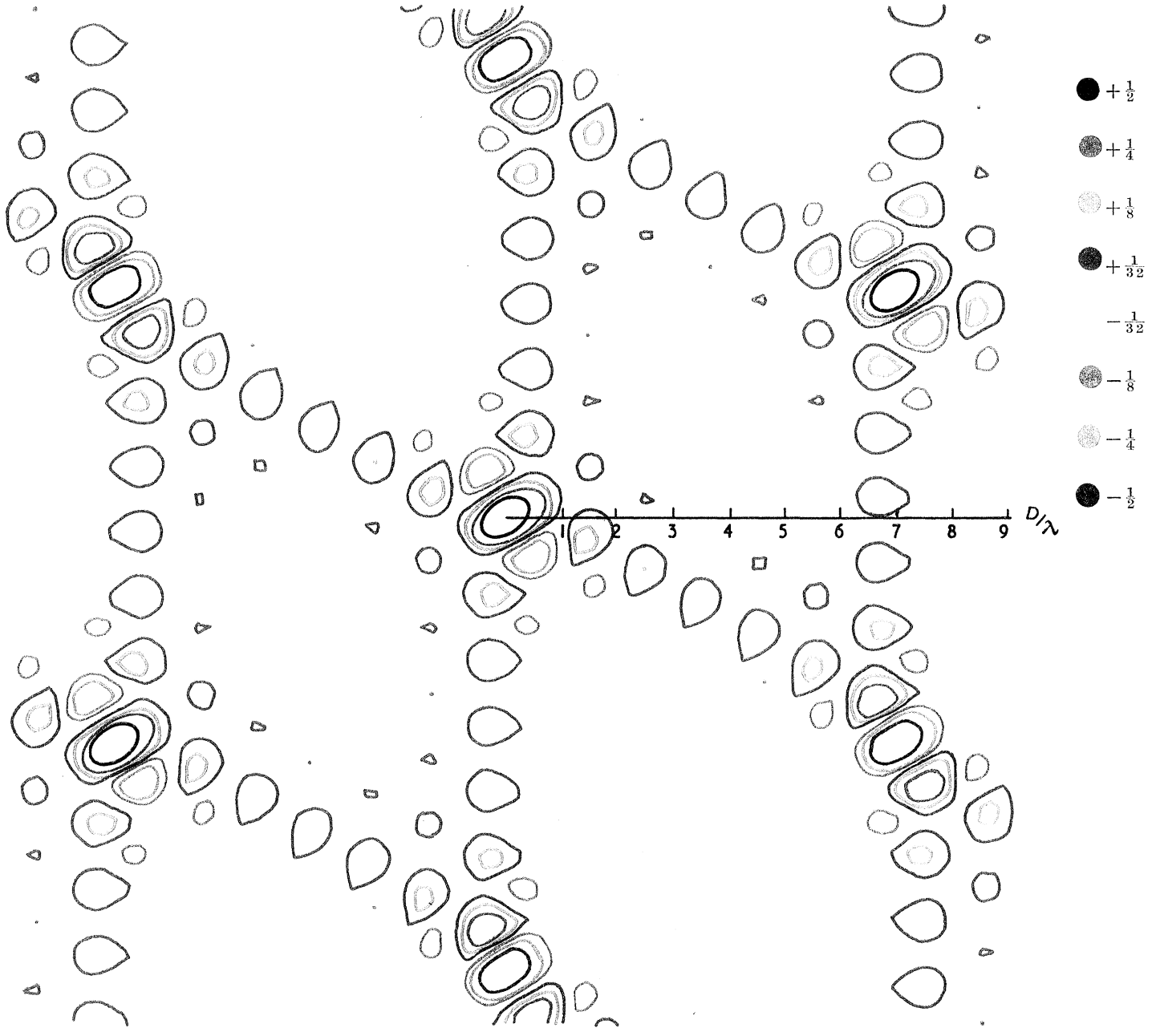

FIGURE 11. Correlator response of 14 element V-shaped array.

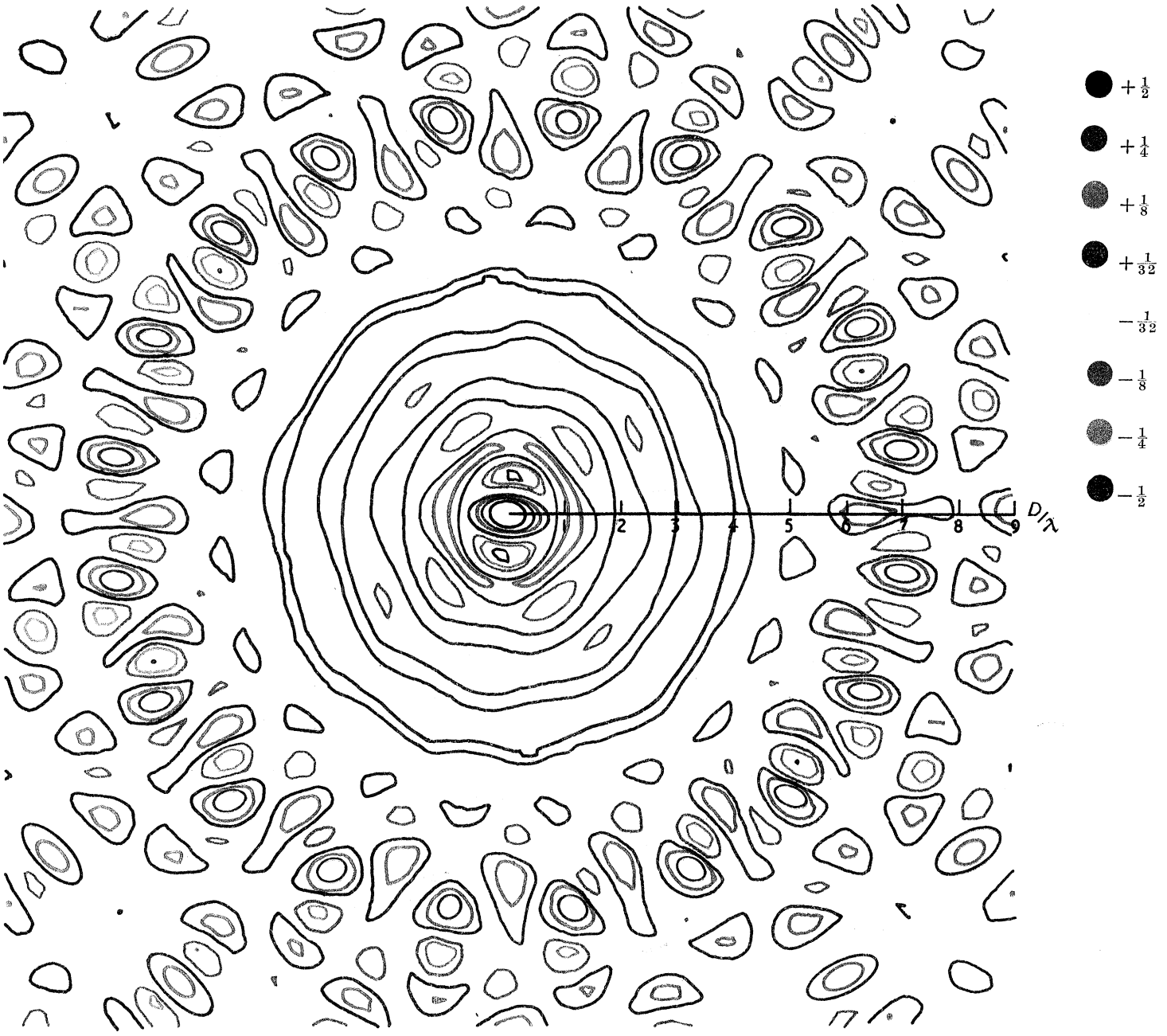

FIGURE 12. Correlator response of 20 element circular array.

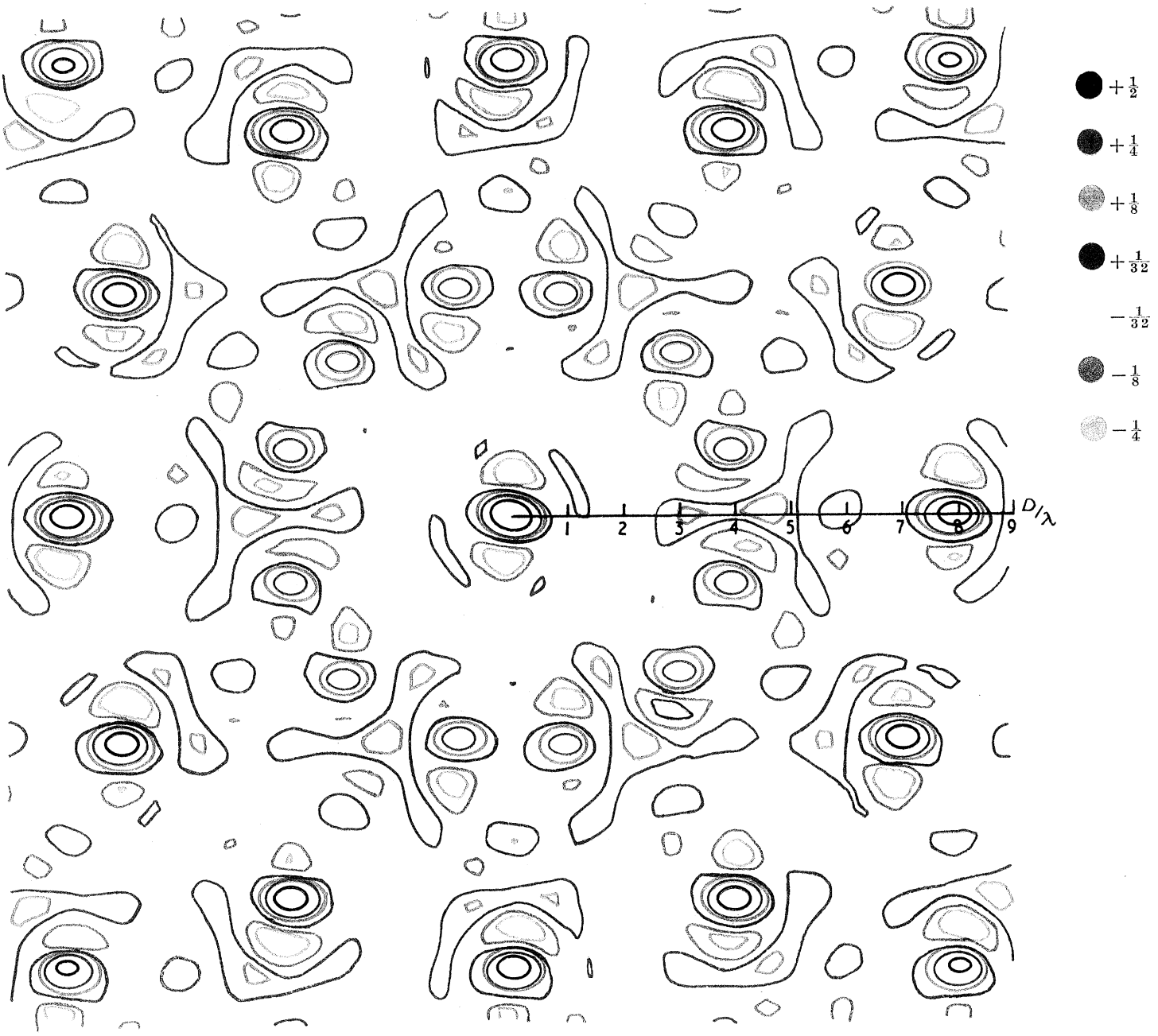

FIGURE 13. Correlator response of 18 element cluster.

signal, or through a range of velocity and/or azimuth. If this signal has a velocity V_1, azimuth θ_1, then the resultant phase shift for the rth seismometer in figure 2 (a) for any other signal (V, θ) is given by

$$\begin{aligned}\beta_r &= 2\pi \frac{d_r}{D}\frac{D}{\lambda}\cos(\theta-\alpha) - 2\pi \frac{d_r}{D}\frac{D}{\lambda_1}\cos(\theta_1-\alpha)\\ &= 2\pi \frac{d_r}{D}\left[\cos\alpha\left(\frac{D}{\lambda}\cos\theta - \frac{D}{\lambda_1}\cos\theta_1\right) + \sin\alpha\left(\frac{D}{\lambda}\sin\theta - \frac{D}{\lambda_1}\sin\theta_1\right)\right]\\ &= 2\pi \frac{d_r}{D}\frac{D}{\lambda'}\cos(\theta'-\alpha), \qquad (18)\end{aligned}$$

where

$$\frac{D}{\lambda'}\cos\theta' = \left(\frac{D}{\lambda}\cos\theta - \frac{D}{\lambda_1}\cos\theta_1\right), \qquad (19)$$

$$\frac{D}{\lambda'}\sin\theta' = \left(\frac{D}{\lambda}\sin\theta - \frac{D}{\lambda_1}\sin\theta_1\right). \qquad (20)$$

In these equations, λ and λ_1 correspond to the same frequency. The resultant phase shift given by equation (18) corresponds to that which would be produced by a signal of azimuth θ', wavelength λ'. From equations (19) and (20), it is seen that the vector representing this signal is equal to the difference in the two vectors $(D/\lambda, \theta)$, $(D/\lambda_1, \theta_1)$. Similarly, the summed or correlator response for the whole array corresponds to the difference vector $(D/\lambda', \theta')$. In order to determine the response as a function of (V, θ) for the above condition, it is only necessary to move the origin to the point $(fD/V_1, \theta_1+\pi)$. The same procedure can be adopted to determine the response to a signal component of velocity V_1, azimuth θ_1, when the array is tuned through a range of velocity V, azimuth θ. Since the responses are symmetrical about the first origin, the response as a function of (V, θ) can again be obtained by moving the origin to the point $(fD/V_1, \theta_1+\pi)$.

When the signal covers a band of frequency, the locus of the signal vector can only be fully represented by introducing frequency as a third dimension. The contoured response is shown as before in terms of $(D/\lambda, \theta)$ with no delay inserted, and is independent of frequency. However, since the value of D/λ is equal to fD/V, the locus of the point $(fD/V, \theta)$, without inserted delays and for constant velocity is the surface of a right circular cone, as illustrated by figure 14 (a). If the array is tuned to a signal (V_1, θ_1), the axis of the cone is displaced, and lies along OO_1' (figure 14 (b)). The displaced cone has a circular cross-section in the plane corresponding to a fixed frequency. Figure 14 (b) shows the displaced cones for several values of V/V_1.

The response can be obtained for discrete values of frequency by use of a single two-dimensional polar diagram, using the relationship $(D/\lambda_1 = fD/V_1)$. For given values of f and V_1, the locus of the resultant signal vector for constant values of V is a series of concentric circles centred on O' (for example), as shown in figure 14 (c). For another value of f or V_1, the centre is moved, e.g. to O''. The effect of doubling the frequency is the same as halving the value of V_1, since D/λ_1 (and hence the position of the new origin) remains the same. For given values of V_1, V, θ_1 and θ, the locus of the difference vector is a straight line through the origin. The distance from the origin is proportional to frequency, and thus the response can be determined as a function of frequency. The integral of the product of the sum squared or correlator response with the power spectrum of the signal gives the total signal power in

the output. Thus if the signal has a flat spectrum over a 2:1 frequency range and zero elsewhere, the relative signal power output is given by the average sum squared or correlator response over this range. This smooths the response, and isolated peaks are less important than for very narrow band spectra. Furthermore, since the correlator response varies about zero, the result of integrating the response over a band of frequency is to reduce the output towards zero. On the other hand, when the array is receiving isotropic, coherent noise of wide bandwidth, the sum squared output tends to the level $1/n$, irrespective of array configuration.

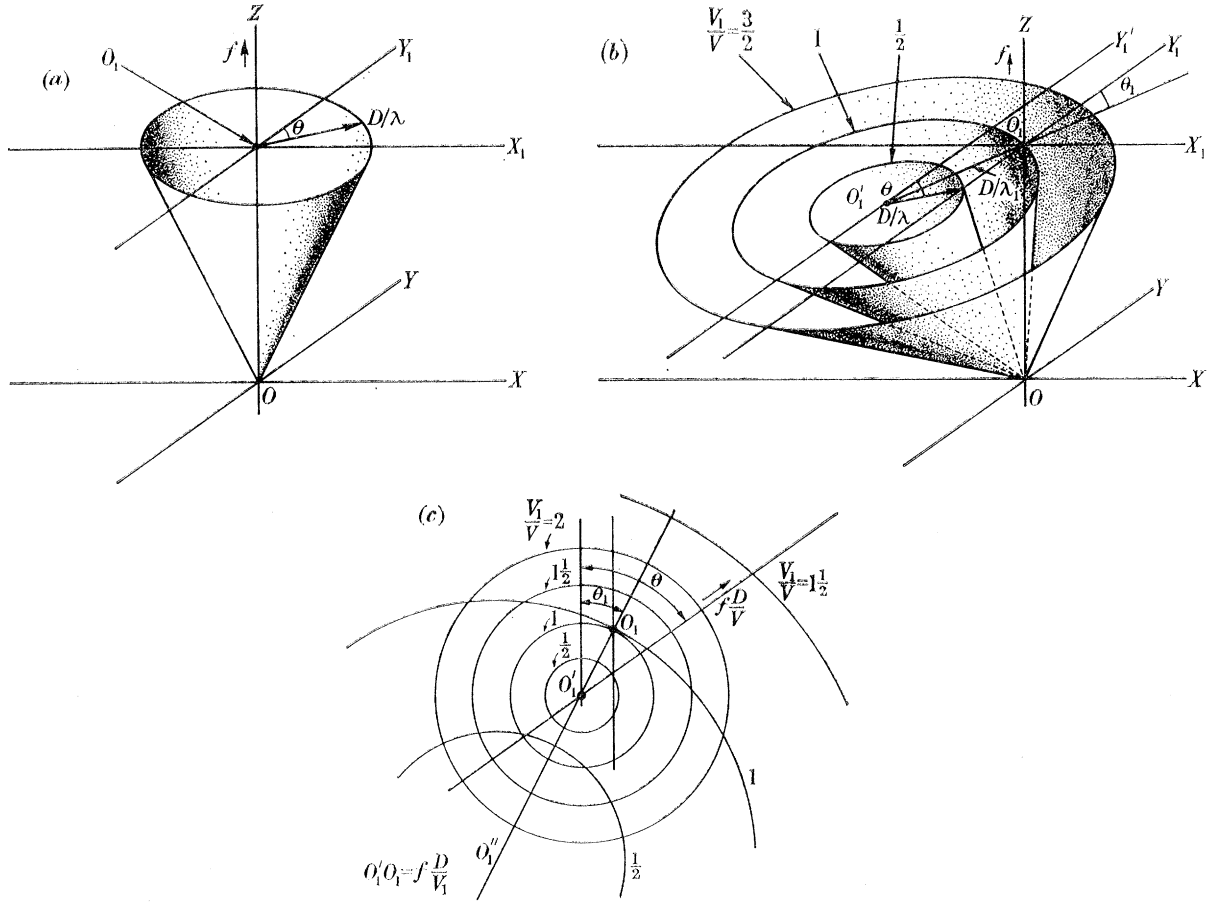

FIGURE 14. (*a*) Locus of constant velocity signal vector $(D/\lambda, \theta)$ for untuned array. (*b*) Locus of signal vector $(D/\lambda, \theta)$ when array tuned to signal of velocity V_1, azimuth θ_1. (*c*) Two dimensional representation of locus of vector $(fD/V, \theta)$ for array tuned to signal (V_1, θ_1).

2·4·4. *Comparison of array responses for different configurations*

The contoured responses can be used to determine the best array configuration. Desirable features in the contoured responses include:

(*a*) Minimum area within positive $\frac{1}{4}$ level contour line for the in-phase peak. This determines the sharpness of the azimuth and velocity responses discussed in §§2·4·5 and 2·4·6.

(*b*) Absence of subsidiary high level contours ($\pm\frac{1}{8}$, say) near origin. Any such contours to have a maximum value of D/λ and minimum enclosed area.

(*c*) Minimum area within $\pm\frac{1}{32}$ and higher contours over complete response.

With these factors in mind, the circle appears to give the best sum squared response, whilst the cross arrays are unsuitable in this respect for the reason previously described (§2·4·2). Comparing the correlator responses, the best response is obtained with the L-shaped array, and is in many ways better than the sum squared response of the circular array, particularly with regard to the total area within the $\pm\frac{1}{32}$ and $\pm\frac{1}{8}$ contours. The main disadvantage is that the correlator response of the L-shaped array is asymmetrical, although never inferior to the correlator response for a symmetrical cross. Furthermore, subsidiary $\pm\frac{1}{8}$ contours occur relatively close to the origin, and further subsidiary $\pm\frac{1}{32}$ contours occur at regular intervals of D/λ at directions at right angles to each of the lines. These subsidiary peaks can be reduced in amplitude by weighting the individual outputs as described in appendix B.

The normalized correlator response for a symmetrical cross array remains the same if one arm of the array is deleted, resulting in a T-shaped array. The number of seismometers can then be increased in each arm, and an improved correlator response obtained. The sum all squared response is inferior to the symmetrical cross, however, in the direction of the missing arm. The triangular array considered has the advantage that the sum all squared response is improved compared to the symmetrical cross, whilst the availability of three lines allows any one line to be discarded in obtaining the correlator response.

2·4·5. *Determination of signal azimuth*

In order to determine the azimuth of a signal, delays are inserted which correspond to the estimated velocity of the signal, and the full range of azimuth. The azimuth is determined from the value which gives the maximum correlator or sum squared output at a given time. The variation of correlator or sum squared output with azimuth (referred to as the azimuth response) can be determined from the general contoured responses for the array concerned in the manner described in §2·4·3, by using figure 3(*a*). The chart is orientated so that the position of the D/λ scale on the contoured response coincides with the correct value of θ_1 on the chart. In this case $(V_1/V = 1)$, and the circle giving the azimuth response passes through the first origin and has a value of unity at $(\theta = \theta_1)$. The sharpness of the azimuth response is dependent upon the general response in the vicinity of the first origin and upon the radius of the circle D/λ_1, i.e. fD/V_1. As this is increased, the azimuth response becomes sharper, and the azimuth can be determined to a greater order of accuracy. However, the azimuth response also becomes more dependent upon an accurate knowledge of V_1, and it may be necessary to carry out the azimuth search at a number of velocities within the estimated range. The sharpest azimuth response for the sum squared output is obtained with a circular array, and is symmetrical. The correlator output for the L-shaped array gives a sharper azimuth response than this in directions $(\theta_1 = \frac{1}{4}\pi, \frac{5}{4}\pi)$, but a comparatively broad azimuth response in directions $(\theta_1 = \frac{3}{4}\pi, \frac{7}{4}\pi)$. The correlator output for the triangular array is also asymmetrical, but the lines can be chosen to give the sharpest response for each sector of 120°.

2·4·6. *Determination of signal velocity*

If the azimuth of the signal is known, delays can be inserted to correspond to a range of signal velocity for the correct azimuth. The velocity of a signal component can then be

determined from the value which corresponds to maximum correlator or sum squared output at a given time. The theoretical response for each value of frequency is obtained simply by constructing a straight line starting at the displaced origin and passing through the first origin on the contoured response. The distance along this line is proportional to V_1/V, the initial origin corresponding to $(V_1/V = 1)$. Figure 3 (*b*) gives the scales for four values of D/λ_1. The sharpness of the response is once more dependent upon the general correlator or sum squared response in the region of the first origin, and upon the distance between the first and displaced origins (i.e. fD/V_1).

The contoured responses only give the velocity and azimuth responses at discrete points. The full curves may be derived from the original equations for specific conditions of interest. Some full curves for cross arrays are included in appendix B, corresponding to three of the values of D/λ_1 used in figures 3 (*a*) and (*b*), namely

$$d/\lambda_1 = \tfrac{1}{2},\ (D/\lambda_1 = 4{\cdot}5); \quad d/\lambda_1 = \tfrac{1}{10},\ (D/\lambda = 0{\cdot}9); \quad d/\lambda_1 = \tfrac{1}{20},\ (D/\lambda_1 = 0{\cdot}45).$$

2·4·7. *Errors in azimuth and velocity determination*

The accuracy of determination of velocity or azimuth depends partly upon the sharpness of the velocity or azimuth response, which in turn depends upon the dimensions of the array in relation to the wavelength of the signal, and the array configuration concerned. The conclusion in appendix B for cross arrays is that, for a single signal component with high signal/noise ratio, an accuracy of about 3° in azimuth and 5 % in velocity is feasible when the length of each line is equal to the wavelength. A similar order of accuracy is feasible with the other types of array considered. The accuracy may be reduced by a number of factors; for example, if the number of search conditions is insufficient. These factors are considered in detail in appendix B for cross arrays, and most of them are equally applicable to other forms of array.

The velocity or azimuth of a signal component may also be determined when it is preceded by an earlier arrival, or by coherent noise. In this case the 'differential correlator' or 'sum squared output' is measured as a function of velocity or azimuth by taking the correlator or sum squared output immediately before the event as a baseline (appendix B). Appreciable errors may be encountered for weak arrivals in the presence of strong unwanted signals, owing to variation of the cross-product terms in the correlator or sum squared output. Such errors can be minimized by using maximum array dimensions, and endeavouring to ensure that the strong signal component is rejected by both groups of seismometers when the correlator output is used. The preferred direction for velocity filtering for a cross array is therefore at an angle of 45° to the two lines. A triangular array allows one line to be discarded if necessary.

2·4·8. *Correlator presentation*

One method of presenting the correlator or sum squared output is to display it as a function of time for each search condition (V, θ). In this way, sudden changes in output may be observed as a function of time, indicating possible new arrivals. Alternatively, the output may be recorded as a function of velocity and/or azimuth as a nested display at discrete time intervals, so that the velocity or azimuth may be rapidly assessed as a function of time.

3. Experimental arrays

3·1. *General*

The remainder of this paper describes experimental applications of the general principles described above. The array configurations used in the experimental arrays represent a compromise between desired theoretical layouts, and factors such as accessibility and local topography. The Eskdalemuir and the original Pole Mountain arrays were designed to record signals at ranges up to 10° and maximum wavelengths of 10 km. At a later stage, interest was concentrated on the detection and analysis of signals at teleseismic ranges. The maximum wavelengths of interest are then about 25 km, corresponding to *P* wave arrivals at a range of 90° and a frequency of 1 c/s. The maximum *P* wave signal amplitude at a range of 90° for an event of magnitude *m*4 is about 1 nm (zero to peak). In order to obtain a signal/noise ratio of at least 4:1 with a 20 element array, the ambient noise level should not exceed $\frac{1}{2}$ nm (r.m.s.) The dimensions and siting of the Yellowknife array were chosen to fulfil these requirements.

3·2. *Siting criteria*

The choice of a suitable site for an array covering an area of 10 to 25 km square is governed by many stringent requirements. First of all it must be in an area which has low seismic noise level, and good coupling at all seismometer positions. The geology of the site should be homogeneous and uncomplicated by major elastic discontinuities. The seismometers should be coupled to well consolidated unweathered rock. Areas with multiple sedimentary layers, particularly those of recent origin, are usually found to have a high seismic noise level. The site must be well away from coasts, major industrial centres and other generators of seismic noise. For example, the siting criteria adopted requires each pit to be at least 5 miles from a railway line (in frequent use), one mile from a busy road, and 200 yd from the nearest tall tree. The bedrock should be only sparsely covered, so that good coupling can be obtained with relatively shallow pits (about 6 ft.). The area should be as flat as possible and a tolerance of ± 200 ft. elevation over the whole array was given in the siting criteria. Other factors include the nature of the farming activity in the area concerned, accessibility, and accommodation for the operational staff.

3·3. *Pole Mountain*

Additional criteria for the choice of a site in U.S.A. were that it should be at least 500 km from the coast, to minimize microseismic noise, and about 1000 km from both the Gnome shot point (N. 32·2°, W. 104·0°) and the Nevada Test Site (N. 37·0°, W. 116·0°). This distance was chosen because it corresponds to the minimum amplitude on the amplitude-distance curve for the first *P* wave arrival in western U.S.A. (Romney 1959). The site selected is situated on Sherman granite at Pole Mountain between Laramie and Cheyenne in Wyoming. It is 1000 km from the Gnome shot point, and 1030 km from the Nevada Test Site. The area is the property of the U.S. Government, which gave permission to install the array quickly, avoiding many administrative difficulties.

The original array (figure 15) comprised 13 seismometer pits spaced at intervals of 1·5 km along two mutually perpendicular lines, and with one pit common to the two lines (co-ordinates N. 41° 12·6′, W. 105° 20·1′). Each pit was constructed with a level concrete floor

grouted to bedrock, and a metal liner sealed by bitumen at the base to prevent water leakage. It contained a vertical Willmore seismometer and head amplifier. Appreciable differences in noise levels were encountered between pits. These differences are believed to be a function of the degree of weathering, which varied considerably over the area. The quietest pit (BW3) was situated on hard exposed rock on a hillside, with small trees within 50 ft. Some of the noisier sites (e.g. RN3) were situated in open country with several feet of badly weathered rock at the surface.

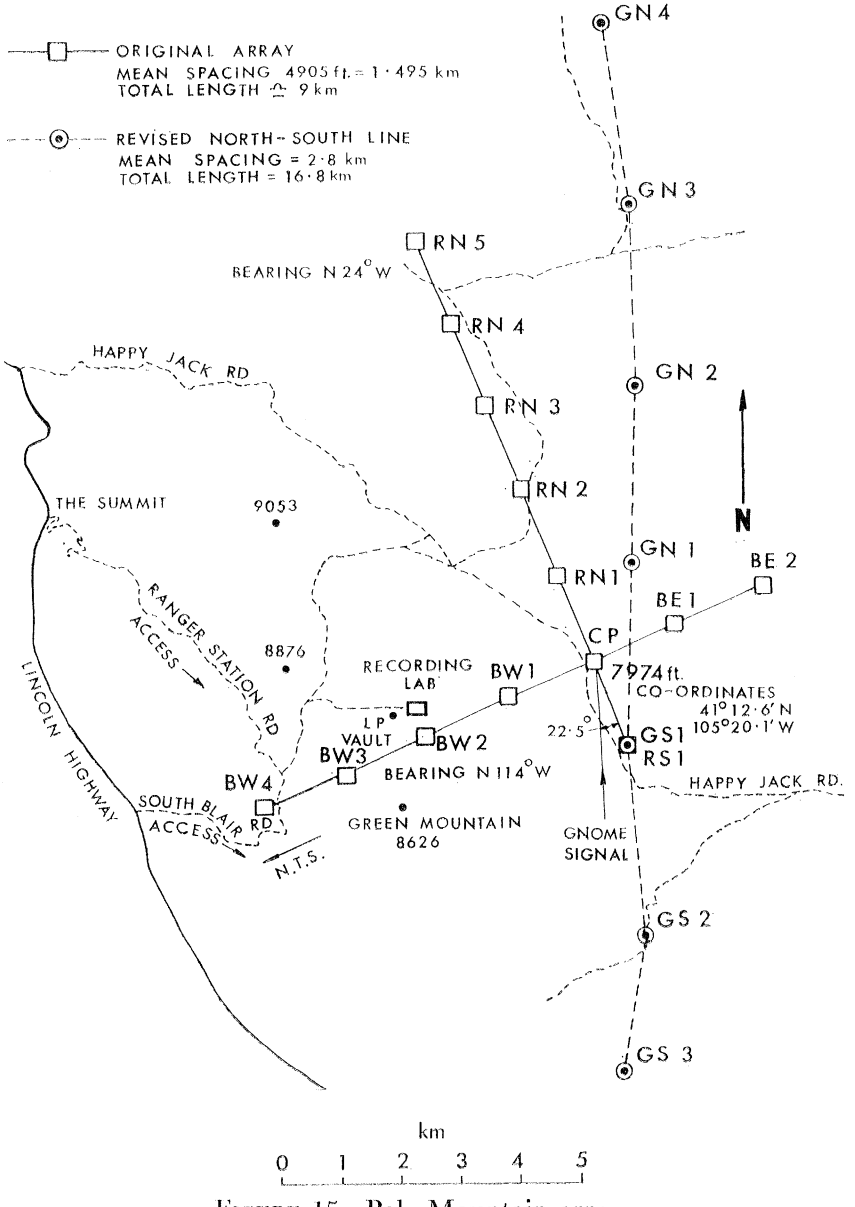

FIGURE 15. Pole Mountain array.

For this reason, nearly all seismometer pits were relocated. The positional tolerance was relaxed, since allowance for positional errors will be possible in future analysis. The length of the north-south line was extended to 18 km to enable velocity filtering techniques to be applied to more distant events. The line was reorientated to allow siting the seismometers on unweathered granite. Each site was chosen after measuring the velocity of the rock

immediately beneath the thin cover. This was achieved by constructing travel-time curves for distances up to 150 ft., using signals generated by hammer blows. In spite of these measures, the improvements in noise levels were disappointing. The plan of the revised array is also shown in figure 15.

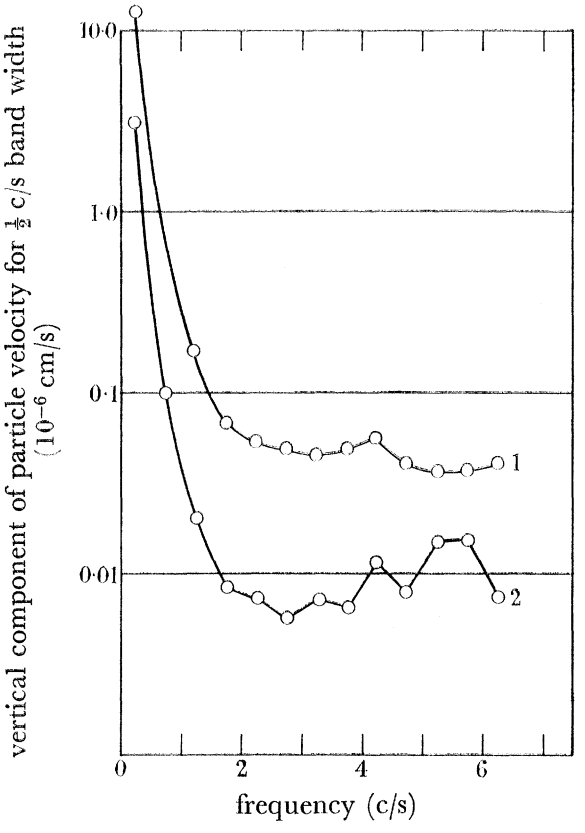

FIGURE 16. Frequency spectra of noise. Curve 1, Eskdalemuir; 2, Yellowknife.

Severe weather conditions were encountered during the winter months, with up to 80° of frost and deep snow drifts. These made most of the array inaccessible for long periods, and the staff had great difficulty in reaching the recording vans to maintain continuous operation. Very little recording time was lost, despite the difficulties, although several individual channels were non-operational for a time. During the summer months, considerable interference was encountered from induced currents, due to lightning, in the long signal cables, causing damage to amplifiers and seismometers. Many cables were damaged by rodents, causing further loss of recording channels. This was greatly reduced by burying the cables.

After operating for nearly 2 years, sufficient data had been accumulated, and the station was dismantled in August 1963. The effort was then concentrated on completing the Yellowknife array, which is on a far better site.

3·4. *Eskdalemuir, Dumfriesshire*

In view of the siting criteria previously described, Scotland is the obvious choice for a site in the United Kingdom. Granite outcrops were considered, but found to be unsuitable due to weathering, high relief or insufficient area. Finally, Eskdalemuir was chosen, being

situated in an extensive area of Silurian Shale (Lower Palaeozoic). Nearly all siting criteria were met, the area being almost devoid of trees, and used for sheep farming. The noise in the 1 to 3 c/s band is very low for the British Isles, and varies between 3 and 20 nm, depending on weather conditions. The frequency spectrum for a quiet day is shown by figure 16, curve 1. This was obtained by measuring the mean square value of the noise passed by filters of $\frac{1}{2}$ c/s bandwidth (−3dB points), correcting for the seismometer and recording system responses.

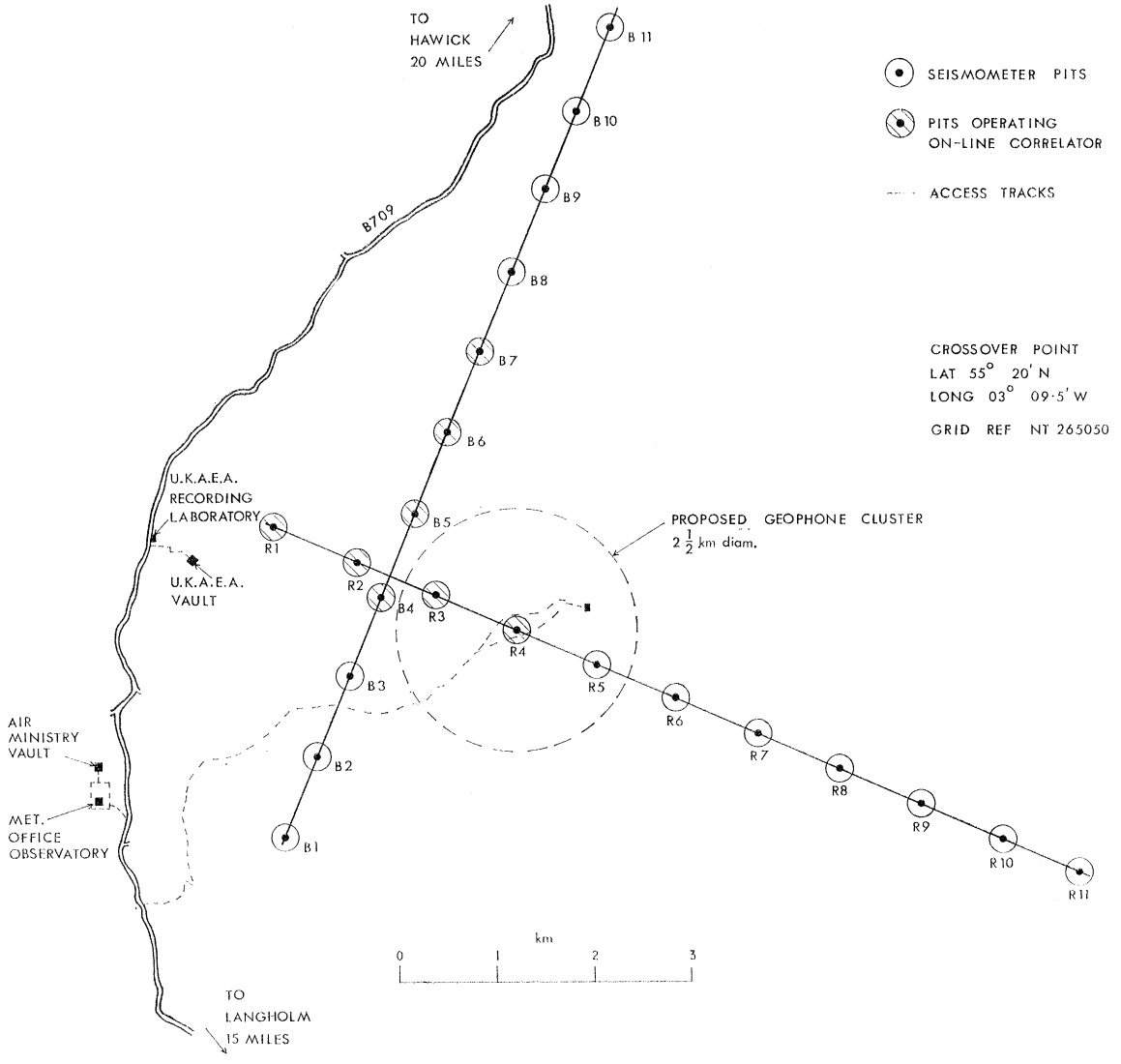

FIGURE 17. Eskdalemuir array.

The plan of the array is shown in figure 17. The array contains 22 seismometer pits, spaced at intervals of about 900 m along two mutually perpendicular lines. A full description of the array, vault and recording system has been given by Truscott (1964).

3·5. *Yellowknife*

The Canadian Shield is an ideal area in which to site an array. The large-scale structure is very uniform, with considerable exposure of hard rock, and low relief. After a noise survey, an array was installed near Yellowknife and is being operated by the Canadian

Department of Mines and Technical Surveys. Figure 16, curve 2 shows the frequency spectrum of the ambient noise. Yellowknife is on the northern shore of the Great Slave Lake. The plan of the final array is shown in figure 18, and consists of two lines of 10 seismometers spaced at 2·5 km intervals. A limited array, consisting of seven pits shown by the shaded circles, commenced operation in December 1962. The remainder of the main array was completed by December 1963. The original instrumentation was similar to that at Eskdalemuir. A new recording system is now installed using amplitude modulated tones, with a

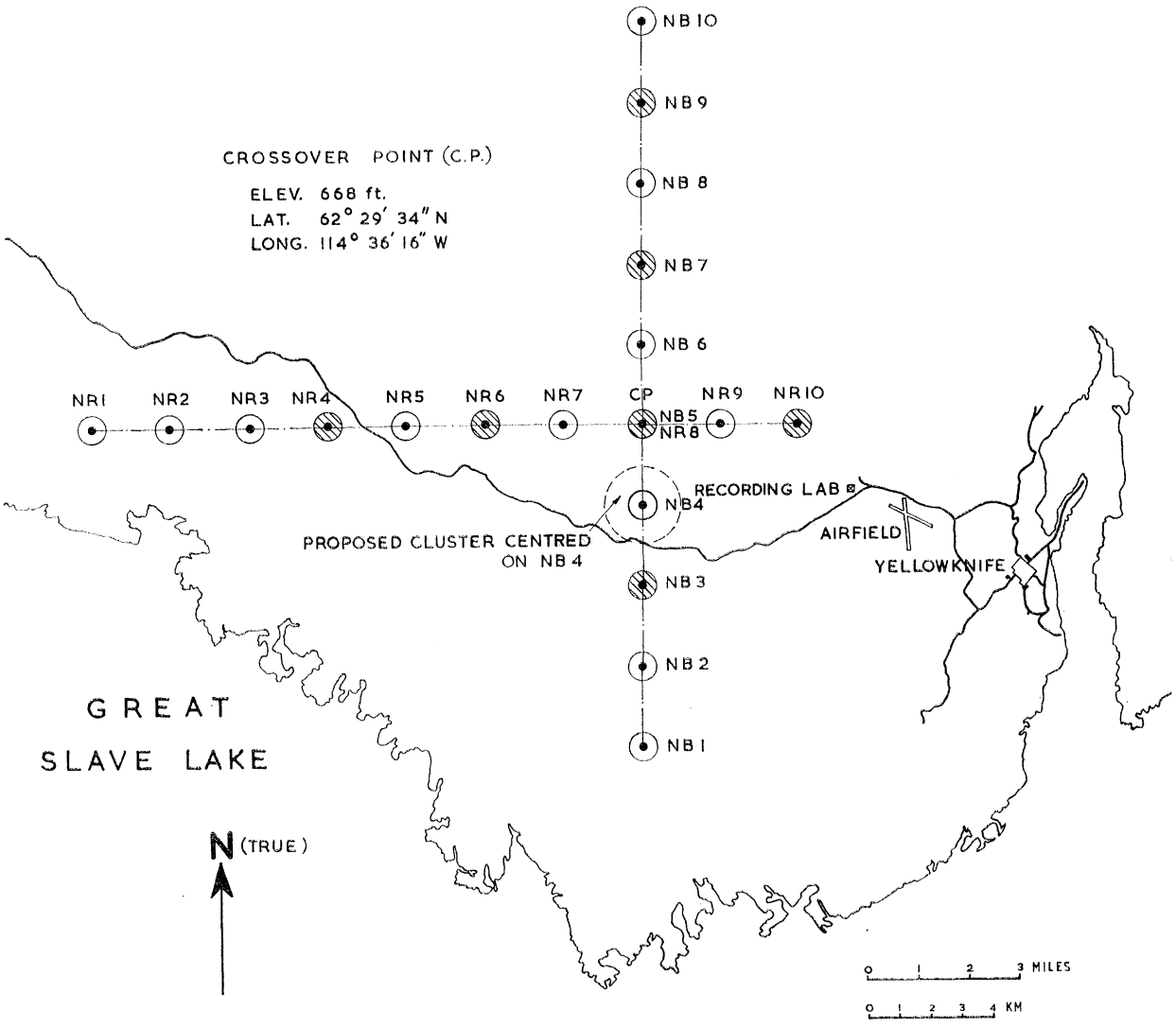

FIGURE 18. Yellowknife array.

single semi-armoured cable serving two pits. The object of the new system is, first, to improve reliability against storm and animal damage, and second, to reduce cable costs. The array includes a 2 km diameter solid pattern cluster of mk II Willmore seismometers centred about NB4. This will comprise up to 24 seismometers, although only two are being recorded at present. The cluster will be summed into two groups, without inserted delays, and recorded on magnetic tape. The summed outputs will also be cross correlated in an on-line processor, and will trigger an 8 channel heated stylus paper recorder and an auxiliary magnetic tape recorder when the correlator output reaches a pre-set level. In this way, nearly

all signals of interest will be recorded on paper at a suitable speed (about 3 mm/s), and the load on the off-line processor and transcription facility reduced. A similar correlator, with the gain automatically controlled by the ambient noise level, has been installed at Eskdalemuir.

Results from the Yellowknife array have been very promising. During the winter 1962–63 the noise level in the band 1 to 3 c/s was well below $\frac{1}{2}$ nm (r.m.s.). As a result, it was possible to detect many more events on the single channel helicorder records than at Pole Mountain or Eskdalemuir. During the summer months, the noise level was higher, and exceeded 1 nm at times.

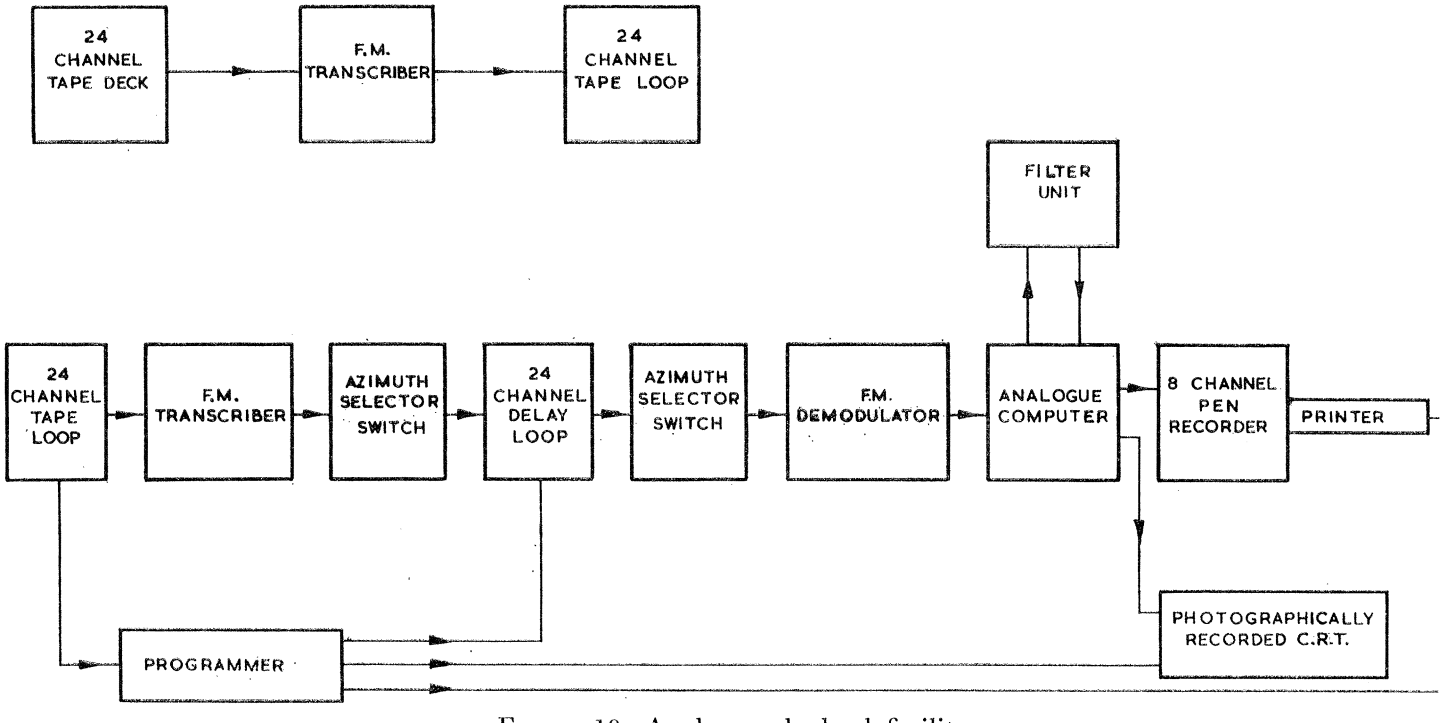

FIGURE 19. Analogue playback facility.

4. DATA ANALYSIS EQUIPMENT

There are several possible methods of performing the processes required for the combination of array outputs. One method uses a general purpose off-line analogue computer in conjunction with equipment designed for inserting the required delays, and is currently in use by the A.W.R.E. Seismological Group. A second method is to use an off-line general purpose digital computer, and it is hoped to implement this shortly. A third uses a special purpose computer, capable of operating on-line, for the analysis of array data. A feasibility study on this machine has been carried out and design work is proceeding. Details of these three methods are given below.

4·1. *Analogue facility*

The analogue playback and analysis system, illustrated by figure 19, is installed at Blacknest, near Aldermaston. All tape and paper records are sent to the data library there. Paper monitor records from each station are studied and details of events logged. These are compared with the U.S. Coast and Geodetic Survey lists of epicentres, and with other seismological bulletins. Events are selected for detailed analysis from those identified,

and are located on the original tapes with the aid of the coded time track. The signal in frequency modulated form is then transcribed onto a permanent tape store and onto a tape loop. The cycle time of the loop is adjusted to correspond to the duration of the signal, which can therefore be reproduced repeatedly in frequency modulated form at the output of playback heads mounted on the loop tape deck. The signal is then transcribed continuously onto a delay loop. This contains a 24 channel in-line recording head, 22 staggered 2 channel playback heads and two single channel heads. The delay deck enables equal incremental delays to be inserted in 22 signal channels with wow and flutter compensation. A 2 channel playback head is required for each signal channel since it is necessary for the appropriate error correction channel to be delayed by the same amount as the signal. The incremental delay between playback heads can be varied from 0·0125 to 0·125 s by changing tape speed, corresponding to a 10:1 range in seismic signal velocity. The delay deck can be programmed to insert up to 50 selected delays, the value being changed automatically at the end of each cycle of the primary tape loop. The head configuration is suitable for single line arrays of up to 22 equally spaced seismometers, but for a cross array it is only possible to arrange the delays for a restricted number of azimuths and seismometer outputs without introducing time errors. This is one of the reasons for changing to the digital methods.

The signals from the delay deck are demodulated and the error correction channels combined with the corresponding signal channels. They are then fed through a filter bank to a Pace analogue computer type 231 R. This is a versatile computer with an accuracy of 0·01 % for each linear element. The computer is used to normalize the seismic signals, to weight them if required, and to perform the addition, multiplication and time averaging processes required for cross correlation. The output is recorded on an 8 channel rectilinear heated stylus recorder associated with the computer. This is typically switched to record a single channel output, the summed outputs of the two lines (A, B), the summed output of the complete array ($\Sigma A + \Sigma B$), the correlator output $\overline{(\Sigma A \Sigma B)}$ at two levels of sensitivity, the modified correlator output $\overline{(\Sigma A \Sigma B)}^{\frac{1}{2}}$ and time.

The computer has also been used for other purposes, such as the determination of power spectra, inverse filtering and probability distributions of noise. These probability distributions are now carried out by using a pulse height analyser in conjunction with a sampling system.

4·2. *Use of general purpose digital computer*

A program is being written for the I.B.M. 7030 digital computer, installed at A.W.R.E., Aldermaston. Equipment necessary for converting the array data to the required format has been constructed. This system operates as follows.

Signals from 19 channels are demodulated and combined with the appropriate wow and flutter correction channel. They are normalized and passed through a bank of high and low pass filters to a 20 channel sampling switch. The recorded time signal is fed to the 20th channel. Each channel is sampled in turn at a rate of 20 samples per second of recorded time, and converted to digital form. The output of the analogue-digital converter has a rate of 400 words per second, and is in 12 bit binary coded decimal form (b.c.d.). The data are written continuously into a 1000 word core store, being read out in bursts of 1000 words at a rate of 5000 words per second. The digits are then recorded on 7 channel $\frac{1}{2}$ in. wide

digital tape, which moves at 75 in. per second while the words are being read out of the core store. The tape is stationary in the quiescent phase. Each data block is contained on 15 in. of tape followed by a gap of $\frac{3}{4}$ in. The words are recorded on four tracks of the magnetic tape in standard I.B.M. format at a packing density of 200 bits per inch of tape. A fifth channel is used for lateral parity for each digit; longitudinal parity bits are recorded at the end of each data block. The record is identified on the tape by an alpha-numeric code using all seven channels, including parity.

The input data to the computer include the polar co-ordinates of seismometers in the array and the search conditions, namely 72 chosen combinations of velocity and azimuth (V, θ). A table of delays, relating each seismometer output to a fixed point in the array for the 72 values of (V, θ), is then computed by a subroutine, and stored in the memory of the computer. Alternatively the input can accept a similar table of delays previously computed.

The signal data are read sequentially from the tape. The program at present allows for a total of 120000 words, corresponding to data from 20 channels sampled at a rate of 20 per second for a duration of 5 min. As the data are read, the channels are summed in two groups for each search condition, one instrument being common if required. Normally these groups will correspond to the two lines. The two groups are then multiplied, integrated, and the cross correlation integral thus obtained stored on disc. There are 72 values for each sample period.

After exhaustion of the data two outputs can be called:

(i) A print of the correlation integral and total sum for each search condition and sample time.

(ii) A print of the conditions corresponding to the main maxima of the correlation integral at each sample time. Thus if the search conditions correspond to azimuth at three velocities, the computed direction of the signal is recorded for each velocity. Similarly, if the search conditions correspond to velocity filtering at fixed azimuth, the velocity(ies) corresponding to the peak(s) of the correlation integral is recorded.

A graph of correlation integral against search conditions can be recorded on the off-line SC4020 output device.

4·3. *Special purpose computer*

The third method is to use a computer designed specifically for the purpose, and figure 20 illustrates the general principles of the system which is under development. The input section is designed for analogue operation, and accepts input data either from an array of seismometers in the field (on-line working) or from a magnetic tape recording (off-line working). The signals are filtered and normalized in analogue form, then passed to the next section for insertion of delays. This operation is performed digitally, using a core store. The channels are digitized sequentially at a rate of 20 samples per second per channel, and written into a 4096 word store. This will store information for about 10 s. Thus, relative delays of ± 5 s can be inserted in each of 22 channels (including time) by reading the appropriate cores. These delays are selected by a separate program store, which stores up to 9 tables of delays, each table corresponding to the array configuration concerned and 20 values of (V, θ). Alternative programs are computed off line and stored on punched cards. The channels are read out sequentially for each of the 20 search conditions (V, θ) at each sample time. The output from the core store is thus multiplexed both with respect to channel

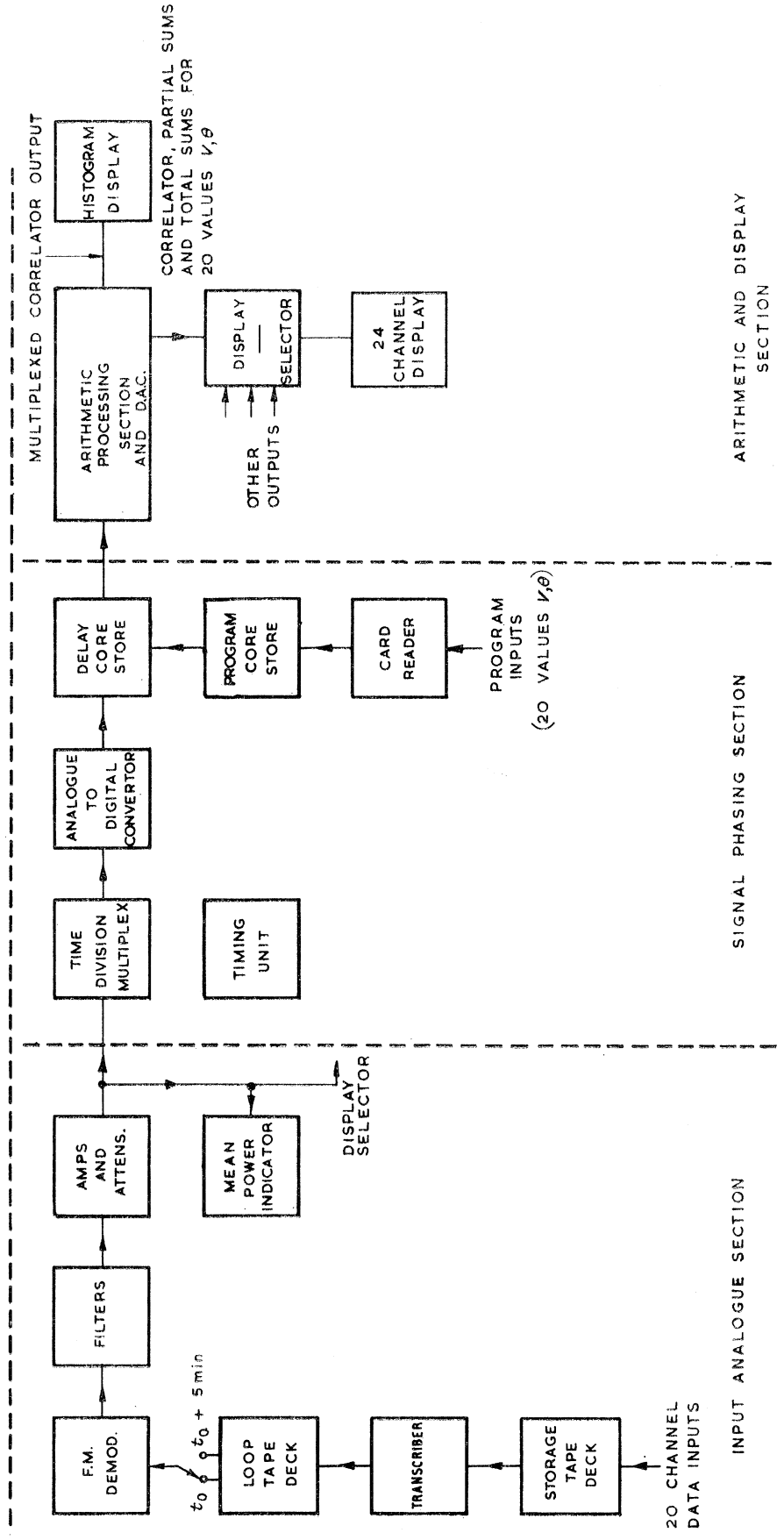

FIGURE 20. Seismic array data analyser.

number and also with the value of (V, θ). The channels are then summed into two groups and these groups multiplied together using digital arithmetic. A total sum is also computed. The product and total sum are converted back to analogue form, and demultiplexed. The averaging process is performed on the product in analogue form, and the summed and correlator outputs are available separately for each search condition (V, θ). The information is then re-multiplexed to give a histogram showing the correlator output as a function of (V, θ). By choosing the values of (V, θ) to correspond to the full azimuth range at the expected signal velocity the azimuth of the signal may be determined. The program can

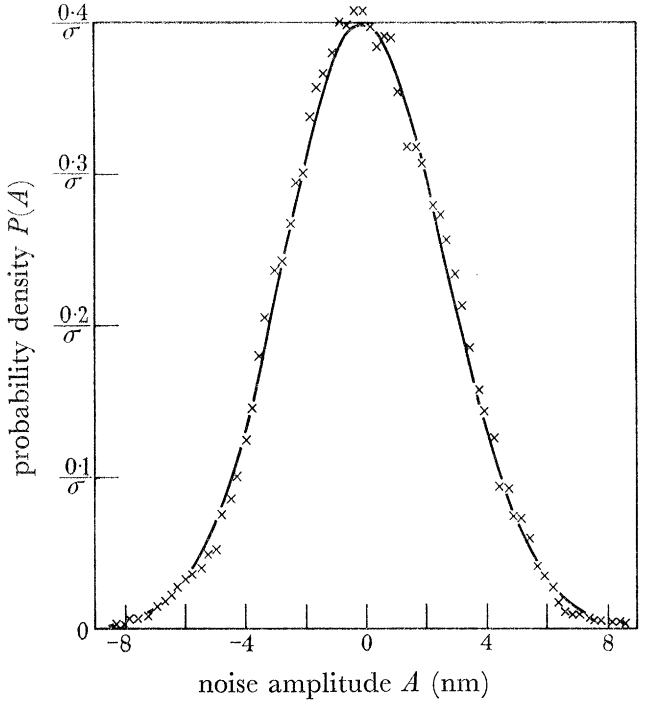

FIGURE 21. Amplitude probability density of noise at Eskdalemuir. ——, Normal distribution, $\sigma = 2{\cdot}7$ nm; ×, observed distribution.

then be changed so that the full velocity range is swept at this azimuth. A five minute delay loop has been incorporated to enable the signal to be repeated for this purpose.

Up to 24 summed and correlator outputs may be recorded as a function of time on an ultra-violet recorder. The histogram is recorded on film from a cathode ray oscillograph.

5. Analysis of experimental results

5·1. *Signal/noise improvement for summed array*

The improvement in signal/noise amplitude obtained by summing the outputs of an array was investigated experimentally using the noise outputs from the 21 vertical seismometers of the Eskdalemuir array. The outputs were frequency filtered with a pass band of 1 to 4 c/s to correspond to P wave signals at ranges of 5 to 90°, excluding the microseism band below 1 c/s. The amplitude probability distribution of the noise from a typical seismometer output was obtained with a 100 channel pulse height analyser of the type used in nuclear measurements. This required the noise to be gated to produce pulses of approximately 5 μs in duration. The sample rate used for the noise analysis was 100 samples/s.

The analyser enabled the amplitude range to be divided into 100 sections. The number of pulses, whose amplitudes lay within a particular section, were counted. At the end of the experiment the counts recorded in the 100 channels gave the amplitude probability distribution of the noise. The probability distribution obtained, after normalizing the individual counts by the total number of counts, is shown by figure 21 and conforms closely to a normal distribution with zero mean. The cumulative probability distribution, which shows the probability of the noise amplitude lying below a given level, is shown by figure 22.

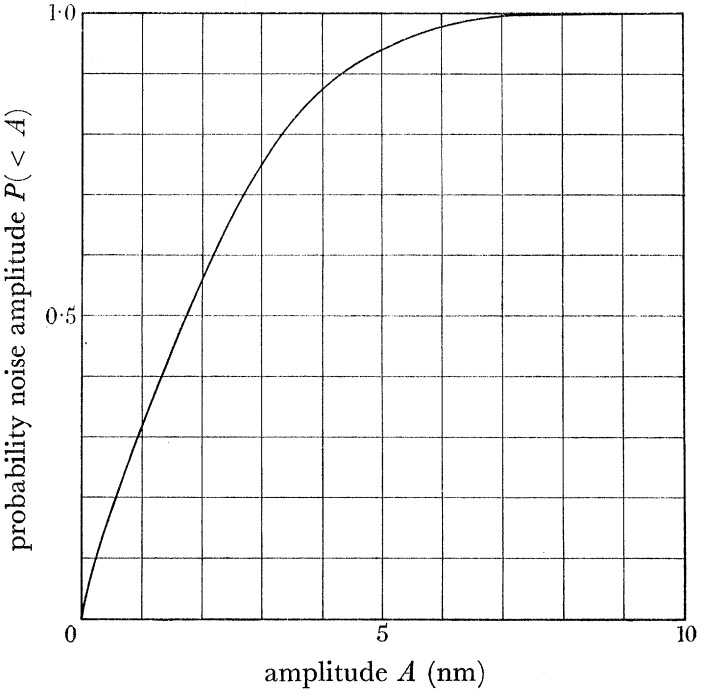

FIGURE 22. Cumulative probability distribution of noise at Eskdalemuir.

The probability distribution for a single output having been determined, the outputs of the remaining 20 seismometers were approximately normalized to have the same r.m.s. value, equivalent to 2·8 nm. The probability distribution for the summed output was obtained as before, and also conformed closely to the normal distribution, with an increase of $n^{\frac{1}{2}}$ compared to the single output.

5·2. *Recognition of signal onset*

The ability to recognize the signal onset in the presence of noise of known statistics may only be expressed as a probability for a given signal amplitude. Various methods of combining the array outputs were investigated to determine which method gave the highest probability. The same normalized noise sample was used as for the experiment described in §5·1. A synthetic sinusoidal signal, consisting of a number of cycles of constant amplitude, was added to each output. This signal was repeated at random intervals and with a varying number of cycles. Three correlation methods were applied, namely:

(*a*) Cross correlate the summed outputs of lines A and B, $(\overline{\Sigma A \Sigma B})$.

(*b*) Sum the cross correlation integrals of 183 pairs (§2·3·3).

(*c*) Obtain the mean square value of the summed array, $(\overline{\Sigma A + \Sigma B})^2$.

About 100 bursts of signal were recorded for each of seven different signal amplitudes. The start of the signal was deduced in each case from the correlator records without reference to the signal channel. This was then compared to the actual signal onset, and the probability of picking first motion ascertained for each signal amplitude. This probability is shown as a function of signal/noise ratios σ_s/σ_n and $S_{\text{max.}}/N_{\text{max.}}$ by figure 23, where

$S_{\text{max.}}$ = peak signal amplitude from one seismometer

$N_{\text{max.}}$ = noise amplitude from one seismometer at a cumulative probability of 0·99.

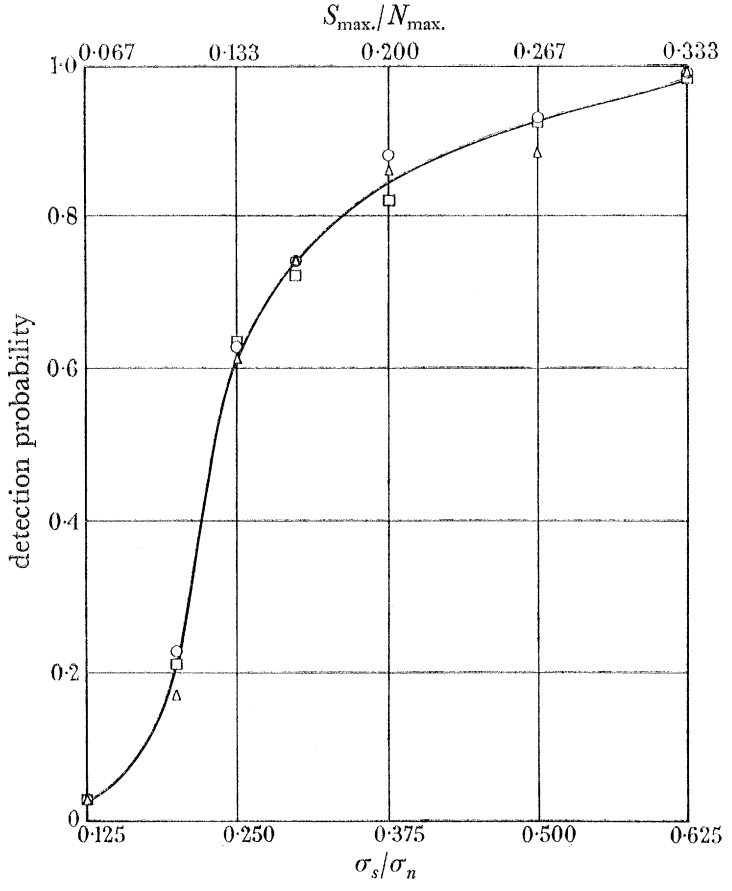

FIGURE 23. Probability of detecting first motion.
○, 183 Pairs; △, $\overline{\Sigma R \Sigma B}$; □, $\overline{(\Sigma R + \Sigma B)^2}$.

In comparing the correlation methods used it was found that spurious bursts of noise occurred which resulted in pulses of large amplitude in the correlator output for method (*c*). Nevertheless, these were not sufficient in number to cause any significant difference in detection probability, and similar results were obtained for all three correlator methods. Method (*a*) is preferred since it has improved azimuth and velocity discrimination for coherent signals. Another experiment, using two channels of narrow band frequency filtered noise, showed that the probability of detection from the summed trace was similar to that obtained for the correlation methods used separately. However, if both summed and correlator traces were used simultaneously, a small increase in probability was obtained. From the above, it is concluded that correlation methods do not increase the probability of detecting first motion significantly. Their advantage for random noise lies in the ability to detect signals having low signal/noise ratio and duration of many cycles.

5·3. *Velocity filtering of Gnome data*

The analysis of data recorded at Pole Mountain from the Gnome nuclear event demonstrates the advantages of velocity filtering. Nine seismometers were in operation, comprising six in the *red* line and four in the *blue* line, one seismometer being common. The azimuth of the signal relative to that of the *red* line was 22°. The records were processed by cross correlating the summed outputs of the two lines with an exponential window of 2 s time constant, for a velocity range of 2·0 to 14·0 km/s.

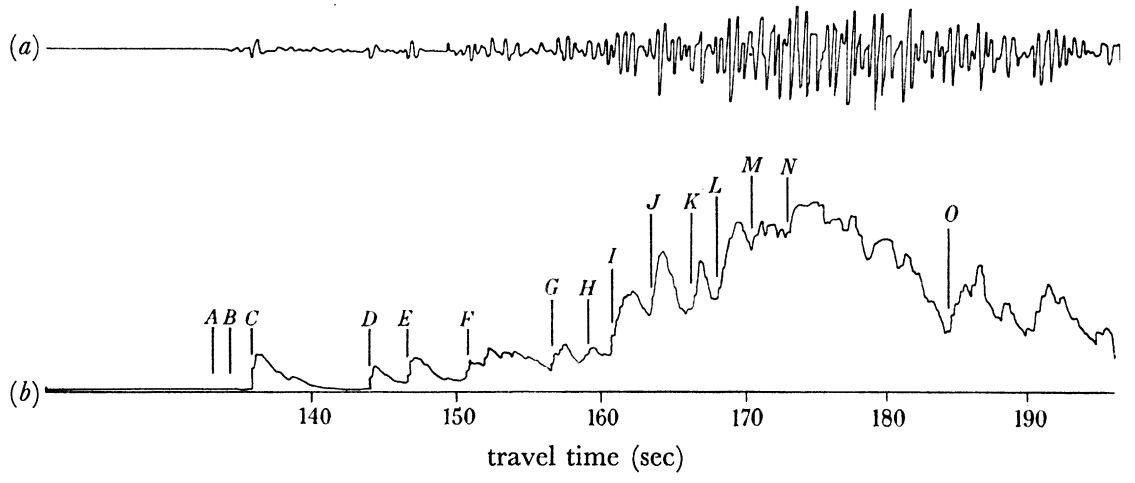

FIGURE 24. (*a*) Summed (ΣR) and (*b*) correlator output $(\overline{\Sigma R \Sigma B})^{\frac{1}{2}}$ for Gnome (*P* wave arrivals).

Figure 24 shows the first minute of the signal recorded by the Pole Mountain array, showing the summed and correlator output for a velocity of $7\frac{1}{4}$ km/s. Many abrupt changes in correlator output occur. It is considered that these correspond to onsets of new signal components. For each of these arrivals the difference in correlator output immediately before and immediately after the onset was measured and plotted as a function of velocity. The velocity of the new arrival was then determined from the peak of the differential correlation curve thus obtained. In this method, the effect of earlier arrivals on the velocity determination was minimized. It was found that most of the arrivals in the first part of the signal had a velocity of 7·0 to 8·0 km/s. Figure 25 shows the differential correlation curve for arrival *D*, which was the first with an apparent ground velocity of about 7 km/s. This was followed by other arrivals having increasingly higher velocities. Arrivals *D*, *E*, *F*, *G*, *J*, *N* and *O* appeared to be multiple reflexions from the same discontinuity, from their apparent ground velocities and times between successive onsets. For a single uniform layer such reflexions would be related by the expression

$$t_k^2 = (L^2 + 4k^2h^2)/V_p^2,$$

where

t_k = total travel time for k reflexions,

L = distance from shot point,

k = number of reflexions from lower discontinuity,

h = thickness of layer,

V_p = P wave velocity in layer.

A very good least squares fit was obtained for the first five arrivals under consideration, giving $h = 55{\cdot}4$ km and $V_p = 7{\cdot}0$ km/s. These reflexions were therefore deduced to be from the Mohorovičić discontinuity, although the depth calculated is greater than is generally accepted for this area, about 48 km (Steinhart & Meyer 1961). The last two arrivals considered did not fit the simple single layer model determined, but could be explained by

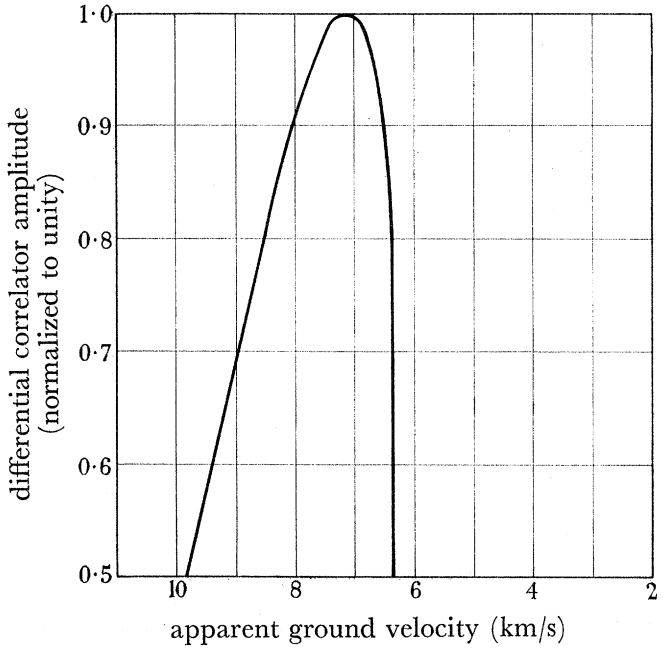

FIGURE 25. Correlation function for Gnome, arrival *D*.

TABLE 1. REFLEXIONS FROM MOHOROVIČIĆ DISCONTINUITY

arrival	number of reflexions	observed travel time (sec)	calculated travel time (sec)	observed apparent velocity (km/s)	calculated apparent velocity (km/s)
D	1	144·1	144·1	7·2	7·0
E	2	146·8	146·7	7·3	7·2
F	3	150·8	150·9	7·0	7·4
G	4	156·5	156·6	7·5	7·6
J	5	163·7	163·7	7·6	7·8
N	6	173·2	173·2	7·9	8·4
O	7	184·4	184·4	8·6	8·9

assuming a depression of about 5 km in the Mohorovičić discontinuity for a distance of about 80 km south of Pole Mountain. This appears to be possible from isostasy considerations. The agreement then obtained between the calculated and observed travel times, and also between the corresponding apparent ground velocities, is evident from table 1. In order to explain the amplitudes of the reflected arrivals it is necessary to assume that a low velocity layer exists near the surface. This is evident from the solutions to Zoeppritz equations obtained by McCamy, Meyer & Smith (1962). The amplitudes of the reflected arrivals for the model considered would be expected to decrease rapidly after the 6th or 7th reflexion. Thin low velocity layers having sufficient velocity contrast have been shown to exist at the shot point (Byerly, Stewart & Roller 1960). The arrival at *K* had an apparent ground velocity of 6·0 km/s and a travel time of 166·2 s. Assuming this arrival to be direct (*Pg*), it

had a mean velocity of 6·0 km/s. Attempts were made to derive a two-layer model to fit this arrival and the reflected arrivals. The general solution is given by Slotnick (1959) and involves the elimination of p in the following equations:

$$L/k = 2[h_1 p V_{P_1}/(1-p^2V_{P_1}^2)^{\frac{1}{2}} + h_2 p V_{P_2}/(1-p^2V_{P_2}^2)^{\frac{1}{2}}], \quad (22)$$

$$t_k/k = 2[h_1/V_{P_1}(1-p^2V_{P_1}^2)^{\frac{1}{2}} + h_2/V_{P_2}(1-p^2V_{P_2}^2)^{\frac{1}{2}}], \quad (23)$$

where t_k = total travel time for k reflexions,

L = distance from shot point,

k = number of reflexions from second discontinuity,

h_1, h_2 = thickness of first and second layers, respectively,

V_{P_1}, V_{P_2} = P wave velocity in first and second layers, respectively,

p = reciprocal of apparent ground velocity at recording site.

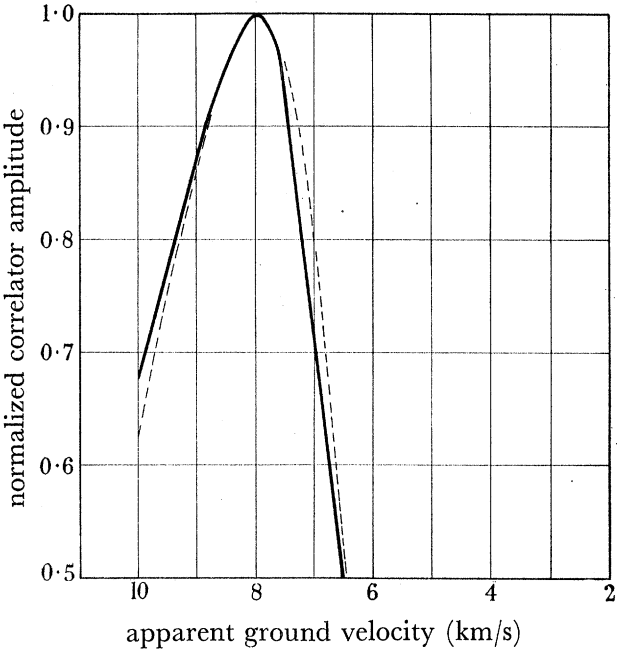

FIGURE 26. Correlation function for Gnome, arrival B. ——, Practical at 1·7 c/s; – – –, theoretical at 1·7 c/s for V_1 = 8 km/s.

The value of V_{P_1} was obtained from arrival K. The apparent ground velocity $1/P$ could not be obtained accurately from the values observed, since these could have been affected by local variations. The solution of equations (22) and (23) is difficult. Approximate manual solutions obtained show that the upper layer, if present, is very thin. In practice, the crust must be more complex than the simple models considered, and may contain velocity gradients. These would affect the calculated depth of the Mohorovičić discontinuity. Nevertheless, the results obtained strongly indicate that the arrivals concerned are in fact multiple reflexions from this discontinuity. If such reflexions could be reliably detected they would be of considerable assistance in the determination of mean crustal structure, since the crust is sampled at regular intervals.

The arrival at B had an apparent ground velocity of 8·0 km/s, and was assumed to be P_n. The correlation function at this time is shown by figure 26 and compares well with the

theoretical curve. The first motion was compressional, but had a very low amplitude (1·8 nm) compared with later parts of the signal (44 nm peak maximum). The mean velocity of P_n was deduced to be 7·9 km/s, assuming the model derived above. Arrival B was followed shortly afterwards by a strong arrival C, which had an apparent ground velocity of 8·5 km/s.

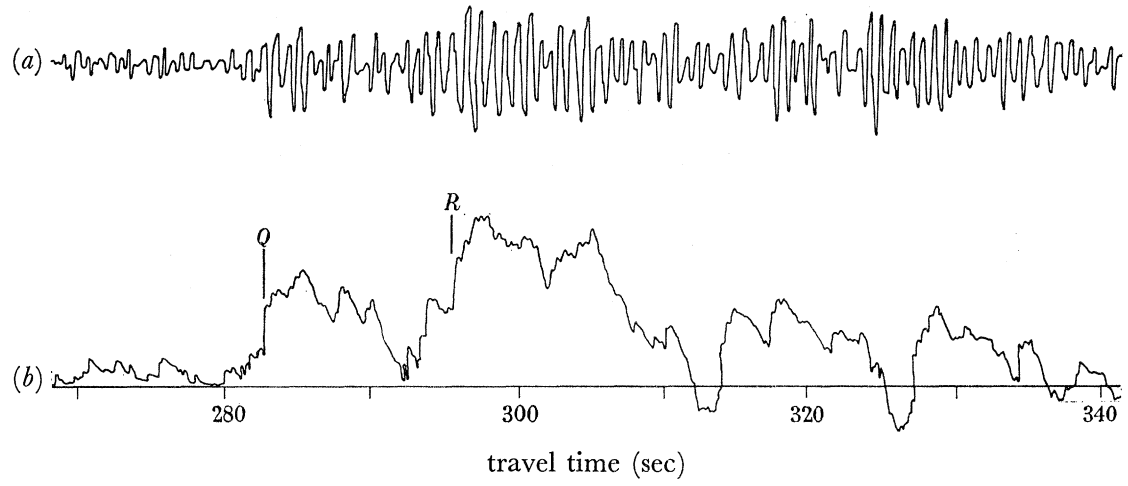

FIGURE 27. (*a*) Summed (ΣR) and (*b*) correlator outputs $(\overline{\Sigma R \Sigma B})^{\frac{1}{2}}$ for Gnome (shear wave arrivals).

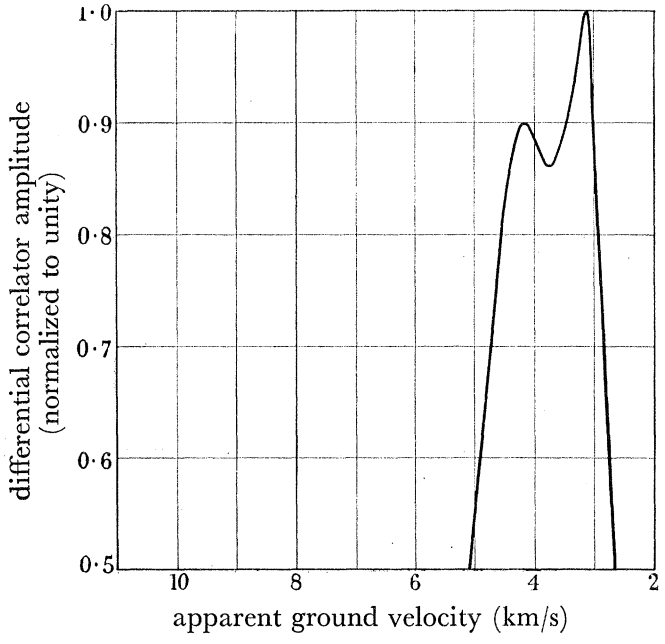

FIGURE 28. Correlation function for Gnome, arrival *R*.

In view of the large amplitude it is thought likely that this arrival was a reflexion from a deeper discontinuity. The depth of this discontinuity was deduced from the travel time of arrival C to be 133 km, assuming the velocity between the two discontinuities to be constant. The apparent ground velocity derived is in agreement with the value observed. On a few channels there were indications that arrival B was preceded by another complete cycle of very low amplitude (arrival A). This could be the head wave from the lower discontinuity. The travel time of A would require a velocity below the discontinuity of 8·5 km/s.

No explanation has been found for the arrivals at *I*, *L* and *M* to fit the apparent ground velocities. Many forms of mode converted signals have been considered, but none identified.

Figure 27 shows part of the record associated with the shear wave arrivals. The summed and correlator traces correspond to a velocity of $4\frac{1}{2}$ km/s. The traces are complex, and there are undoubtedly a number of components present. A longer seismometer period would have been desirable for recording shear waves at this distance. The first shear waves of large amplitude occur at *Q*. These have an apparent velocity of about $4\frac{1}{2}$ km/s, and appear to be related to the 7 km/s *P* wave arrivals. However, the onset is later than expected. It may be that earlier arrivals of this velocity are of low amplitude and are obscured by the remainder of the *P* wavetrain. A second main burst of energy starts at *R*. This has an apparent velocity and travel time compatible with L_g. The differential correlation function is shown by figure 28. A second peak occurs at $4\frac{1}{4}$ km/s, presumably due to the presence of another arrival. These and other arrivals are summarized in table 2.

TABLE 2. ARRIVALS OTHER THAN REFLEXIONS FROM MOHOROVIČIĆ DISCONTINUITY

arrival	observed travel time (sec)	mean velocity for model (km/s)	observed apparent velocity (km/s)	interpretation
A	133·6	—	9 approx.	head wave from 133 km discontinuity
B	134·2	7·9 below Moho.	8·0	P_n
C	136·1	—	8·5	reflexion from 133 km discontinuity
H	159·3	—	10·8	reflexion from 420 km discontinuity
I	161·0	—	7·0	unidentified *P*
K	166·2	6·0	6·0	P_g or Π_g
L	168·0	—	7·0	unidentified *P*
M	170·8	—	7·8	unidentified *P*
Q	282·8	3·6	4·5	unidentified *S*
R	295·8	3·4	3·2	L_g

Figure 29 shows the correlator output for the Gnome event as a function of time and velocity with variable area recording. While this record is not suitable for making accurate measurements, it presents the correlator output in a compact form and shows the general distribution of seismic energy as a function of time and velocity.

5·4. *Analysis of teleseismic events*

Teleseismic events at ranges of 30 to 90° have propagation paths which are relatively simple, since the paths of *P* waves lie mainly in the deep mantle. The angles of emergence to the vertical are 25 to 10°, for a crustal velocity of 6 km/s. Therefore the reflected energy from horizontal discontinuities within the crust will be relatively small, as shown by the Zoeppritz equations. The signal components are more coherent across the array compared to near events and are often well separated in time, as seen in table 3. There is therefore a greater possibility, between these ranges, of detecting differences in the character of the *P* signal arising from the nature of the source function, or from focal depth (Thirlaway 1963). Recent recordings of large underground nuclear explosions have demonstrated the existence of this 'source window'. Figure 30 shows the phased summed outputs of the Eskdalemuir,

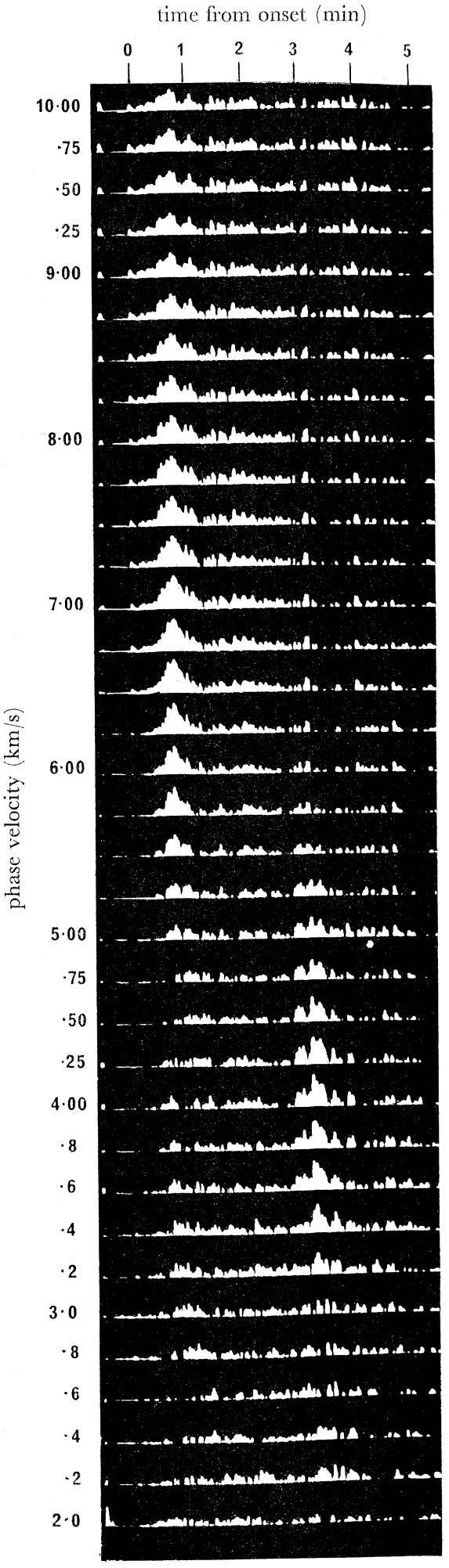

FIGURE 29. Variable area presentation of correlator output for Gnome.

Yellowknife and Pole Mountain arrays for the French underground nuclear test which took place in the Sahara on 18 March 1963. The ranges are respectively 32, 82 and 88°. Despite large range differences, and azimuth differences of about 40°, the three records are all characterized by a simple *P* pulse of a few cycles followed by a low amplitude tail or coda. This would be expected from a simple symmetrical source generating mainly compressional waves. In contrast to this simple signal, the recordings at Yellowknife of the signals from the explosions at the Nevada Test Site at a range of 25° are of very long duration. The change from complex to simple *P* wave signals occurs within a few degrees of range below 30°.

TABLE 3. TELESEISMIC SIGNAL COMPONENTS FOR SURFACE FOCUS EVENTS

range (degrees)	signal component (phase)	time from *P* onset min	time from *P* onset sec	apparent ground velocity (km/s)
30	*P*	0	0	12·5
60		0	0	16·2
90		0	0	23·8
30	*PP*	0	57·5	8·5
60		2	14·3	12·5
90		3	35·3	13·8
30	*PPP*	1	11·5	8·1
60		3	40·3	10·5
90		5	34·3	12·5
30	*PcP*	3	2·4	43·5
60		0	45·9	27·8
90		0	1·5	25·2
30	*S*	4	57·7	7·0
60		8	11·9	8·7
90		10	51·8	12·3
30	*PcS*, *ScP*	6	44·6	34
60		4	46·7	25
90		—		—

Figure 31 shows recordings at the three array sites for an earthquake near Barce, Libya, which occurred on 21 February 1963. The depth given by the U.S. Coast and Geodetic Survey was 33 km. The signals are more complex than for the Sahara explosion, and differ considerably in character at the three stations. From the evidence of the explosion records it must be supposed that the observed complexity is source-generated and that the contribution of the transmission path is negligible. Such records are consistent with an asymmetrical source within the crust, generating both *P* and *S* waves at source.

Not all earthquakes give complex *P* wavetrains. Most of those which give simple seismograms have a considerable focal depth. A few occur which have a shallow calculated focal depth. An analysis of about 100 earthquakes reported to have a shallow focal depth showed about 5 % to be simple. In view of the errors often incurred in the measurement of focal depth it is by no means certain that there are, in fact, any shallow focus earthquakes which result in simple seismograms. Furthermore, a suggestion that the percentage of simple seismograms increases with decreasing magnitude was disproved by analysing 30 earthquakes, recorded at Yellowknife, with magnitudes of *m*3·4 to *m*4.

The terms 'simple' and 'complex' are relative, and an objective test for the degree of simplicity is necessary. One such test is to measure the ratio between the correlated energy in the first 6 s of the recorded *P* wave to that of the succeeding 30 s. This method requires the exclusion of interfering signals, including signal generated noise, by azimuth and velocity

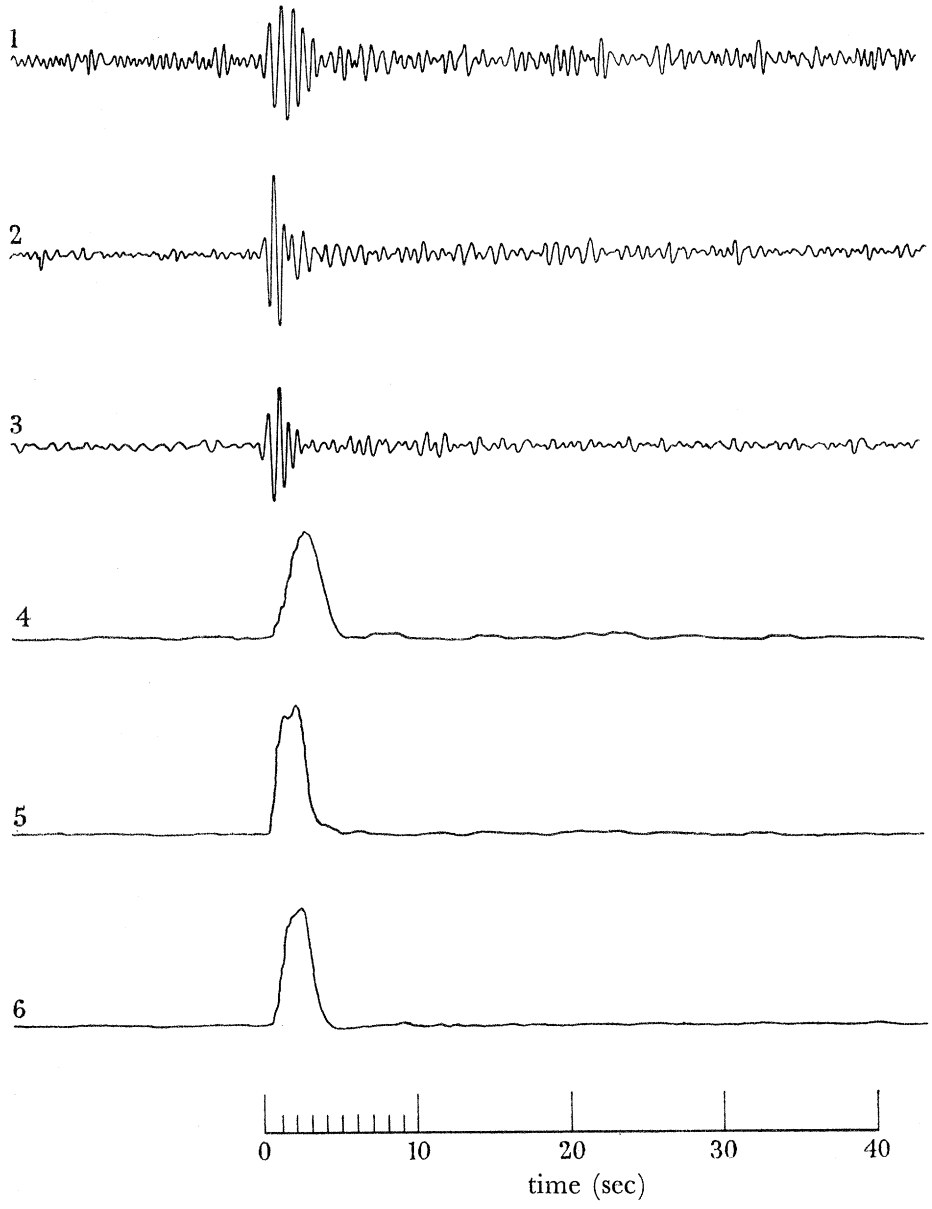

FIGURE 30. Sahara event (18 March 1963). U.S.C.G.S. data: co-ordinates 24·1° N., 05·0° E., H 10·02. 00·8 G.M.T.; depth 0 km. Filter 1 to 2 c/s. Curve 1, Pole Mountain summed array, range 88°; 2, Yellowknife summed array, range 82°; 3, Eskdalemuir summed array, range 32°; 4, Pole Mountain correlator output $\overline{\Sigma R\,\Sigma B}$, 2 s square window; 5, Yellowknife correlator output $\overline{\Sigma R\,\Sigma B}$, 2 s square window; 6, Eskdalemuir correlator output $\overline{\Sigma R\,\Sigma B}$, 2 s square window.

filtering. Figure 32 shows the outputs of individual seismometers of the Eskdalemuir array for the same French underground nuclear test. The signals differ appreciably, and are more extended than the summed signal shown in figure 30, owing to the presence of signal-generated noise.

Although the signal components of teleseismic events are generally more separated in time than for near events, it is nevertheless, useful to be able to measure their apparent ground velocities. This is particularly true when there are interfering signal components, or when doubt exists as to the identity of a particular signal component. An example of the use of velocity filtering at teleseismic distances is shown in figure 33 for a Fox Island earthquake recorded at Yellowknife on 7 April 1964 ($h = 200$ km). It was originally thought

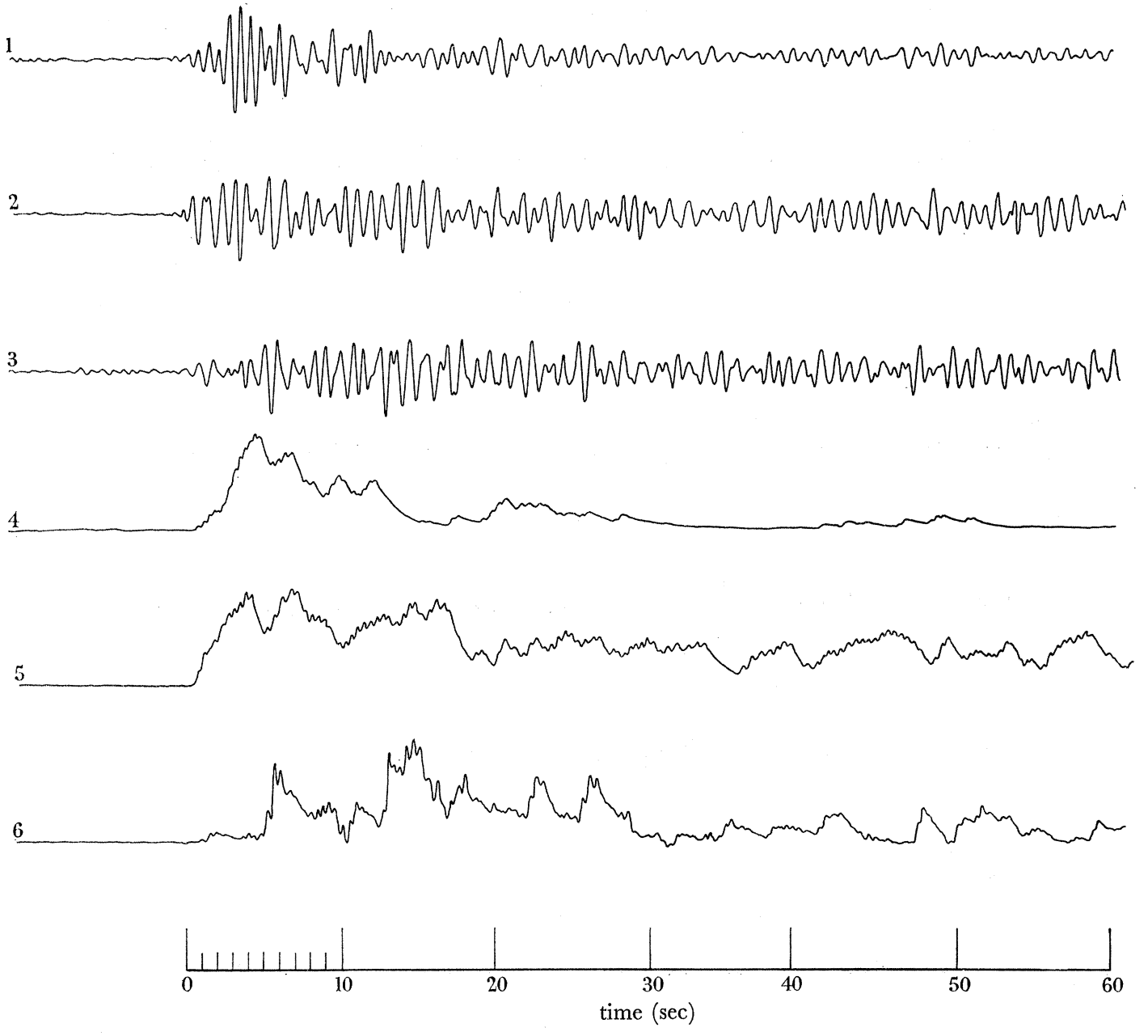

FIGURE 31. Barce earthquake (21 February 1963). U.S.C.G.S. data: co-ordinates 32·7° N., 20·9° E., H 17.14.35·7 G.M.T.; depth 33 km. Filter 1 to 2 c/s. Curve 1, Pole Mountain summed array, range 91·3°; 2, Yellowknife summed array, range 78·6°; 3, Eskdalemuir summed array, range 28·2°; 4, Pole Mountain correlator output $\overline{\Sigma R\,\Sigma B}$, $1\frac{1}{2}$ s exponential window; 5, Yellowknife correlator output $\overline{\Sigma R\,\Sigma B}$, $1\frac{1}{2}$ s exponential window; 6, Eskdalemuir correlator output $\overline{\Sigma R\,\Sigma B}$, $1\frac{1}{2}$ s exponential window.

that the simple impulsive signal which occurred at *A* on the single seismogram was an interfering signal from another source. This was because the arrival time did not fit that of *PcP*, although the later signal component at *B* fitted *ScP*. A velocity run was made on the data and this showed conclusively that the two later signal components were both core phases, having the same azimuth as the *P* signal and apparent ground velocities of about 40 km/s.

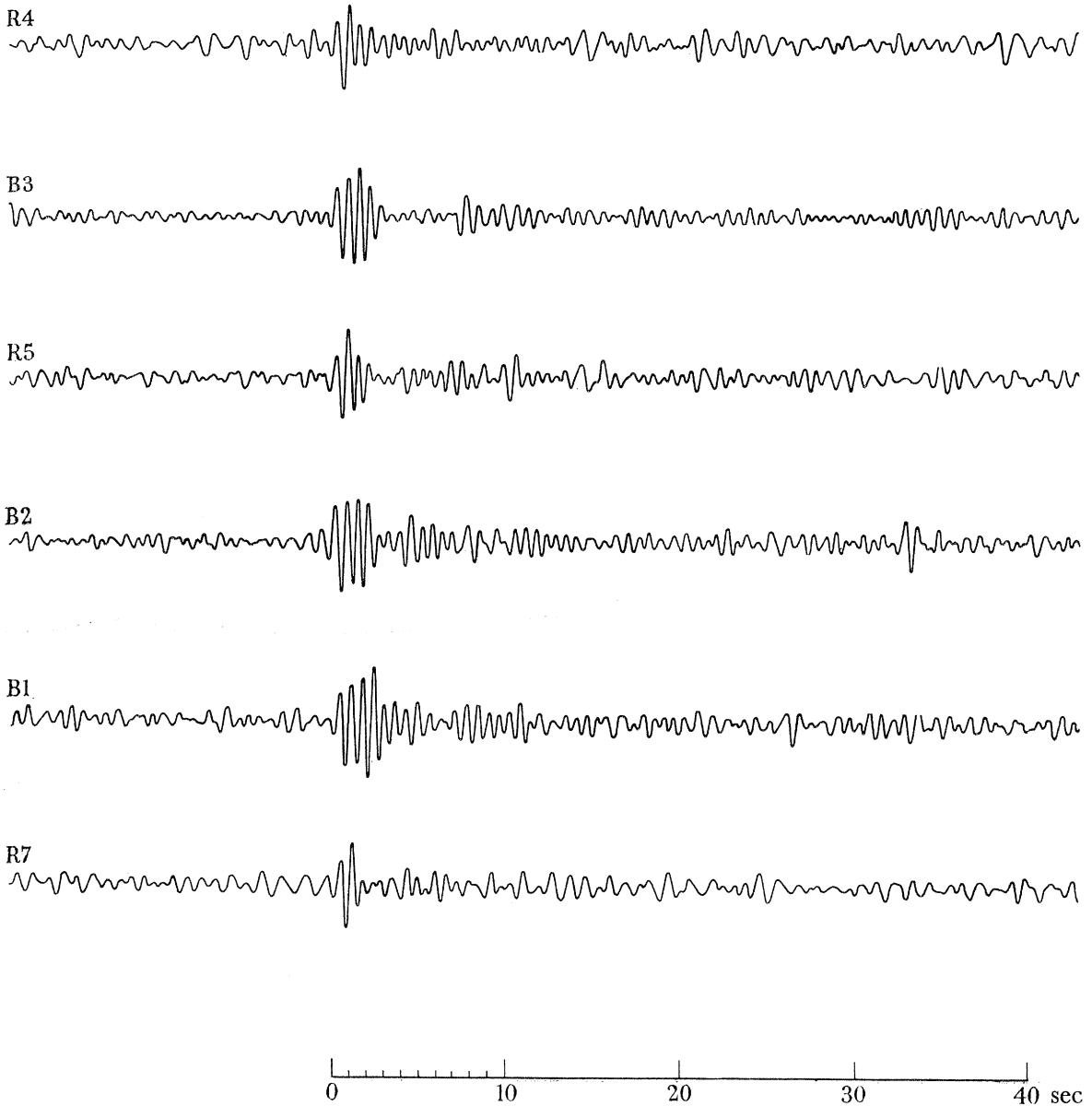

FIGURE 32. Sahara event; individual seismometer outputs of Eskdalemuir array.

The first of these core phases was then identified as *pPcP*. This is further evidence that the radiation pattern of earthquake sources is commonly asymmetrical. In this particular example the fault must have been orientated so that a high *S*/*P* ratio developed in the direction of the core, and a high *P*/*S* ratio towards the surface. Also, despite the complex main *P* arrival, the simplicity of the core phases shows that the source function was a single stress release. When the apparent signal wavelength is much larger than the size of the array,

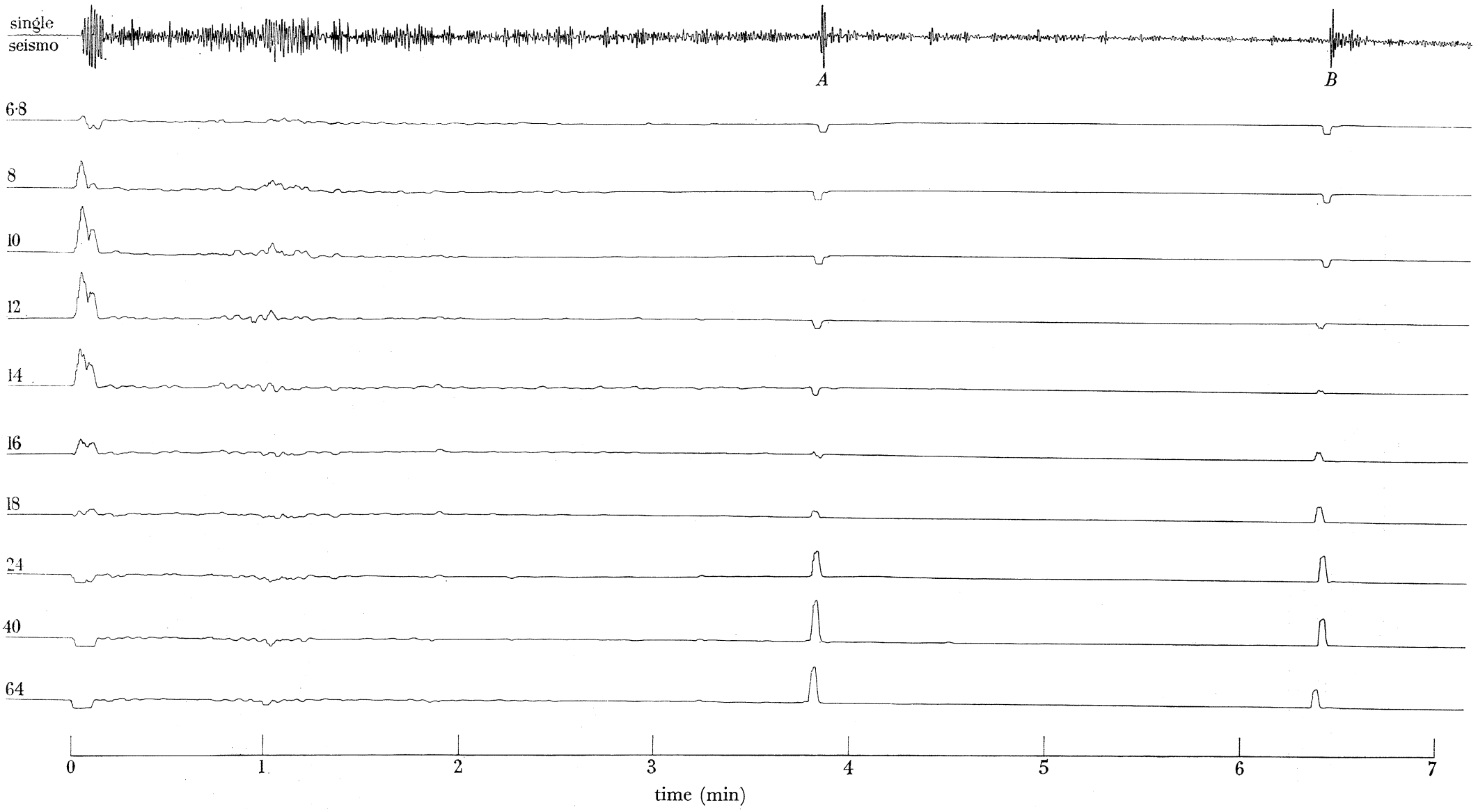

FIGURE 33. Fox Island earthquake (7 April 1963). U.S.C.G.S. data: co-ordinates 53·7° N., 170·1° W., H 15.28.01·8 G.M.T.; depth 202 km; magnitude $m6$; range 29·7°. Filter 1 to 2 c/s. Single seismometer output, and correlator output $\overline{\Sigma R\,\Sigma B}$. 2 s square window (7 seismometers), for range of velocity.

the array outputs can be summed and correlated without phasing to give a useful signal/noise improvement. Figure 34 shows how this method was applied to the detection of *PcP* at Eskdalemuir for the Sahara event.

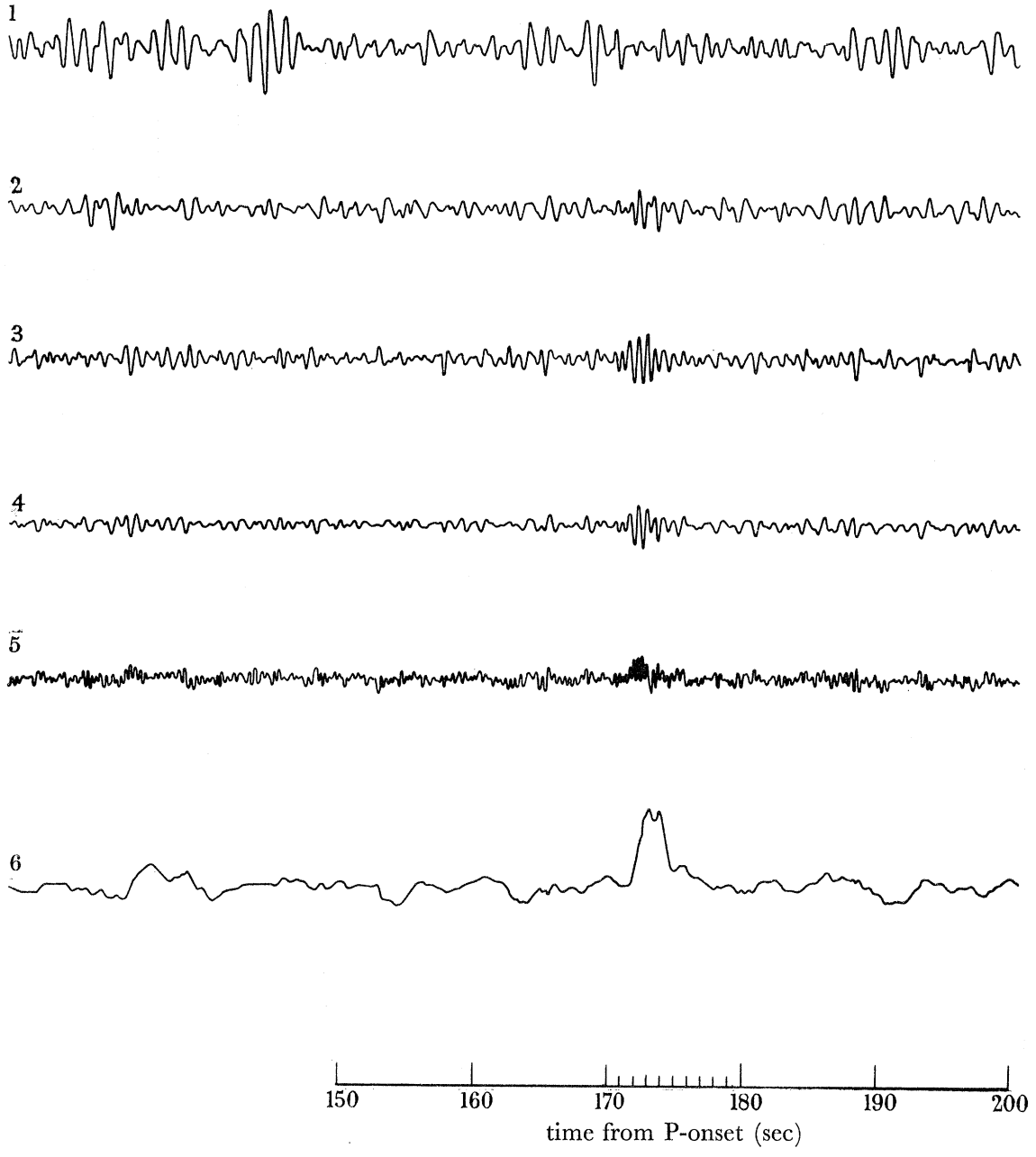

FIGURE 34. Sahara event; detection of *PcP* at Eskdalemuir. Curve 1, single seismometer; 2, summed blue line, ΣB; 3, summed red line, ΣR; 4, summed array, $\Sigma B + \Sigma R$; 5, $\Sigma R \Sigma B$; 6, correlator output, $\overline{\Sigma B \Sigma R}$, 2 s square window.

6. CONCLUSIONS

The analysis of seismic body waves, with the use of phased arrays, has enabled significantly more information to be obtained than would have been possible with a single seismometer or three component set. It has been shown that an array may be used as a velocity and azimuth filter to improve signal recognition in the presence of microseisms and unwanted

signal components. The velocity and onset times of individual signal components have been ascertained, using correlation techniques, and this information used for the determination of crustal structure. Analysis of the array data recorded at Pole Mountain, Wyoming, from the Gnome nuclear explosion, enabled a large number of signal components to be identified. These included at least five components which had undergone one or more reflexions from the Mohorovičić discontinuity. From this analysis, the crustal structure between Carlsbad and Pole Mountain was deduced.

Seismograms recorded at ranges of less than 25° are so complex that little information can be deduced concerning the nature of the source. However, analysis of array data from explosions has shown that the effect of the propagation path at ranges of 30 to 90° is small. The analysis of *P* wave array data at these ranges therefore provides maximum information on source functions. The results from explosions are in agreement with a simple, symmetrical impulsive source function. Nearly all earthquakes at these ranges had more complex *P* signals, which differed in character between array sites, indicating asymmetric source functions.

A large number of events are detected each day at very quiet sites such as Yellowknife. Velocity and azimuth filtering is useful in separating and identifying the signal components from these events, many of which have apparent wavelengths of at least 20 km. In order to provide adequate resolution, arrays of comparable dimensions are necessary. At ranges of 30 to 50° identification of reflections from the core is particularly easy because of their high apparent velocity.

The total noise power obtained by summing the normalized noise outputs from the Eskdalemuir array was found to be approximately equal to the sum of the individual noise powers. This is consistent with random noise or wideband isotropic coherent noise, and yields an improvement in signal/noise amplitude ratio for coherent signals equal to the square root of the number of seismometers. It has been shown theoretically that, for random noise, the optimum improvement is obtained when the seismometer outputs are weighted in proportion to their signal/noise power ratios, after normalizing for equal signal amplitude. Greater improvements are possible for sites where noise is coherent and anisotropic, or narrow band, coherent and isotropic, as shown by the contoured responses. There is then an advantage, for linear cross arrays, in weighting the seismometer outputs in accordance with the Tchebyscheff polynomials.

Theoretical sum squared and correlator responses for coherent components have been given as a function of azimuth and normalized wave number D/λ for several array configurations. These show that correlation techniques are essential for obtaining a satisfactory directivity response in the case of arrays comprising two lines of seismometers. This is not so for the circular and cluster configurations considered. The main advantage of cross correlating the two summed groups in these cases, compared with averaging the sum squared response, lies in the ability to discriminate against bursts of noise which are not coherent across the whole array. This is particularly important in the case of automatically triggered recorders which operate above a preset threshold. Of the array configurations and processing methods considered, the widest rejection band in terms of D/λ was obtained for the correlator output of the L-shaped array. The sum squared response for the circular array has a wider rejection band than that of the cluster. Either of these arrays is suitable

for the rejection of stationary, coherent isotropic noise. In the case of a teleseismic array, the signal wavelengths are often much higher than the noise wavelengths, and cluster or circular arrays of small dimensions may be summed without delays to give good signal/noise improvement. Such arrays do not give any velocity or azimuth information, and should be used as subarrays of a larger pattern.

Simple on-line correlators are in operation and enable high quality edited paper and magnetic tape records of distant events to be produced automatically at source. This considerably reduces the burden on the central analysis facility. A more comprehensive data analyser is under construction, capable of working on-line and of giving velocity and azimuth information. However, this system is complex, and simplified on-line systems for azimuth/velocity search are being investigated.

The work described in this paper was performed by numerous planning, engineering and scientific staff directly or indirectly employed by the Atomic Weapons Research Establishment. The authors particularly wish to acknowledge the overall direction of the project by Mr I. Maddock (Chief of Applied Physics), and the advice of Dr H. I. S. Thirlaway, in charge of the seismological group of A.W.R.E. The authors are indebted to Dr H. Hulme for the symmetrical solution given in appendix A, and wish to acknowledge the significant contributions of the following staff:

J. R. Truscott, K. G. Beauchamp, W. Hutchins and J. Fyson (Instrumentation design).

E. Yeo, J. Milne and F. Ridsdale (Planning and Engineering).

D. C. Platt and W. Mowat (System Design and Station Management).

References

Agger, H. E. & Carpenter, E. W. 1964 *Geophys. J.R. Astr. Soc.* **9**, no. 1, 69–93.

Bendat, J. S. 1958 *Principles and applications of random noise theory.* London: Chapman and Hall Ltd. p. 57.

Byerly, P. E. Stewart, S. W. & Roller, J. C. 1960 U.S.G.S. Rep. no. TE 1-761.

Dolph, C. L. 1946 *Proc. Inst. Radio Engrs,* **34**, 335–348.

Frantti, G. E., Willis, D. E. & Wilson, J. T. 1962 *Bull. Seism. Soc. Amer.* **52**, 113–121.

Jacobson, M. J. 1957 *J. Acoust. Soc. Amer.* **29**, 1342–1347.

Kraus, J. D. 1950 *Antennas.* New York: McGraw-Hill Book Co. Inc.

McCamy, K., Meyer, R. P. & Smith, T. J. 1962 *Bull. Seism. Soc. Amer.* **52**, 923–955.

Romney, C. 1959 *J. Geophys. Res.* **64**, 1489.

Slotnick, M. M. 1959 *Lessons in seismic computing.* Wisconsin: S.E.G. Publication.

Steinhart, J. S. & Meyer, R. P. 1961 Explosion studies of continental structure. Publ. no. 622. Carneg. Instn.

Symposium on Sonar Systems 1962 Univ. Birmingham.

Thirlaway, H. I. S. 1963 *New scientist,* **18**, no. 338, 311–316.

Truscott, J. R. 1964 *Geophys. J. R. Astr. Soc.* **9**, no. 1, 59–68,

Tullos, F. N. & Cummings, L. C. 1961 *Geophys.* **26**, 298–308.

Wainstein, L. A. & Zubakov, V. D. 1962 *Extraction of signals from noise.* New Jersey: Prentice-Hall Inc.

Willmore, P. L. 1962 *Nature, Lond.* **195**, 1250–1252.

Appendix A. Optimum seismometer weighting for discrimination against random noise

It is assumed that the noise has a zero mean, and that there is no coherence between seismometer outputs. The mean square value of the noise output of the jth seismometer is therefore equal to its variance σ_{nj}^2. It is further assumed that the signals are coherent and in phase. The signal/noise power ratio of the jth seismometer is $\sigma_{sj}^2/\sigma_{nj}^2$. The requirement is to maximize the signal/noise ratio of the summed array.

Let the output of the jth seismometer be multiplied by a constant b_j. Then the signal/noise power output of the summed array of n seismometers is given by

$$Q = \frac{\sigma_{s0}^2}{\sigma_{n0}^2} = \left(\sum_{j=1}^{n} b_j \sigma_{sj}\right)^2 \Big/ \sum_{j=1}^{n} b_j^2 \sigma_{nj}^2, \tag{A1}$$

$$\frac{\partial Q}{\partial b_j} = \left[2\sigma_{sj}\left(\sum_{j=1}^{n} b_j \sigma_{sj}\right)\left(\sum_{j=1}^{n} b_j^2 \sigma_{nj}^2\right) - 2b_j \sigma_{nj}^2 \left(\sum_{j=1}^{n} b_j \sigma_{sj}\right)^2\right] \Big/ \left(\sum_{j=1}^{n} b_j^2 \sigma_{nj}^2\right)^2.$$

Equating to zero to find the maximum value of Q and simplifying, we have

$$\frac{b_j \sigma_{nj}^2}{\sigma_{sj}} = \left(\sum_{j=1}^{n} b_j^2 \sigma_{nj}^2\right) \Big/ \left(\sum_{j=1}^{n} b_j \sigma_{sj}\right). \tag{A2}$$

The right-hand side of equation (A2) is independent of the particular j on the left-hand side of the equation. Thus

$$b_j = k_1 \sigma_{sj}/\sigma_{nj}^2, \tag{A3}$$

where k_1 is a constant.

Equation (A3) gives the relative seismometer weighting; the absolute values are unimportant since all outputs can be multiplied by a common factor without affecting the value of Q (equation (A1)).

Substituting for b_j in equation (A1) we have

$$\begin{aligned} Q &= \left(\sum_{j=1}^{n} k_1 \sigma_{sj}^2/\sigma_{nj}^2\right)^2 \Big/ \left(\sum_{j=1}^{n} k_1^2 \sigma_{sj}^2/\sigma_{nj}^2\right) \\ &= \sum_{j=1}^{n} (\sigma_{sj}^2/\sigma_{nj}^2). \end{aligned} \tag{A4}$$

Thus, for optimum weighting, given by equation (A3), the signal/noise power ratio of the summed output is equal to the sum of the individual signal/noise power ratios.

Appendix B. The theoretical response of linear cross arrays

B. 1. *The summed response of uniform line arrays*

The normalized amplitude response for sinusoidal signals for a summed line array A (figure 2(d)) consisting of m equally spaced detectors of identical sensitivity is given by Kraus (1950)

$$E_A = \frac{\sin\left(\frac{1}{2}m\Delta_A\right)}{m \sin\left(\frac{1}{2}\Delta_A\right)}. \tag{B1}$$

Similarly for line B

$$E_B = \frac{\sin\left[\frac{1}{2}(n-m)\,\Delta_B\right]}{(n-m)\sin\left(\frac{1}{2}\Delta_B\right)}. \tag{B2}$$

The response curve for 10 seismometers as a function of $\Delta/2\pi$ is given by figure B1. The first null occurs when

$$\Delta/2\pi = \tfrac{1}{10}.$$

In general, nulls occur in lines A and B when

$$\Delta_A/2\pi = q/m, \quad \Delta_B/2\pi = r/(n-m),$$

where q and r are any integers. If the delay inserted is zero, then

$$\Delta_A = 2\pi(d/\lambda)\cos\theta, \quad \Delta_B = 2\pi(d/\lambda)\sin\theta.$$

The first nulls therefore occur in line A when

$$md = \lambda/\cos\theta. \tag{B3}$$

Similarly for line B

$$(n-m)\,d = \lambda/\sin\theta. \tag{B4}$$

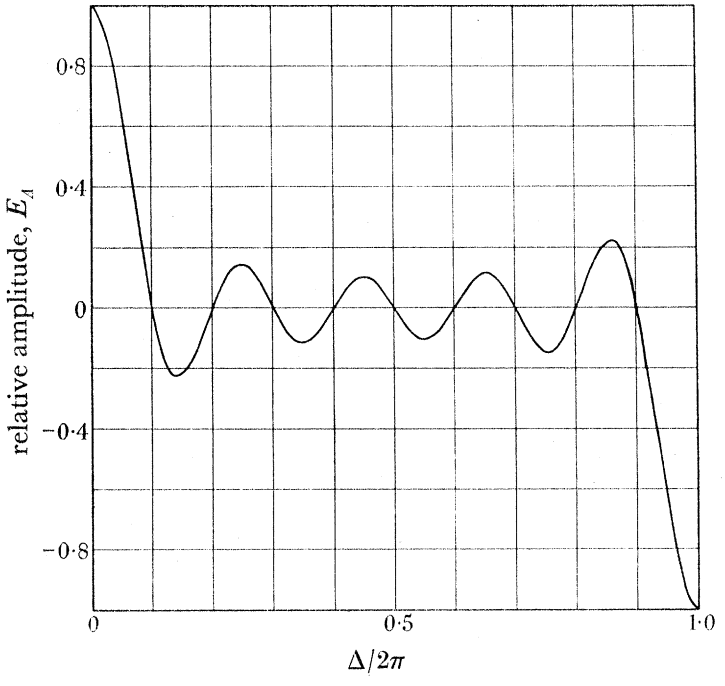

FIGURE B1. Summed response of 10 element line array, equal sensitivity.

Equations (B3) and (B4) show that, for uniform in-line arrays summed without inserting delays, the total effective lengths md, $(n-m)\,d$ must be at least equal to the wavelength of the coherent signal or noise component for total rejection. The length required for line A increases to $1{\cdot}4\lambda$ at $\theta = \frac{1}{4}\pi$, and to infinity at $\theta = \frac{1}{2}\pi$. Referring to figure B1, there are 9 equally spaced nulls between $\Delta/2\pi = 0$ and $\Delta/2\pi = 1$. In general there are $m-1$ and $n-m-1$ equally spaced nulls for lines A and B, respectively. At $\Delta/2\pi = 1$, there is a complete wavelength between adjacent seismometers, and the relative response rises to unity. The whole pattern is repeated between successive integral values of $\Delta/2\pi$. In practice, it is unlikely that the signal will be of a sufficient number of cycles relative to m for the curves to apply beyond $\Delta/2\pi = 1$, and even at this value the response is very dependent upon tolerances of seismometer position.

For high values of m, and for $\frac{1}{2}\Delta_A \ll \pi$, equation (B1) may be written

$$E_A \simeq \frac{\sin(\frac{1}{2}m\Delta_A)}{\frac{1}{2}m\Delta_A}. \tag{B5}$$

Figure B2 shows the response plotted as a function of $m\Delta_A/2\pi$, and represents the limiting case for an infinite number of detectors. Comparing this with figure B1, it can be seen that the amplitudes of the first peaks are virtually the same. The effect of increasing the value of m is to increase the width of the rejection band. Coherent noise having a flat spectrum extending from $\Delta_A/2\pi = 0$ to $\Delta_A/2\pi = 1$ is rejected by the power ratio m, which is the same as for random noise.

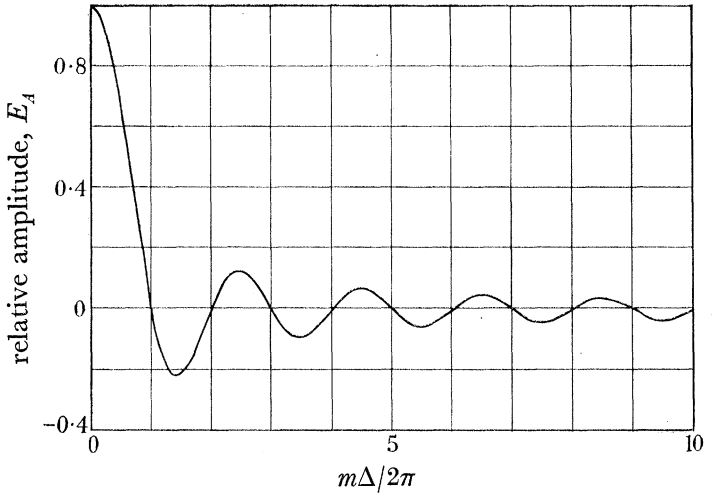

FIGURE B2. Summed response of continuous line array.

In deriving the response for the total summed array, the phase difference $(\gamma_A - \gamma_B)$ between the centre points must be taken into account. It is readily shown that the total normalized amplitude squared response of the summed array is given by

$$E_n^2 = \tfrac{1}{4}[E_A^2 + E_B^2 + 2E_A E_B \cos(\gamma_A - \gamma_B)], \tag{B6}$$

where $(\gamma_A - \gamma_B) = (D_A\Delta_A - D_B\Delta_B)/d$.

For a symmetrical cross array, $D_A = D_B = 0$, and hence

$$E_n^2 = \tfrac{1}{4}(E_A + E_B)^2. \tag{B7}$$

If the array is tuned to receive a signal of velocity V_1 and azimuth θ_1, and receives a signal of velocity V, azimuth θ, there will be phase differences between adjacent seismometers in lines A and B given by

$$\Delta_A = 2\pi fd\left(\frac{\cos\theta}{V} - \frac{\cos\theta_1}{V_1}\right), \tag{B8}$$

$$\Delta_B = 2\pi fd\left(\frac{\sin\theta}{V} - \frac{\sin\theta_1}{V_1}\right). \tag{B9}$$

The frequency f corresponds to the actual signal (V, θ). Normally, this signal will cover a band of frequency and the output may be obtained as a function of frequency from the product of E_n^2 and the power spectrum.

B. 2. *Amplitude weighted line arrays*

It will be seen from figure B1 that secondary peaks of unequal amplitude occur in the rejection band. The first of these peaks has a maximum amplitude of 0·22, although the summed signal has a phase shift of 180° with respect to the incident signal at the centre of the array. The signal corresponding to the next peak is in phase, and has a maximum relative amplitude of 0·13. The amplitude of the subsidiary peaks can in theory be equalized and adjusted to any desired value by weighting the seismometer outputs. This method results in the nulls occurring at non-uniform increments of $\Delta/2\pi$. However, it minimizes the width of the primary peak for a given maximum subsidiary peak level.

The method of doing this was originally proposed by Dolph (1946), and involves equating the coefficients of the Tchebyscheff polynomial of degree $m-1$ to those of the polynomial representing the array response.

For a ten element array the ninth order Tchebyscheff polynomial required is given by

$$T_9(x) = 256x^9 - 576x^7 + 432x^5 - 120x^3 + 9x. \tag{B10}$$

In order to arrange the expression for the response of the array in a similar form it is necessary to sum the seismometers in pairs, and expand the resultant expression in terms of $\cos\frac{1}{2}\Delta$. The sum of the first and tenth seismometer relative to the centre of the array is equal to $2\cos\frac{9}{2}\Delta$. The expression is given by the 9th order Tchebyscheff polynomial $T_9(y)$, where $y = \cos\frac{1}{2}\Delta$. The combined response is therefore

$$E_{10}(y) = c_1T_1(y) + c_2T_3(y) + c_3T_5(y) + c_4T_7(y) + c_5T_9(y), \tag{B11}$$

where c_1 to c_5 are coefficients which determine the relative sensitivities of the seismometers. Before equating the two polynomials it is necessary to relate y to x. Putting $y = x/x_0$ we have

$$E_{10}(x) = c_1T_1\left(\frac{x}{x_0}\right) + c_2T_3\left(\frac{x}{x_0}\right) + c_3T_5\left(\frac{x}{x_0}\right) + c_4T_7\left(\frac{x}{x_0}\right) + c_5T_9\left(\frac{x}{x_0}\right). \tag{B12}$$

The value of x_0 governs the ratio R between the maximum primary and subsidiary peak levels, and may be obtained by substituting R for $T_9(x)$ in equation (B10). A more straightforward solution for x_0 is given by

$$x_0 = \tfrac{1}{2}[(R + (R^2-1)^{\frac{1}{2}})^{1/(m-1)} + (R - (R^2-1)^{\frac{1}{2}})^{1/(m-1)}]. \tag{B13}$$

For $R > 1$, the value of x_0 is always greater than unity. The polynomial $E_{10}(x)$ given by equation (B12) may now be determined for a given value of R, and the coefficients c_1 to c_5 determined by equating $T_9(x)$ to $E_{10}(x)$. Figure B3 shows the relative seismometer sensitivity as a function of position and value of R for a 10 element array. It is clear from this that the sensitivities are most nearly uniform for values of R between 5 and 10. For higher ratios, the sensitivities of the central seismometers are very high in comparison to those near the ends of the array. This is very undesirable, since it would accentuate any imperfections in signal waveform at these positions. Furthermore, it would reduce the discrimination against random noise. A rejection ratio of 10 is a practical limit for a ten element array. The response for this condition is given by equation (B10), substituting $x = x_0\cos\frac{1}{2}\Delta$

and is shown by figure B4. It can be seen that the width of the primary peak is slightly greater than that in figure B1, but that the amplitude of the first subsidiary peak has been more than halved.

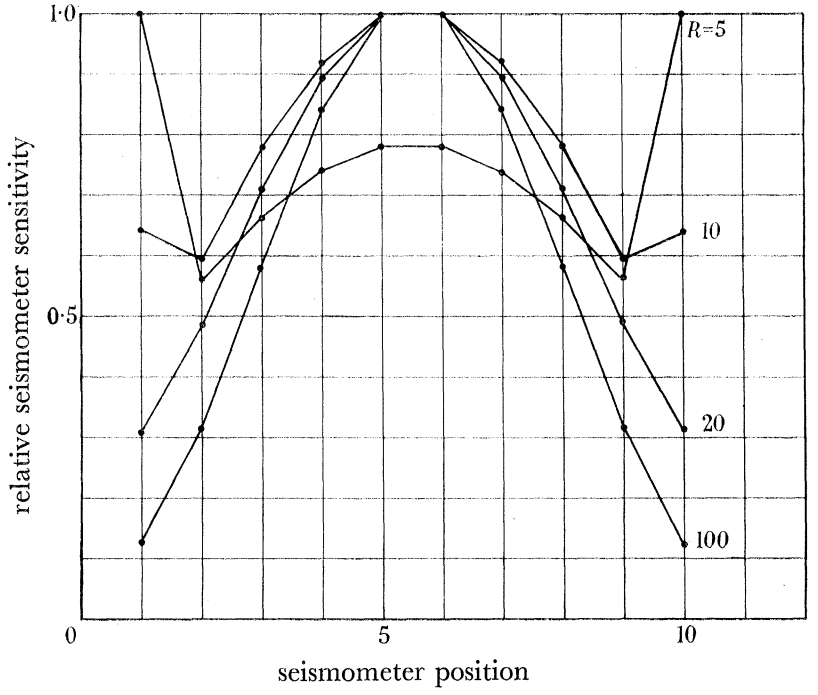

FIGURE B3. Relative seismometer sensitivity for Dolph–Tchebyscheff optimum weighting (10 seismometers).

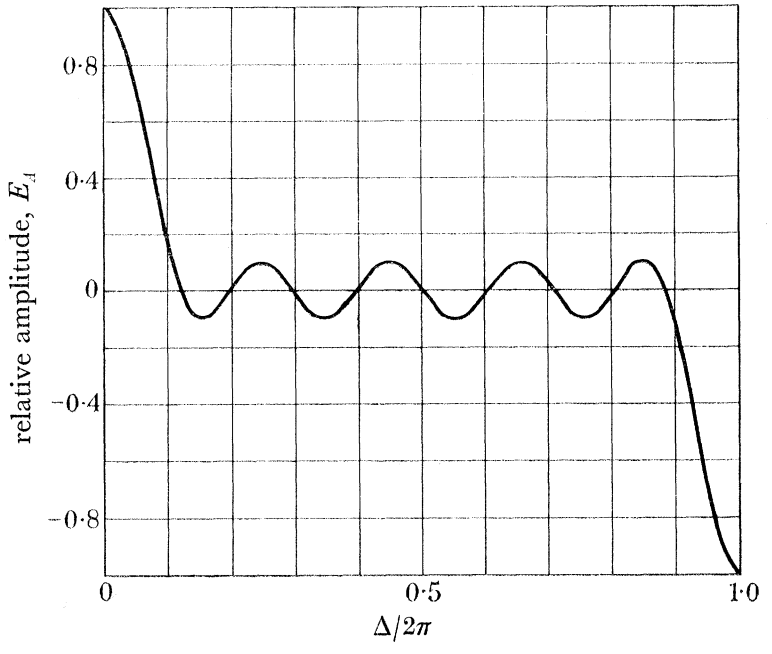

FIGURE B4. Summed response of 10 element line array, Dolph–Tchebyscheff weighting ($R = 10$).

B. 3. *Cross correlation of summed outputs of two uniform line arrays at right angles*

The normalized cross correlation response for a square window of integration T_1 is given by

$$2\varphi_{AB} = \frac{2}{T_1}\int_{t_1-T_1}^{t_1} E_A E_B \cos\omega t \cos(\omega t+\gamma_A-\gamma_B)\,\mathrm{d}t$$

$$= E_A E_B {}_{t_1-T_1}^{t_1}[\sin(2\omega t+\gamma_A-\gamma_B)]/2\omega T_1 + E_A E_B \cos(\gamma_A-\gamma_B).$$

The first term is oscillatory, and its amplitude diminishes as T_1 is increased. For $\omega T_1 \gg 1$, we have

$$2\varphi_{AB} \simeq E_A E_B \cos(\gamma_A-\gamma_B). \tag{B14}$$

This approximation does not hold when $(\gamma_A-\gamma_B)$ is close to $\frac{1}{2}(2r-1)\,\pi$, where r is any integer. However, the value of φ_{AB} is very small under these conditions.

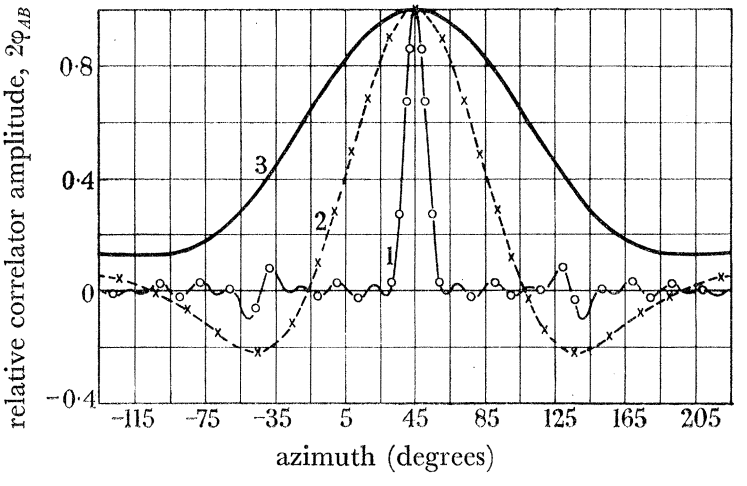

FIGURE B5. Correlator azimuth response for symmetrical cross array. $\theta_1 = \frac{1}{4}\pi$; $m = n-m = 10$; $V = V_1$; $D_A = D_B = 0$. Curve 1, $d/\lambda_1 = \frac{1}{2}$; 2, $d/\lambda_1 = \frac{1}{10}$; 3, $d/\lambda_1 = \frac{1}{20}$.

From equation (B14) it is seen that the correlator output is reduced by three factors for unwanted signals. These are the individual responses of the two lines, and the cosine of the phase difference between the centre points of the two lines. Expanding equation (B14) gives

$$2\varphi_{AB} = \frac{\sin(\frac{1}{2}m\Delta_A)}{m\sin(\frac{1}{2}\Delta_A)}\,\frac{\sin[\frac{1}{2}(n-m)\,\Delta_B]}{(n-m)\sin(\frac{1}{2}\Delta_B)}\cos[(D_A\Delta_A - D_B\Delta_B)/d]. \tag{B15}$$

B. 4. *Azimuth filtering or determination*

The method of applying the contour diagrams for determining azimuth response has already been given. However, such diagrams only give a series of points, and become very complex if a large number of contour values are involved. Thus, if a detailed azimuth response is required, it is better to determine the response from the original equations. The correlator response as a function of azimuth is given by equations (B8), (B9), and (B15). If $(V = V_1)$, the values of Δ_A and Δ_B are given by

$$\Delta_A/2\pi = d(\cos\theta - \cos\theta_1)/\lambda_1, \tag{B16}$$

$$\Delta_B/2\pi = d(\sin\theta - \sin\theta_1)/\lambda_1. \tag{B17}$$

Figure (B5) shows a typical azimuth response of the correlator for a symmetrical cross array tuned to ($\theta_1 = \frac{1}{4}\pi$). Figure (B6) shows the corresponding curves for an L-shaped array.

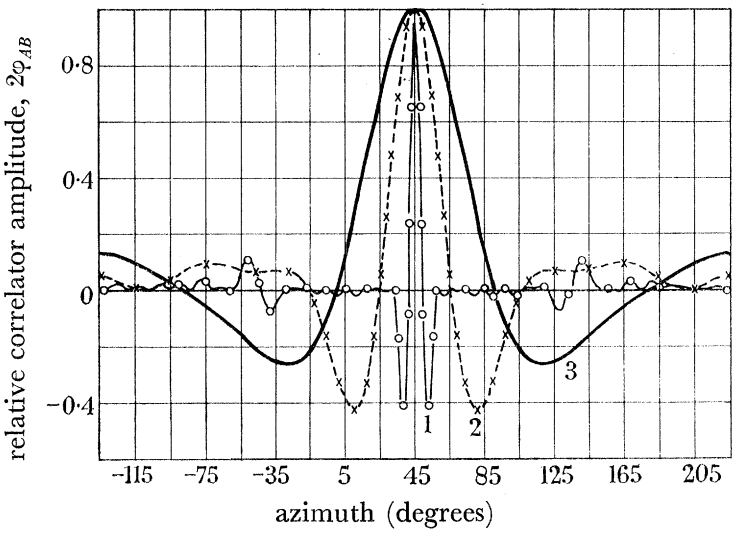

FIGURE B6. Correlator azimuth response for L-shaped array. $\theta_1 = \frac{1}{4}\pi$; $m = n-m = 10$; $V = V_1$; $D_A = D_B = 5d$. Curve 1, $d/\lambda_1 = \frac{1}{2}$; 2, $d/\lambda_1 = \frac{1}{10}$; 3, $d/\lambda_1 = \frac{1}{20}$.

It is clear from these and other response curves that the L-shaped array gives a sharper azimuth discrimination than a symmetrical cross, owing to the phase difference between the centre points. The best discrimination is at ($\theta_1 = \frac{1}{4}\pi$ and $\frac{5}{4}\pi$). For the condition ($d/\lambda_1 = \frac{1}{10}$), the wavelength is equal to the effective length of each line. Table B1 compares the beam widths at the half power points ($2\varphi_{AB} = \frac{1}{2}$) for this condition.

TABLE B1. BEAM WIDTH OF CORRELATOR AZIMUTH RESPONSE ($2\varphi_{AB} \geqslant \frac{1}{2}$, $d/\lambda_1 = \frac{1}{10}$)

θ_1 (radians)	beam width (degrees) $D_A = D_B = 5d$	beam width (degrees) $D_A = D_B = 0$
0	36	72
$\frac{1}{4}\pi$	26	73
$\frac{1}{2}\pi$	36	72
$\frac{3}{4}\pi$	63	73
π	36	72

B. 5. *Velocity filtering or determination*

In this case, the values of $\Delta_A/2\pi$ and $\Delta_B/2\pi$ for ($\theta = \theta_1$) are given by

$$\Delta_A/2\pi = d\cos\theta_1(V_1/V-1)/\lambda_1, \tag{B18}$$

$$\Delta_B/2\pi = d\sin\theta_1(V_1/V-1)/\lambda_1. \tag{B19}$$

Figure B7 shows the correlator response as a function of V_1/V for either a symmetrical cross or L-shaped array tuned to ($\theta_1 = \frac{1}{4}\pi$ or $\frac{5}{4}\pi$). These are the only azimuths in which the velocity responses are identical. Figure B8 shows the corresponding curves for an L-shaped array for ($\theta_1 = \frac{3}{4}\pi$). The response is much sharper than in figure B7. The curves for a symmetrical cross for this azimuth are the same as for ($\theta_1 = \frac{1}{4}\pi$).

Table B2 gives the values of V_1/V corresponding to the one-half and one-fifth power points for wavelengths equal to the effective length of each line ($10d$).

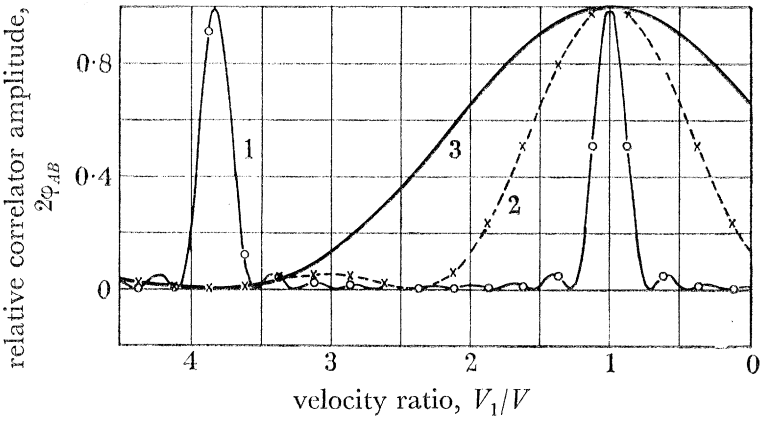

FIGURE B7. Correlator velocity response for L-shaped or symmetrical cross array. $\theta_1 = \frac{1}{4}\pi$; $m = n-m = 10$; $\theta = \theta_1$; $D_A = D_B$. Curve 1, $d/\lambda_1 = \frac{1}{2}$; 2, $d/\lambda_1 = \frac{1}{10}$; 3, $d/\lambda_1 = \frac{1}{20}$.

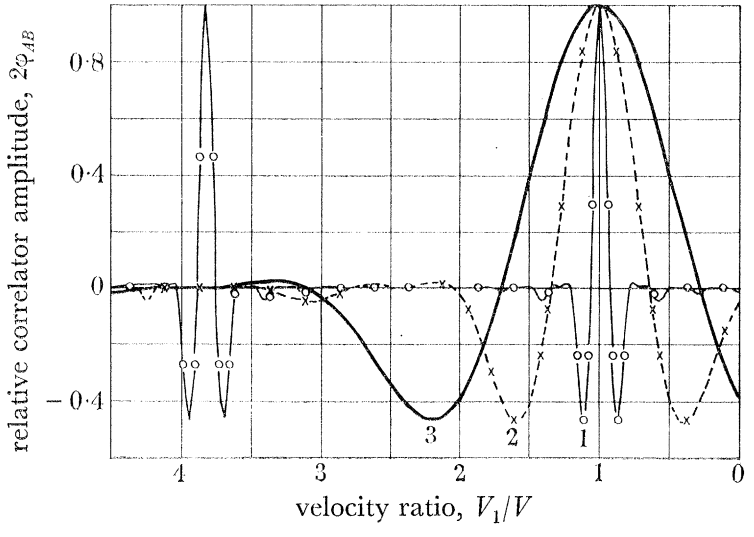

FIGURE B8. Correlator velocity response for L-shaped array. $\theta_1 = \frac{3}{4}\pi$; $m = n-m = 10$; $\theta = \theta_1$; $D_A = D_B = 5d$. Curve 1, $d/\lambda_1 = \frac{1}{2}$; 2, $d/\lambda_1 = \frac{1}{10}$; 3, $d/\lambda_1 = \frac{1}{20}$.

TABLE B2. RESOLUTION OF CORRELATOR VELOCITY RESPONSE ($d/\lambda_1 = \frac{1}{10}$)

		V_1/V			
		$D_A = D_B = 5d$		$D_A = D_B = 0$	
$2\varphi_{AB}$	θ_1 (radians)	$V > V_1$	$V < V_1$	$V > V_1$	$V < V_1$
0·5	0	0·70	1·30	0·38	1·62
	$\frac{1}{4}\pi$	0·37	1·63	0·37	1·63
	$\frac{1}{2}\pi$	0·70	1·30	0·38	1·62
	$\frac{3}{4}\pi$	0·78	1·22	0·37	1·63
	π	0·70	1·30	0·38	1·62
0·2	0	0·59	1·41	0·17	1·83
	$\frac{1}{4}\pi$	0·10	1·90	0·10	1·90
	$\frac{1}{2}\pi$	0·59	1·41	0·17	1·83
	$\frac{3}{4}\pi$	0·71	1·29	0·10	1·90
	π	0·59	1·41	0·17	1·83

These results show that, for a symmetrical cross array, the amplitudes of undesired signal components are only reduced by a factor 10 for velocities less than one-half that of the required signal, or for virtually infinite velocities. This also applies to an L-shaped array for ($\theta_1 = \frac{1}{4}\pi$). In the direction ($\theta_1 = \frac{3}{4}\pi$), the discrimination is much sharper, although the correlator output reaches a significantly high negative value. For significant discrimination against signal components having a velocity close to V_1, it is evident that the dimensions of the array should exceed the value of λ_1. Curve 1 of figures B7 and B8 corresponds to values of λ_1 equal to one-fifth of the effective length. It is undesirable for the dimensions to be much greater relative to the wavelength, since the coherence of the required signal component may be low. A further disadvantage of excessive dimensions is discussed in §B. 6.

B. 6. *Errors in azimuth and velocity determination*

B. 6·1. *Determination of centre of correlation peak*

The accuracy to which the azimuth or velocity can be determined depends upon the accuracy to which the centre of the correlation peak can be estimated. For the ideal curves given (figures B5 to B8), the error should not exceed one-twentieth of the beam width at the half power points. Thus, from table B1 for wavelengths equal to the effective length of each line, the range of error in determining azimuth is $1\frac{1}{2}$ to $3\frac{1}{2}°$, depending on array configuration and signal azimuth. From table B2, the corresponding range of error for velocity determination is 2 to 6 %. In practice, the azimuth and velocity responses will be obtained in discrete steps, and further inaccuracies will result if these steps are too large, because of the difficulty of interpolation. Steps of 10° in azimuth, and 10 % in velocity, will normally suffice.

B. 6·2. *Errors in inserted delays*

The accuracy also depends upon a knowledge of inserted delays, since

$$\theta_1 = \tan^{-1}(\tau_B/\tau_A), \tag{B20}$$

$$V_1 = d/(\tau_A^2+\tau_B^2)^{\frac{1}{2}}. \tag{B21}$$

The magnitude of errors in τ_A and τ_B, and the relation between them, depends upon the method used for inserting the delays. One method is to use a magnetic drum or tape loop, with a number of record and replay heads. An error in drum or tape speed will cause equal percentage errors in τ_A and τ_B. The error caused by this in estimating the value of θ_1 will be zero (equation (B20)), whilst the percentage error in estimating V_1 will be equal to the error of the drum or tape speed. Other analogue methods are possible in which a systematic error may be present in either τ_A or τ_B. A systematic error of $\delta\tau_B$ in the value of τ_B will produce an error in the estimated value of θ_1 given by

$$\tan(\theta_1+\delta\theta_1) - \tan\theta_1 = \delta\tau_B/\tau_A = \delta\tau_B(\tan\theta_1)/\tau_B.$$

For $\delta\tau_B/\tau_B \ll 1$, this reduces to

$$\delta\theta_1 \simeq \delta\tau_B(\sin 2\theta_1)/2\tau_B. \tag{B22}$$

The corresponding error in velocity determination is given by

$$\delta V_1/V_1 \simeq -\delta\tau_B(\sin^2\theta_1)/\tau_B. \tag{B23}$$

Thus an error in $\delta\tau_B/\tau_B$ of 10 % produces a maximum error in velocity determination of 10 % at $\theta_1 = \frac{1}{2}\pi$ and $\frac{3}{2}\pi$. The corresponding maximum error in azimuth determination is 3° at $\theta_1 = \frac{1}{4}\pi$, $\frac{3}{4}\pi$, $\frac{5}{4}\pi$ and $\frac{7}{4}\pi$.

In a simple digital system, it is only possible to insert delays which are an integral multiple of the sampling interval (t_s). Any seismometer output may have an error in delay lying in the range $-\frac{1}{2}t_s$ to $+\frac{1}{2}t_s$. These errors result in a reduction in the amplitude of the summed outputs and hence of the correlator output. With a line array consisting of equally spaced detectors, there will be certain search conditions for which the required incremental delay is an exact multiple of the sampling period, and hence no error is incurred. The condition of maximum error is when the errors are equally distributed from $-\frac{1}{2}t_s$ to $+\frac{1}{2}t_s$. In this condition, the relative output is given by equation (B1) or (B2) for the summed response of the line array, substituting ft_s/m for $\Delta_A/2\pi$, i.e.

$$E_A = \sin(\pi f t_s)/m \sin(\pi f t_s/m). \tag{B24}$$

The value of t_s will normally be chosen such that $ft_s \ll 1$. In this case, equation (B24) reduces to

$$E_A \simeq \sin(\pi f t_s)/\pi f t_s. \tag{B25}$$

Expanding equation (B25) gives

$$E_A \simeq 1 - \tfrac{1}{6}\pi^2 f^2 t_s^2$$
$$= 1 - 1{\cdot}64 f^2 t_s^2 \tag{B26}$$

e.g. if $t_s = 0{\cdot}05$ s, $f = 2$ c/s, $\quad E_A = 1 - 0{\cdot}0164.$

Thus in this case the reduction in amplitude is 1·64 %. The maximum possible reduction in correlator amplitude is twice the value given in equation (B26), and is therefore $3{\cdot}3 f^2 t_s^2$. As the search conditions are varied over a range of velocity or azimuth, the reduction in correlator amplitude will vary between zero and the above maximum. This will cause errors in estimating the peak of the correlation function. The errors will be minimized by having a large number of search conditions, and a very small value of ft_s.

B. 6·3. *Errors due to incorrect assumed velocities*

So far it has been assumed that the azimuth is known when determining the velocity response. This is usually correct, since for most events the location of the epicentre will have been determined using P onset times at a number of stations. However, if the location of the epicentre is unknown, and an azimuth search is required, then this must be carried out at one or more assumed velocities. These may not correspond to the actual velocity, and it is necessary to determine whether any significant errors are introduced in the value of azimuth obtained.

If the actual signal has a velocity V_1, azimuth θ_1, and the array is tuned to a constant velocity V and variable azimuth θ, then the values of Δ_A and Δ_B are given by

$$\Delta_A = 2\pi d\{\cos\theta_1 - (V_1/V)\cos\theta\}/\lambda_1, \tag{B27}$$

$$\Delta_B = 2\pi d\{\sin\theta_1 - (V_1/V)\sin\theta\}/\lambda_1. \tag{B28}$$

Figure B9 shows the correlator response as a function of azimuth for a 20 element symmetrical cross array for $\theta_1 = 0$, $d/\lambda_1 = 0{\cdot}1$ for the correct velocity ($V_1/V = 1$), and for two incorrect velocities ($V_1/V = \frac{3}{4}$ and $\frac{4}{3}$). The peak correlator output occurs at the correct

azimuth each time, although its amplitude, when the velocity is incorrect, is reduced compared with that for the correct velocity. The beam width for $V_1/V = \frac{3}{4}$ is increased from 68 to 84° at the points corresponding to one-half of the maximum output. Figure B10 shows the corresponding curves for $d/\lambda_1 = 0{\cdot}5$, i.e. for wavelengths equal to one-fifth of the effective length of each line. It can be seen that the array response is very much sharper for the

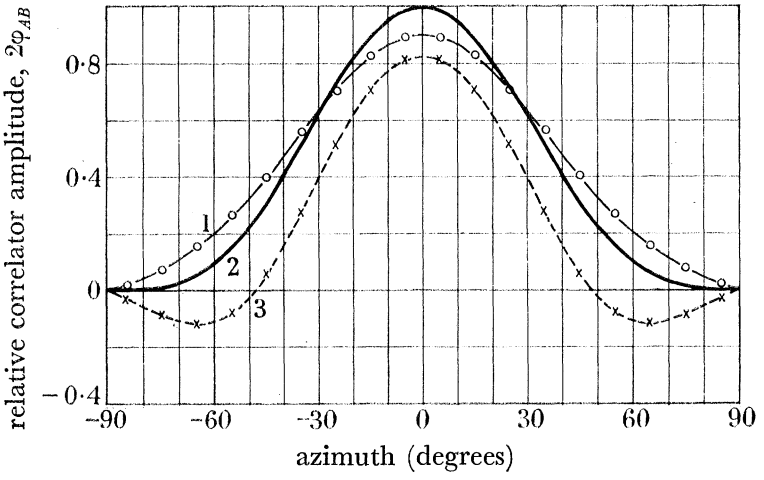

FIGURE B9. Correlator azimuth response for symmetrical cross array. $\theta_1 = 0$; $m = n-m = 10$; $d/\lambda_1 = \frac{1}{10}$; $D_A = D_B = 0$. Curve 1, $V_1/V = \frac{3}{4}$; 2, $V_1/V = 1$; 3, $V_1/V = \frac{4}{3}$.

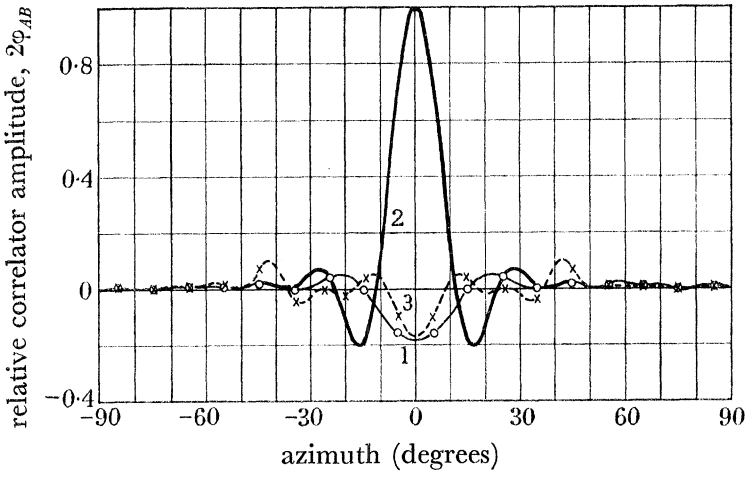

FIGURE B10. Correlator azimuth response for symmetrical cross array. $\theta_1 = 0$; $m = n-m = 10$; $d/\lambda_1 = \frac{1}{2}$; $D_A = D_B = 0$. Curve 1, $V_1/V = \frac{3}{4}$; 2, $V_1/V = 1$; 3, $V_1/V = \frac{4}{3}$.

correct velocity. However, it is completely mistuned for the two incorrect velocities, small negative peaks occurring at $\theta = 0$. This illustrates a serious disadvantage of choosing array dimensions which are many times the signal wavelengths of interest. Figure B11 shows the curves corresponding to figure B9 for an L-shaped array ($\theta_1 = 0$, $d/\lambda_1 = 0{\cdot}1$). In this case, the peak correlator output occurs at $\theta = -13°$ for $V_1/V = \frac{3}{4}$, and at $\theta = 11°$ for $V_1/V = \frac{4}{3}$. Figure B12 shows the corresponding curves for an L-shaped array for $\theta_1 = \frac{1}{4}\pi$. In this case the peak is not displaced, although the beam width is increased for $V_1/V = \frac{3}{4}$.

The above curves, and the contoured responses, show that errors in estimating azimuth can occur with an L-shaped array if an incorrect velocity is assumed. The maximum error

occurs at $\theta = 0, \frac{1}{2}\pi, \pi$ and $\frac{3}{2}\pi$, and is about 13° for $V_1/V = \frac{4}{3}$ or $\frac{3}{4}$, $d/\lambda_1 = 0{\cdot}1$. To obtain greater accuracy, the initial value determined for the azimuth may be used in a velocity determination. The velocity thus obtained may then be used in a revised azimuth determination.

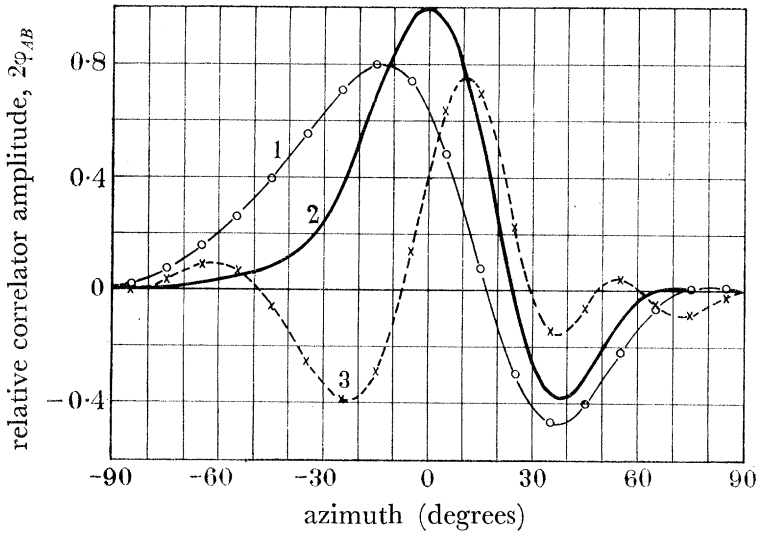

FIGURE B11. Correlator azimuth response for L-shaped array. $\theta_1 = 0$; $m = n-m = 10$; $d/\lambda_1 = \frac{1}{10}$; $D_A = D_B = 5d$. Curve 1, $V_1/V = \frac{3}{4}$; 2, $V_1/V = 1$; 3, $V_1/V = \frac{4}{3}$.

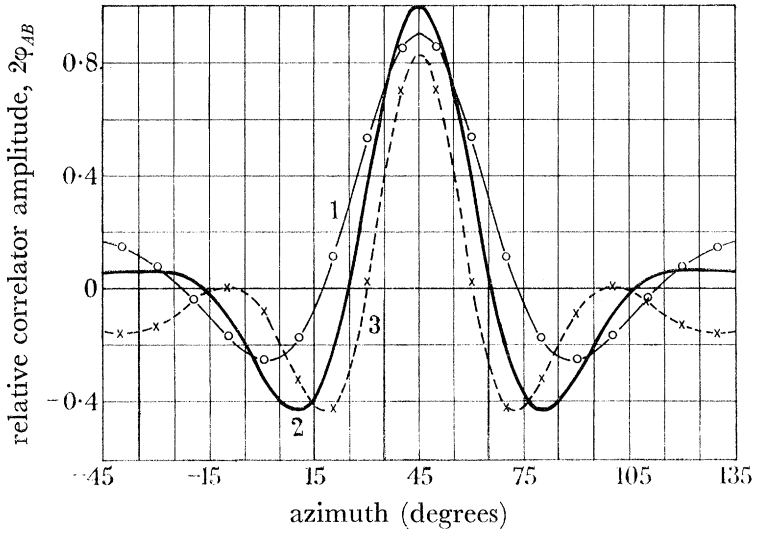

FIGURE B12. Correlator azimuth response for L-shaped array. $\theta_1 = \frac{1}{4}\pi$; $m = n-m = 10$; $d/\lambda_1 = \frac{1}{10}$; $D_A = D_B = 5d$. Curve 1, $V_1/V = \frac{3}{4}$; 2, $V_1/V = 1$; 3, $V_1/V = \frac{4}{3}$.

Normally, it will not be necessary to carry out an iterative procedure of this kind, and an azimuth determination made simultaneously at three fixed velocities in a 2:1 range should be sufficient for a given requirement, e.g. for P signals with ranges of 30 to 90°.

B. 6·4. *Errors due to noise and interfering signals*

Another possible source of error arises from the presence of noise and interfering signals. Coherent components are particularly troublesome, since they produce variations in the correlator level which vary systematically with azimuth and velocity. This condition is

frequently the case when the array is used for determining the velocity of a late signal arrival. The problem will now be considered for a symmetrical cross array.

The correlator output, when an interfering signal component S_1 is present, is given by

$$2\varphi_{AB} = \frac{2}{T_1}\int_{t_1-T_1}^{t_1} [a_{S_1}E_{AS_1}\cos(\omega_1 t+\phi_1) + a_{S_2}E_{AS_2}\cos(\omega_2 t+\phi_2)] \times [a_{S_1}E_{BS_1}\cos(\omega_1 t+\phi_1) + a_{S_2}E_{BS_2}\cos(\omega_2 t+\phi_2)]\,dt.$$

For $\omega_1 T_1 \gg 1$, and $\omega_2 T_1 \gg 1$:

$$2\varphi_{AB} = a_{S_1}^2 E_{AS_1}E_{BS_1} + a_{S_2}^2 E_{AS_2}E_{BS_2} + a_{S_1}a_{S_2}(E_{AS_1}E_{BS_2} + E_{AS_2}E_{BS_1}) \times \frac{2}{T_1}\int_{t_1-T_1}^{t_1} \cos(\omega_1 t+\phi_1)\cos(\omega_2 t+\phi_2)\,dt. \quad \text{(B29)}$$

Evaluating integral term in equation (B29) we have

$$\frac{2}{T_1}\int_{t_1-T_1}^{t_1} \cos(\omega_1 t+\phi_1)\cos(\omega_2 t+\phi_2)\,dt = \frac{1}{(\omega_1+\omega_2)T_1}{}_{(t_1-T_1)}^{t_1}[\sin((\omega_1+\omega_2)t+\phi_1+\phi_2)] + \frac{1}{(\omega_1-\omega_2)T_1}{}_{(t_1-T_1)}^{t_1}[\sin((\omega_1-\omega_2)t+\phi_1-\phi_2)]. \quad \text{(B30)}$$

The first two terms in equation (B29) are the correlator amplitudes for the first and second components, and separately peak at the corresponding values of azimuth and velocity. The sum of these two terms will in general peak at incorrect values of velocity and azimuth, and may have a double-humped response. Thus in order to obtain the velocity or azimuth of the second signal component, it is necessary to take the differential correlator output, which gives the value of the second term only.

The third term in equation (B29) is a form of correlator noise, caused by the cross products of the two signal components. The significance of this term depends upon the characteristics of the two signal components and upon the integration time. If the signals are unrelated and cover a wide frequency band Δf with a substantially flat spectrum, then the third term is unlikely to be significant for ($\Delta f T_1 \gg 1$). On the other hand, the signal spectra may be sharply peaked at two frequencies ω_1 and ω_2 close to each other. Equation (B30) shows the expansion of the time dependent factor of the cross-product terms of equation (B29). This shows that there are sum and difference frequency components present in the correlator output. The difference frequency component predominates, with a maximum relative amplitude ratio of $(\omega_1+\omega_2)/(\omega_1-\omega_2)$. When the signals only exist for a few cycles, the difference frequency component may only exist for a fraction of a cycle, and be substantially constant over the duration of the signal. Its amplitude in the correlator output depends upon the phase difference $(\phi_1-\phi_2)$ at time t_1 and upon the cross product terms $E_{AS_1}E_{BS_2}$ and $E_{AS_2}E_{BS_1}$. The latter vary as the array is tuned through a range of velocity and azimuth and may lead to errors in azimuth/velocity determination, even when the differential correlator output is used. This particularly applies when trying to determine the azimuth or velocity of a relatively weak second arrival. Furthermore, even if the first signal component is sufficiently out of phase in one line such that the first term in equation (B29) is very small, it may nevertheless be in phase in the second line resulting in a cross product term of significant amplitude. It is therefore desirable to ensure that the unwanted signal is rejected by both lines.

Appendix C. Bibliography

C. 1. *Publications on arrays used in radio astronomy and radar*

Andreason, M. G. 1962 Linear arrays with variable interelement spacings. *Trans. Instn Radio Engrs, AP*-**10**, 137–143.

Arsac, J. 1955 Transmissions des frequences spatiales dans les systèmes recepteurs d'ondes courtes. *Opta Actica*, **2**, 112.

Barber, N. F. 1958 Optimum arrays for direction-finding. *N.Z. J. Sci.* **1**, 35.

Barber, N. F. 1958 Compound interferometers. *Proc. Instn Radio Engrs*, **46**, 1951.

Barber, N. F. 1959 Design of 'optimum' arrays for direction-finding. *Elect. Radio Engr*, June, pp. 222–232.

Bloch, A., Medhurst, R. G. & Pool, S. D. 1953 A new approach to the design of super-directive aerial arrays. *Proc. Instn Elect. Engrs*, part III, **100**, 303.

Blythe, J. H. 1957 A new type of pencil beam aerial for radio astronomy. *Mon. Not. R. Astr. Soc.* **117**, 644.

Bracewell, R. N. 1955 Chord construction for aerial smoothing. *Aust. J. Sci. Res.* A, **8**, 200.

Bracewell, R. N., Swarup, G. & Seeger, C. L. 1962 Future large radio telescopes. *Nature, Lond.* **193**, 412.

Brown, F. W. 1962 Note on nonuniformly spaced arrays. *Trans. Instr. Radio Engrs, AP*-**10**, 639.

Christiansen, W. N. & Mathewson, D. S. 1958 Scanning the sun with a highly directional array. *Proc. Instn Radio Engrs*, **46**, 127.

Covington, A. E. & Broten, N. W. 1957 An interferometer for radio astronomy with a single-lobed radiation pattern. *Trans. Instr. Radio Engrs, AP*-**5**, 247.

Dolph, C. L. 1946 A current distribution for broadside arrays which optimises the relationship between beamwidth and sidelobe level. *Proc. Instn Radio Engrs*, **34**, 335.

Hansen, W. W. & Woodyard, J. R. 1938 A new principle in directional receiver design. *Proc. Instn Radio Engrs*, **26**, 333–345.

Harrington, R. F. 1961 Sidelobe reduction by nonuniform element spacing. *Trans. Instn Radio Engrs, AP*-**9**, 187–192.

Ishimaru, A. 1962 Theory of unequally spaced arrays. *Trans. Instn Radio Engrs, AP*-**10**, 691–702.

Jennison, R. C. 1962 Some radio astronomy techniques. *J. Brit. Instn Radio Engrs.* **23**, 121.

Justice, R. 1956 Side-lobe suppression by pattern multiplication. *Trans. Instn Radio Engrs, AP*-**4**, 119–124.

Kraus, J. D. 1950 *Antennas.* New York: McGraw-Hill Book Co. Inc.

King, D. D., Packard, R. F. & Thomas, R. K. 1960 Unequally spaced broadband antenna arrays. *Trans. Instn Radio Engrs, AP*-**8**, 30–34.

Koch, W. E. & Stone, J. L. 1958 Space frequency equivalence. *Proc. Instn Radio Engrs*, **46**, 499.

McReady, L. L., Pawsey, J. C. & Payne-Scott, R. 1947 Solar radiation at radio frequencies and its relation to sunspots. *Proc. Roy. Soc.* A, **190**, 357.

Mills, B. Y. & Little, A. G. 1953 A high-resolution aerial system of a new type. *Aust. J. Phys.* **6**, 272.

Mills, B. Y., Little, A. G., Sheridan, K. V. & Slee, O. B. 1958 A high-resolution radio telescope for use at 3·5 metres. *Proc. Instn Radio Engrs*, **46**, 67.

O'Brien, P. A. 1954 The distribution of radiation across the solar disc at metre wavelengths. *Mon. Not. R. Astr. Soc.* **113**, 597.

Pedinoff, M. E. & Ksienski, A. A. 1962 Multiple target response of data processing. *Trans. Instn Radio Engrs, AP*-**10**, 112–126.

Price, O. R. 1960 Reduction of sidelobe level and beamwidth for receiving antennas. *Proc. Instn Radio Engrs*, June, pp. 1177–1178.

Ryle, M. 1952 A new radio interferometer and its application to the observation of weak radio stars. *Proc. Roy. Soc.* A, **211**, 351.

Ryle, M. & Smith, F. G. 1948 A new intense source of radio-frequency radiation in the constellation of Cassiopeia. *Nature, Lond.* **162**, 462.

Sandler, S. S. 1960 Some equivalence between equally and unequally spaced arrays. *Trans. Instn Radio Engrs, AP-8*, 496.

Schelkunoff, S. A. 1943 A mathematical theory of linear arrays. *Bell. Syst. Tech. J.* **22**, 80.

Schelkunoff, S. A. & Friis, H. T. 1952 *Antennas: theory and practice.* New York: John Wiley. London: Chapman and Hall.

Shanks, H. E. & Bickmore, R. W. 1959 Four-dimensional electromagnetic radiation. *Canad. J. Physics*, **37**, 263–275.

Stanier, H. M. 1950 Distribution of radiation from the undisturbed sun at a wavelength of 60 cm. *Nature, Lond.* **165**, 354.

Swenson, G. W. Jr. & Lo, Y. T. 1961 The univ. of Illinois Radio Telescope. *Trans. Instn Radio Engrs, AP-9*, 9–16.

Unz, H. 1960 Linear arrays with arbitrarily distributed elements. *Trans. Instn Radio Engrs, AP-8*, 222.

Unz, H. 1962 Nonuniform arrays vs. spacings larger than λ. *Trans. Instn Radio Engrs, AP-10*, 647.

Vitkevich, V. V. 1953 Wide band radio interferometer. *Dokl. Akad. Nauk. S.S.S.R.* **91**, 1301.

Wolff, I. 1937 Determination of the radiating system which will produce a specified directional characteristic. *Proc. Instn Radio Engrs*, **25**, 630–643.

Woodwood, P. M. 1953 *Probability and information theory with application to radar.* London: Pergamon Press.

C. 2. *Publications on acoustics and sonar*

Anderson, V. C. 1958 Arrays for the investigation of ambient noise in the ocean. *J. Acoust. Soc. Amer.* **30**, 470–477.

Anderson, V. C. 1960 Digital array phasing. *J. Acoust. Soc. Amer.* **32**, 867–870.

Berman, A. & Clay, C. S. 1957 Theory of time-averaged-product arrays. *J. Acoust. Soc. Amer.* **29**, 805–812.

Broussaud, G. & Spitz, E. 1960 Superdirectivité: supergain. *Ann. Radioelect.* **15**, 289.

Brown, J. L. & Rowlands, R. O. 1959 Design of directional arrays. *J. Acoust. Soc. Amer.* **31**, 1638–1643.

Davies, D. E. N. 1961 A fast electronically scanned radar receiving system. *J. Brit. Instn Radio Engrs*, **21**, 305.

Di Francia, G. T. 1955 Directivity, supergain and information. *Trans. Instn Radio Engrs, AP-4*, 10.

Fakley, D. C. 1959 Comparison between the time averaged product array and the interclass correlator. *J. Acoust. Soc. Amer.* **31**, 1307.

Faran, J. J. & Hills, R. 1952 The application of correlation techniques to acoustic receiving systems. Acoustics Research Lab., Harvard Univ. *Tech. Memo.* no. 28.

Federici, M. 1959 La precisione di mesura della direzione di una sorgente sonora con sistemi riceventi direttivi. *Ric. sci.* **29**, 2301.

Federici, M. 1962 On the improvement of detection and precision capabilities of sonar systems. *Symposium on Sonar Systems.* Univ. Birmingham.

Jerardin, L. 1954 Le signal minimum utilisable en reception radar et son amélioration par certain procédés de correlation. *Onde élect.* January.

Hoover, G. W. 1961 Applications of delay lines in correlation processing. *J. Acoust. Soc. Amer.* **33**, 1657.

Jacobson, M. J. 1957 Analysis of a multiple receiver correlation system. *J. Acoust. Soc. Amer.* **29**, 1342–1347.

Jacobson, M. J. 1958 Correlation with similar uniform collinear arrays. *J. Acoust. Soc. Amer.* **30**, 1030–1034.

Jacobson, M. J. 1959 Correlation of a finite distance point source. *J. Acoust. Soc. Amer.* **31**, 448–453.

Jacobson, M. J. & Talham, R. J. 1959 Use of pressure gradient receivers in a correlator receiving system. *J. Acoust. Soc. Amer.* **31**, 1352–1362.

Jacobson, M. J. & Talham, R. J. 1961 Comparison analysis on four directional receiver correlators. *J. Acoust. Soc. Amer.* **33**, 518–526.

Jacobson, M. J. 1961 Optimum envelope resolution in an array correlator. *J. Acoust. Soc. Amer.* **33**, 1055–1060.

Jacobson, M. J. 1962 Space-time correlation in spherical and circular noise fields. *J. Acoust. Soc. Amer.* **34**, 971–978.

Middleton, D. 1962 Acoustic signal detection by simple correlators in the presence of non-Gaussian noise. *J. Acoust. Soc. Amer.* **34**, 1958.

Remley, W. R. 1963 Correlation of signals having a linear delay. *J. Acoust. Soc. Amer.* **35**, 65.

Rudnick, P. 1960 Small signal detection in the DIMUS array. *J. Acoust. Soc. Amer.* **32**, 871–877.

Shearman, E. D. R. 1962 Synthesis of multi-element directional patterns with a two-element single frequency receiving array. *Symposium on Sonar Systems.* Univ. Birmingham.

Thomas, J. B. & Williams, T. R. 1959 On the detection of signals in non-stationary noise by product arrays. *J. Acoust. Soc. Amer.* **31**, 453–462.

Tucker, D. G. 1957 Arrays with constant beam-width over a wide frequency-range. *Nature, Lond.* **180**, 496.

Tucker, D. G. 1958 Signal/noise performance of super-directive arrays. *Acustica*, **8**, 112.

Tucker, D. G. 1961 Improved directivity using synchronous demodulation. *Acustica*, **11**, 45.

Tucker, D. G. 1962 Multiplicative reception in radio astronomy and sonar systems. *Symposium on Sonar Systems.* Univ. Birmingham.

Tucker, D. G., Welsby, V. G. & Kendell, R. 1958 The rapid swinging of an acoustic beam across a section by electronic means and its application to echo ranging systems. *J. Brit. Instn Radio Engrs*, **18**, 465.

Tucker, D. G. *et al.* 1959 Underwater echo-ranging with electronic sector scanning: sea trials on R.R.S. 'Discovery II'. *J. Brit. Instn Radio Engrs*, **19**, 681.

Vanderkulk, W. 1962 Optimum processing for acoustic arrays. *Symposium on Sonar Systems.* Univ. Birmingham.

Welsby, V. G. 1961 Two-channel sector scanning system using a multi-frequency carrier. *Electron. Tech.* **38**, 160–163.

Welsby, V. G. 1961 Multiplicative receiving array. *J. Brit. Instn Radio Engrs*, **22**, 5.

Welsby, V. G. 1961 The signal/noise gain of ideal receiving arrays. *Instn Elect. Engrs Monograph* 470E, September.

Welsby, V. G. 1962 Two-element electronic scanning array. *Electron. Tech.* **39**, January.

Welsby, V. G. 1962 The angular resolution of a receiving aperture. *Symposium on Sonar Systems.* Univ. Birmingham.

Welsby, V. G. & Tucker, D. G. 1959 Multiplicative receiving arrays. *J. Brit. Instn Radio Engrs*, **19**, 369.

Woodward, P. M. & Lawson, J. D. 1948 The theoretical precision with which an arbitrary radiation-pattern may be obtained from a source of finite size. *J. Instn Elect. Engrs*, **95**, part III, 363.

C. 3. *Publications on seismology and geophysics*

Denham, D. 1963 The use of geophone groups to improve the signal-to-noise ratio of the first arrival in refraction shooting. *Geophys. Prosp.* **11**, 299–408.

Embree, P., Burg, J. P. & Backus, M. M. 1963 Wide-band velocity filtering—the pie-slice process. *Geophysics*, **28**, 948–974.

Fail, J. P. & Grau, G. 1963 Fan filters. *Geophys. Prosp.* **11**, 131–163.

Holzman, M. 1963 Chebyshev optimized geophone arrays. *Geophysics*, **28**, 145–155.

Issayev, V. A. 1959 On the theory of the directional effects of a group of seismometers in case pulse oscillations. *Bull. Acad. Sci. Geophys. Series*, December.

Iyer, H. M. 1958 A study of the direction of arrival of microseisms at Kew Observatory. *Geophys. J.* **1**, 32.

Jones, H. J. 1962 Applications of correlation analysis to seismic exploration. *World Petroleum*, March, p. 60.

Jones, H. J. & Morrison, J. A. 1954 Cross-correlation filtering. *Geophysics*, October, p. 660.

Jones, H. J., Morrison, J. A., Sarrafian, G. P. & Spieker, L. J. 1955 Magnetic delay line filtering. *Geophysics*, October, p. 745.

Melton, B. S. & Bailey, L. F. 1957 Multiple signal correlators. *Geophysics*, **22**, 565–588.

Rieber, F. 1936 A new reflection system with controlled directional sensitivity. *Geophysics*, **1**, 97–106.

Rieber, F. 1937 Complex reflection patterns and their geologic sources. *Geophysics*, **2**, 132–160.

Rykunov, L. N. 1961 A correlation method of determining the velocities of microseisms. *Izv. Acad. Sci.* July, 1037. Translated by American Geophysical Union, October 1961.

Tullos, F. N. & Cummings, L. C. 1961 An analog seismic correlator. *Geophysics*, **26**, 298–308.

Vinnik, L. P. 1963 The space time filtration of seismic signals. *Bull. Acad. Sci. Geophys. Series*, June, no. 6.

C. 4. *Publications on general correlation methods*

Barber, N. F. 1957 A scatter diagram which gives the complex correlation coefficient for normal variables. *N.Z. J. Sci. Tech.* B, **38**, 366.

Bendat, J. S. 1958 *Principles and applications of random noise theory.* London: Chapman and Hall Ltd.

Davenport, W. B., Jr. & Root, W. L. 1958 *Random signals and noise.* New York and London: McGraw-Hill Book Co. Inc.

George, S. F. 1954 Effectiveness of cross-correlation detectors. *Proc. National Electronic Conf.* **10**, 109.

Green, P. E. Jr. 1957 The output signal to noise ratio of correlation detectors. *Trans. Instn Radio Engrs, IT-***3**, 10–18.

Lee, Y. W. 1960 *Statistical theory of communication.* New York and London: John Wiley and Sons Inc.

Middleton, D. 1960 *An introduction to statistical communication theory.* New York: McGraw-Hill Book Co. Inc.

Nodtvedt, H. 1951 The correlation function in the analysis of directive wave propagation. *Phil. Mag.* **42**, 1022.

Stewart, J. L. 1960 *Fundamentals of signal theory.* New York: McGraw-Hill Book Co. Inc.

Wainstein, L. A. & Zubakov, V. D. 1962 *Extraction of signals from noise.* New Jersey: Prentice-Hall Inc.

Wiener, N. 1949 *The extrapolation, interpolation and smoothing of stationary time series with engineering applications.* New York: John Wiley and Sons Inc.

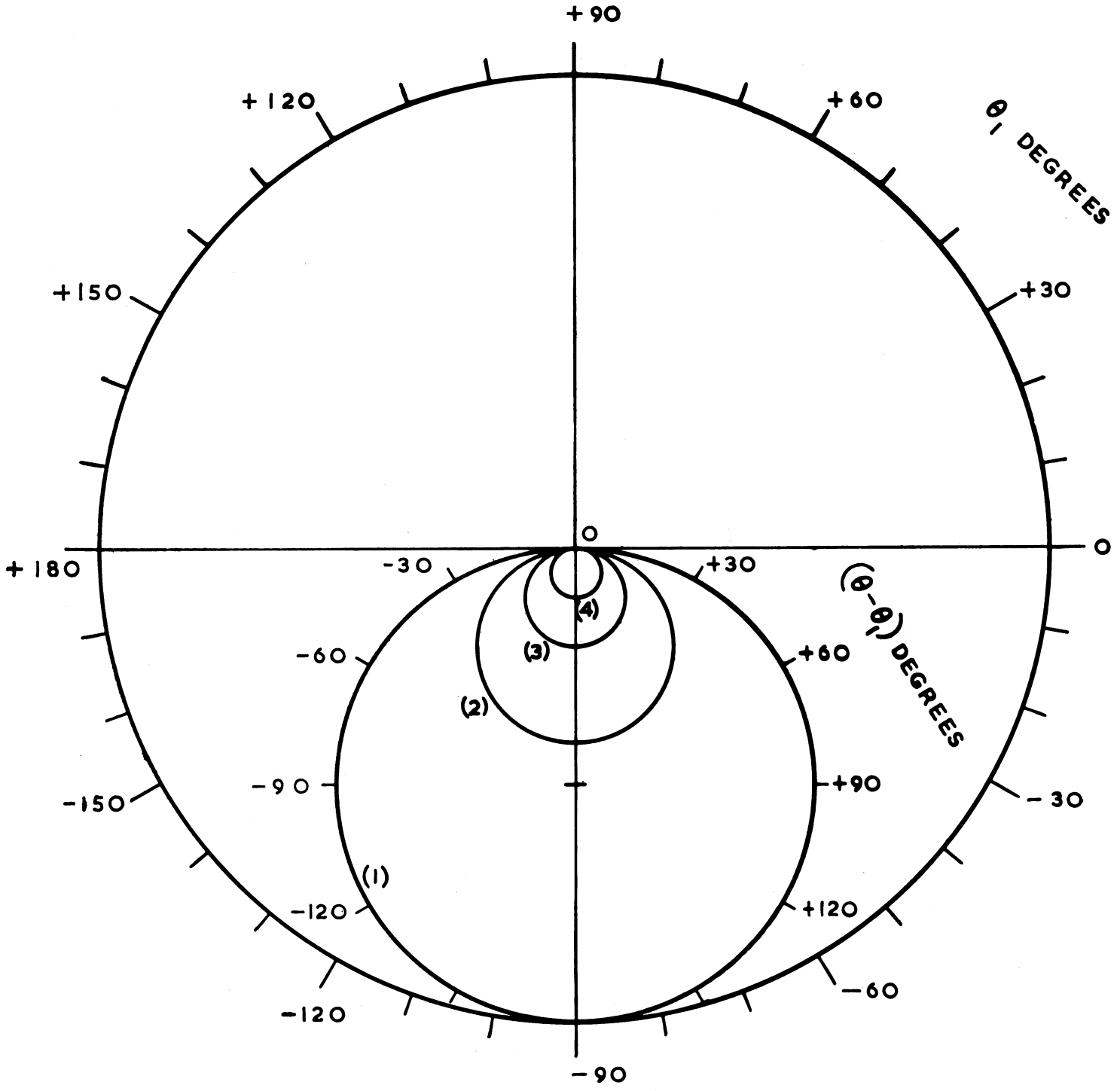

FIGURE 3(*a*). Chart for determining azimuth response.
(1), $D/\lambda_1 = 4{\cdot}5$; (2), $D/\lambda_1 = 1{\cdot}8$; (3), $D/\lambda_1 = 0{\cdot}9$; (4), $D/\lambda_1 = 0{\cdot}45$.

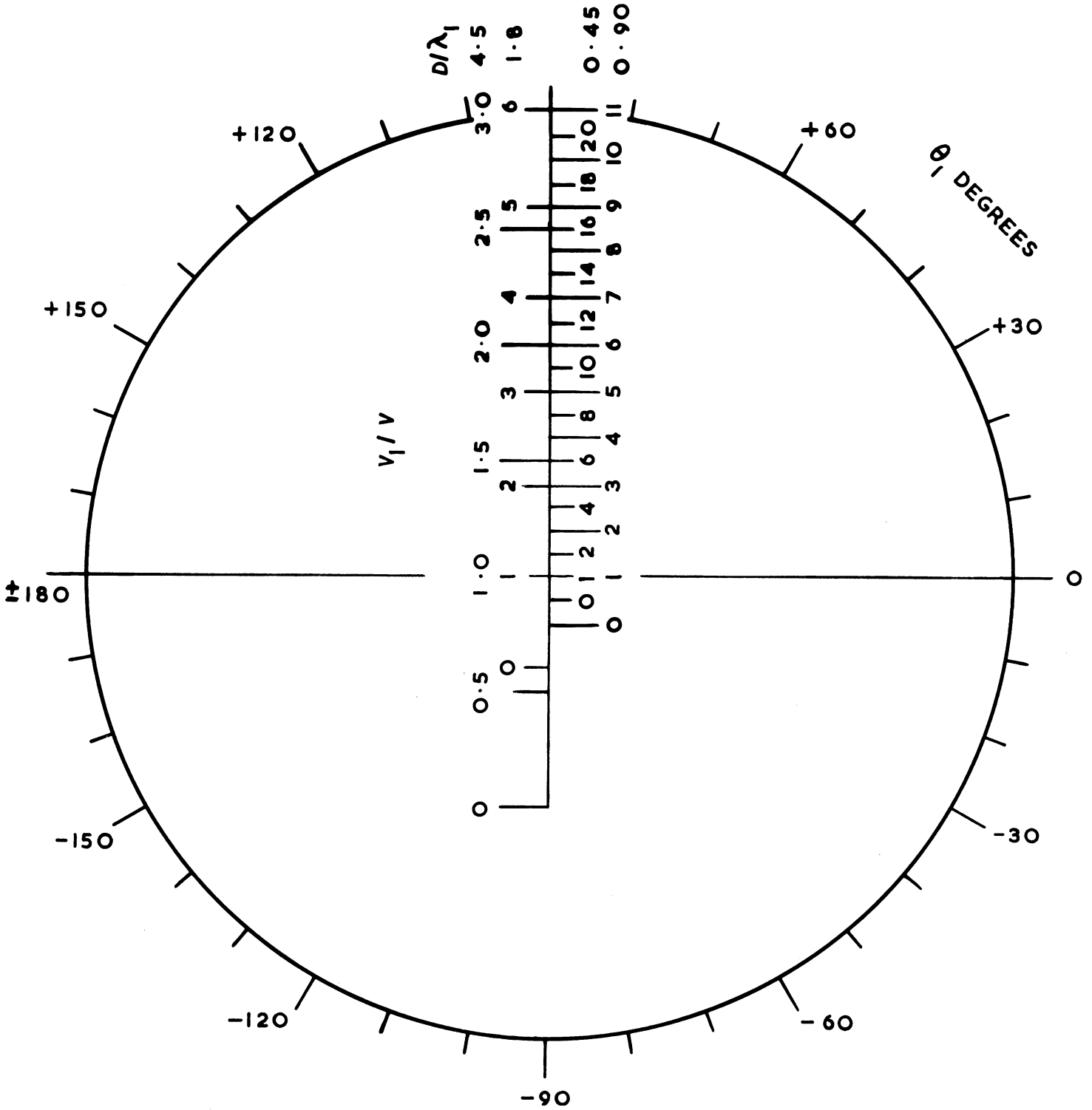

FIGURE 3 (*b*). Chart for determining velocity response (D/λ_1 = 4·5, 1·8, 0·9, 0·45).

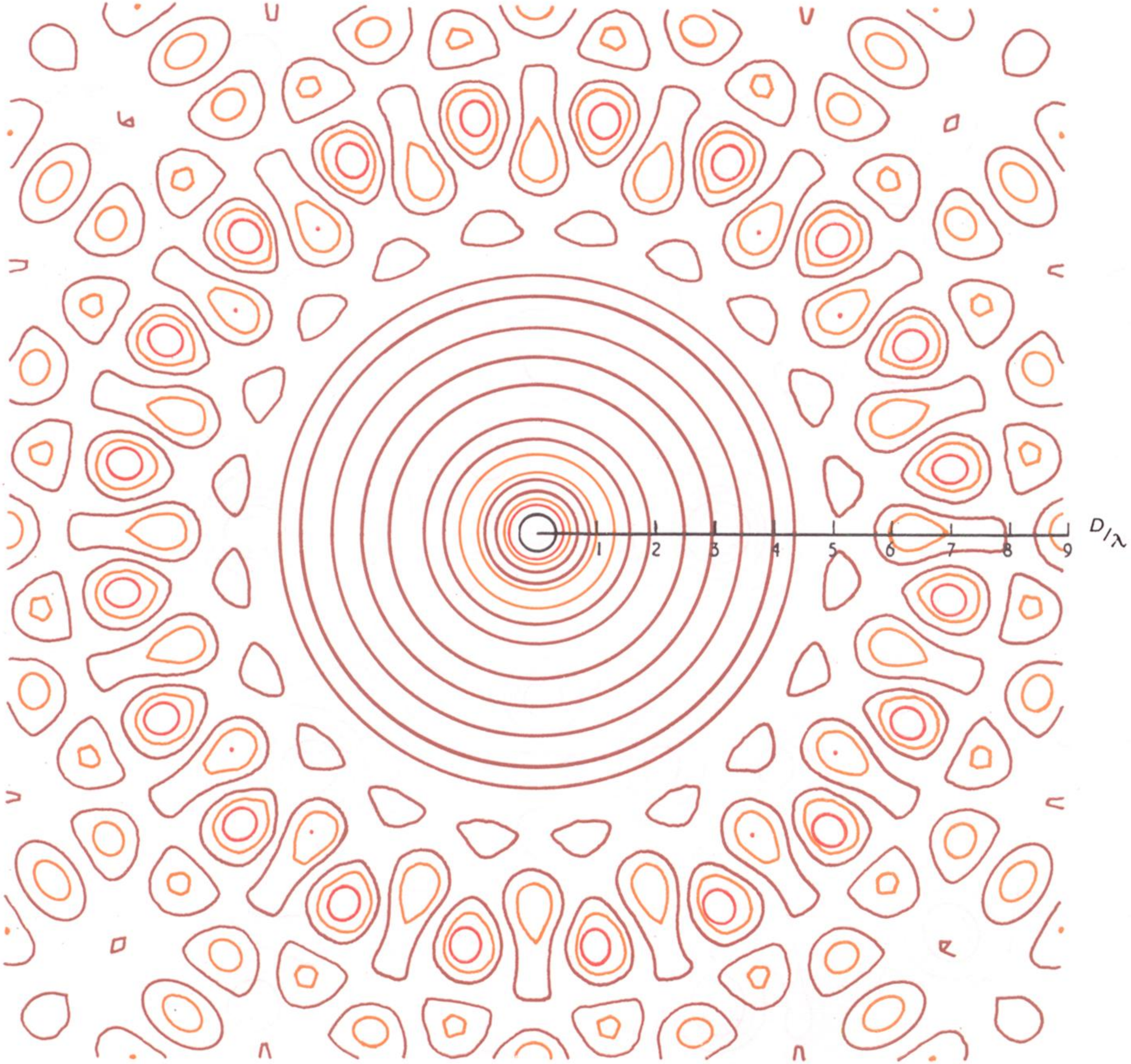

FIGURE 4. Sum squared response of 20 element circular array.

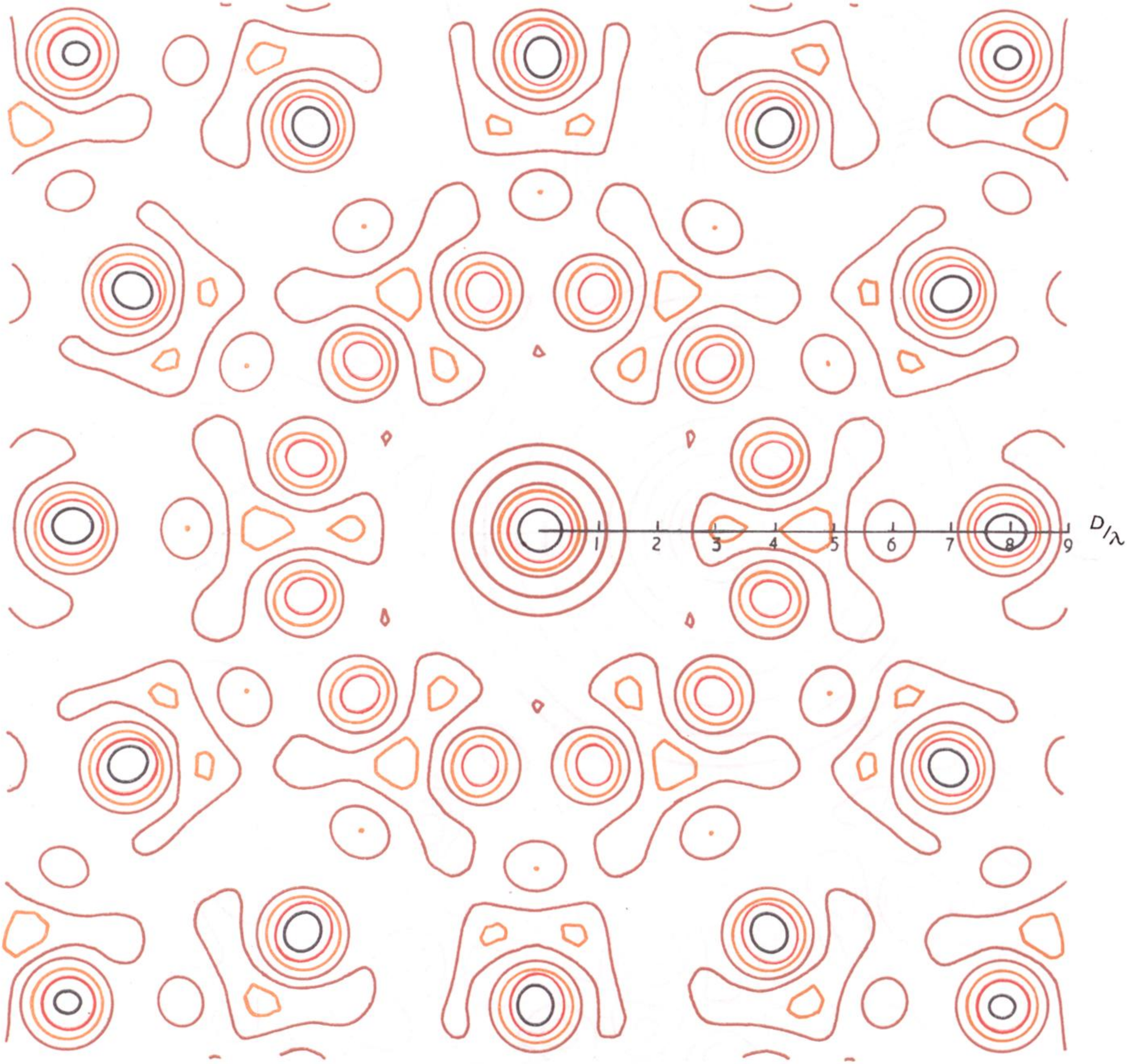

FIGURE 5. Sum squared response of 18 element cluster.

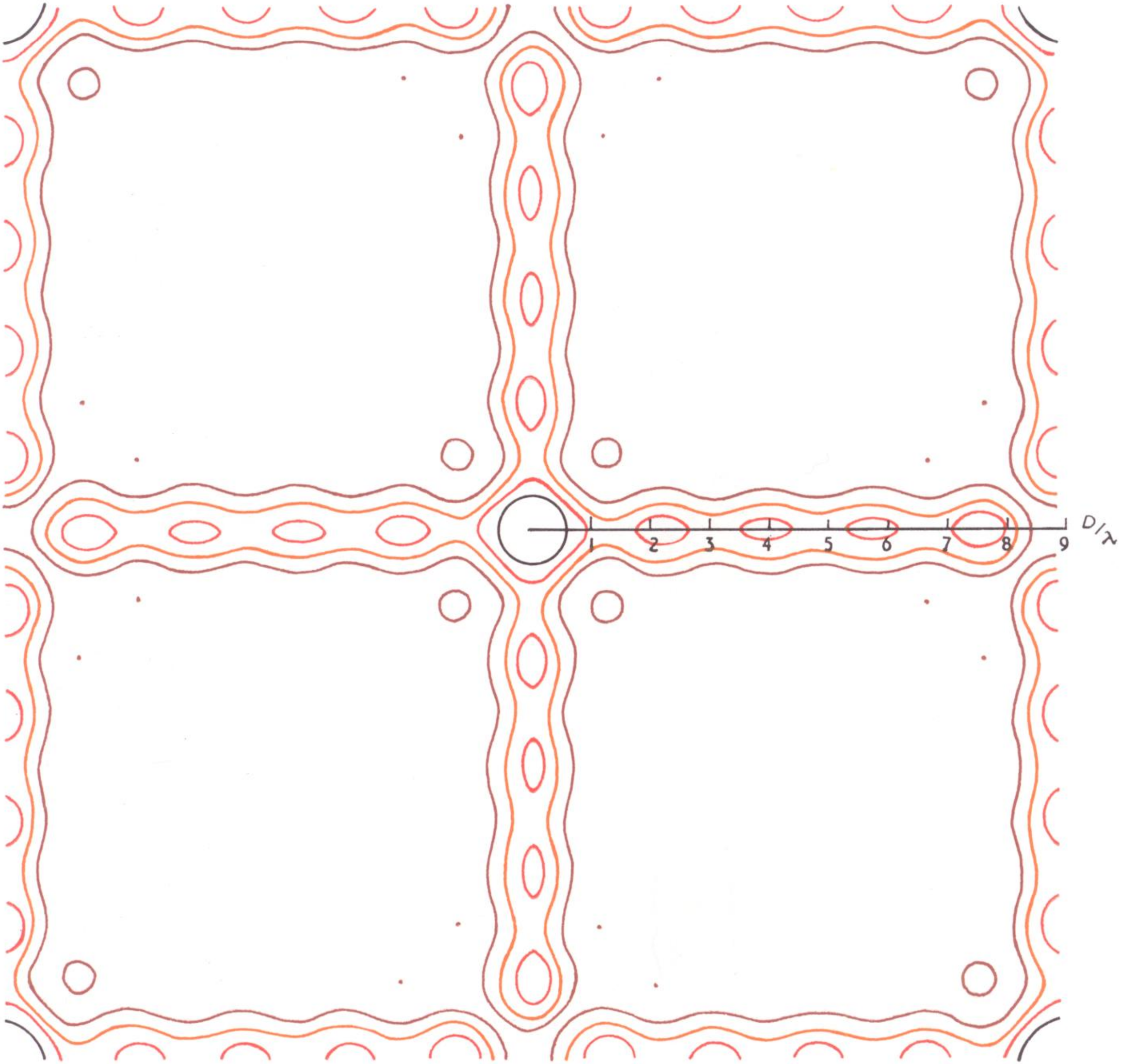

FIGURE 6. Sum squared response of 20 element symmetrical cross array.

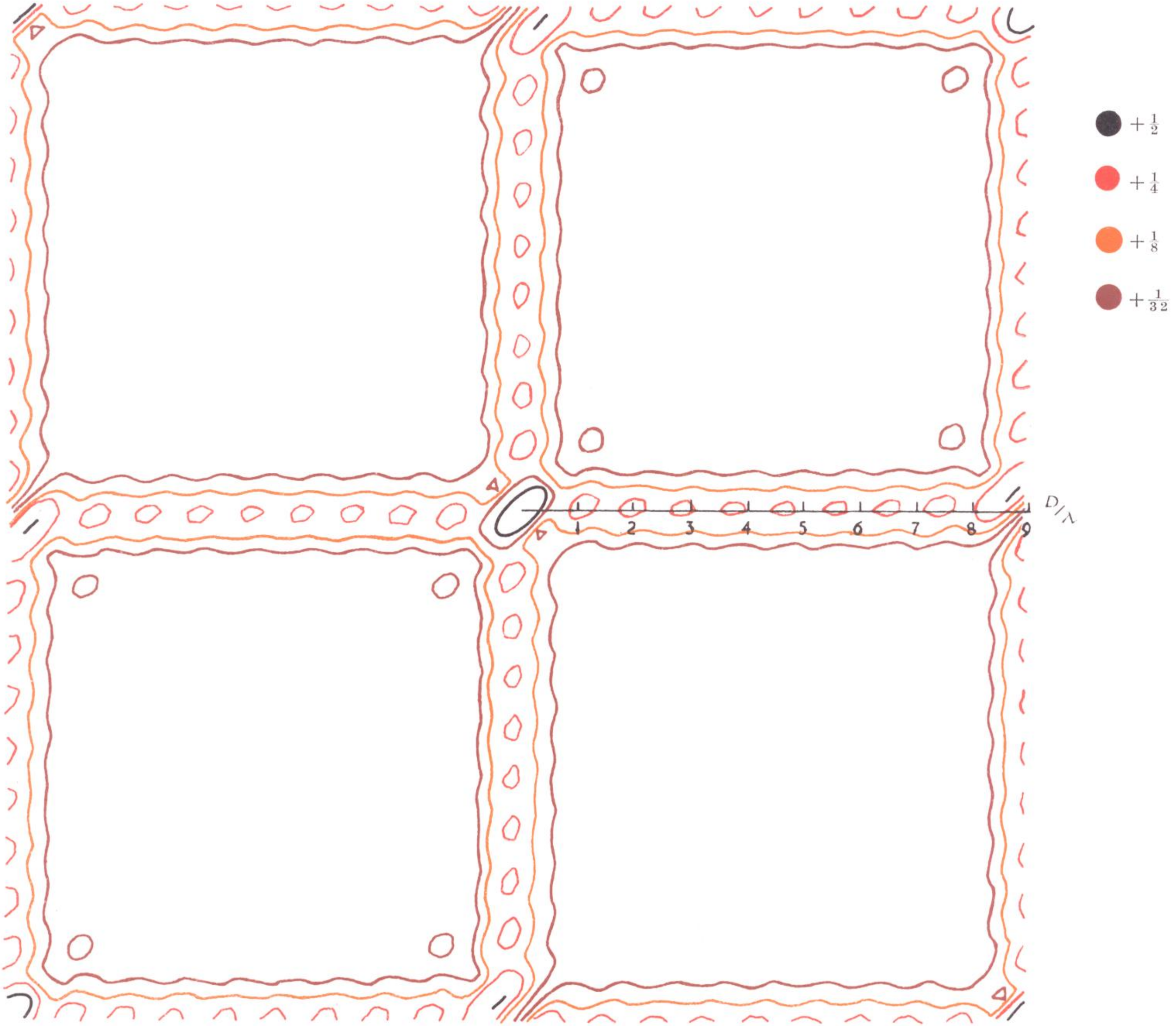

FIGURE 7. Sum squared response of 20 element L-shaped array.

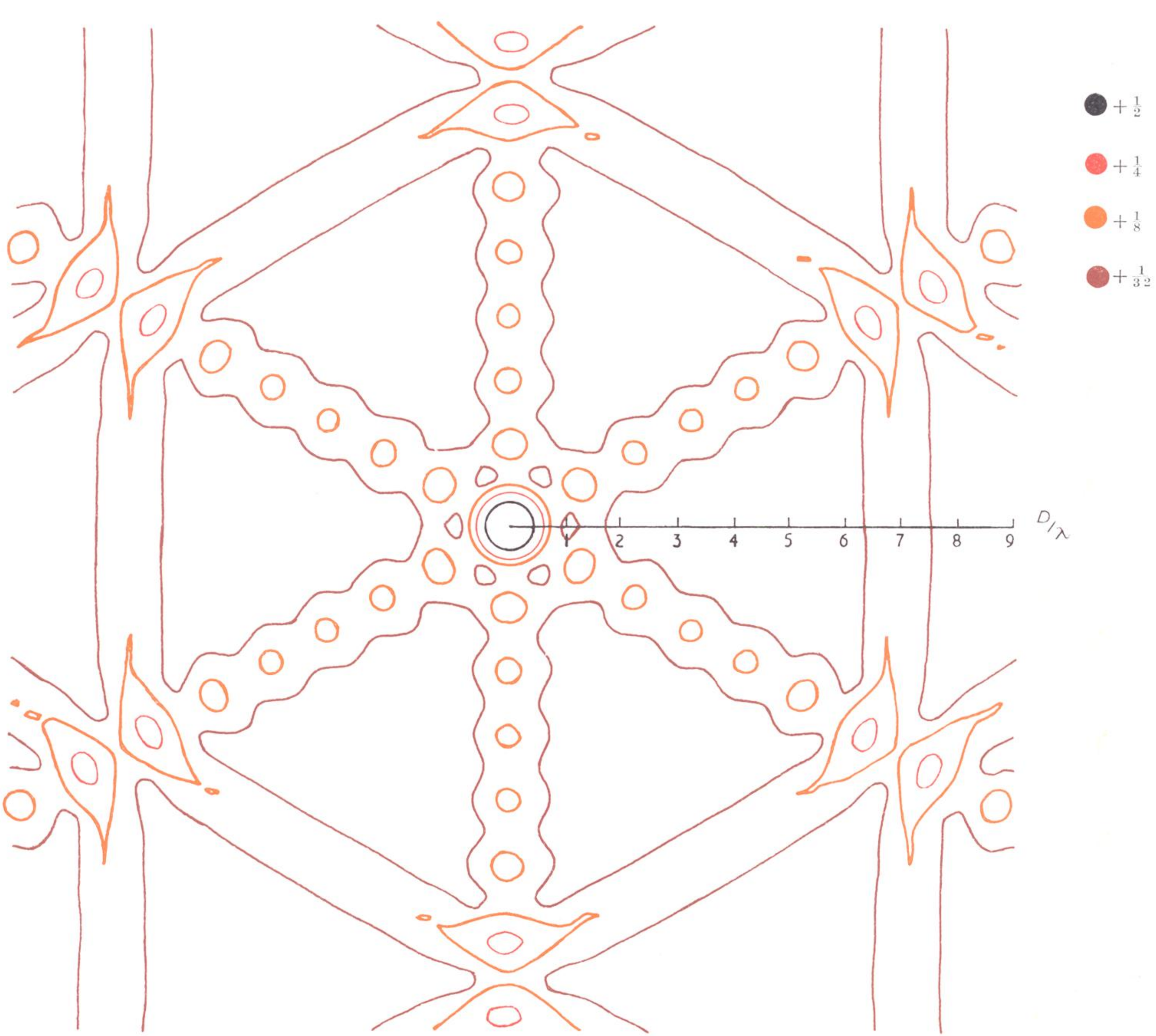

FIGURE 8. Sum squared response of 21 element triangular array.

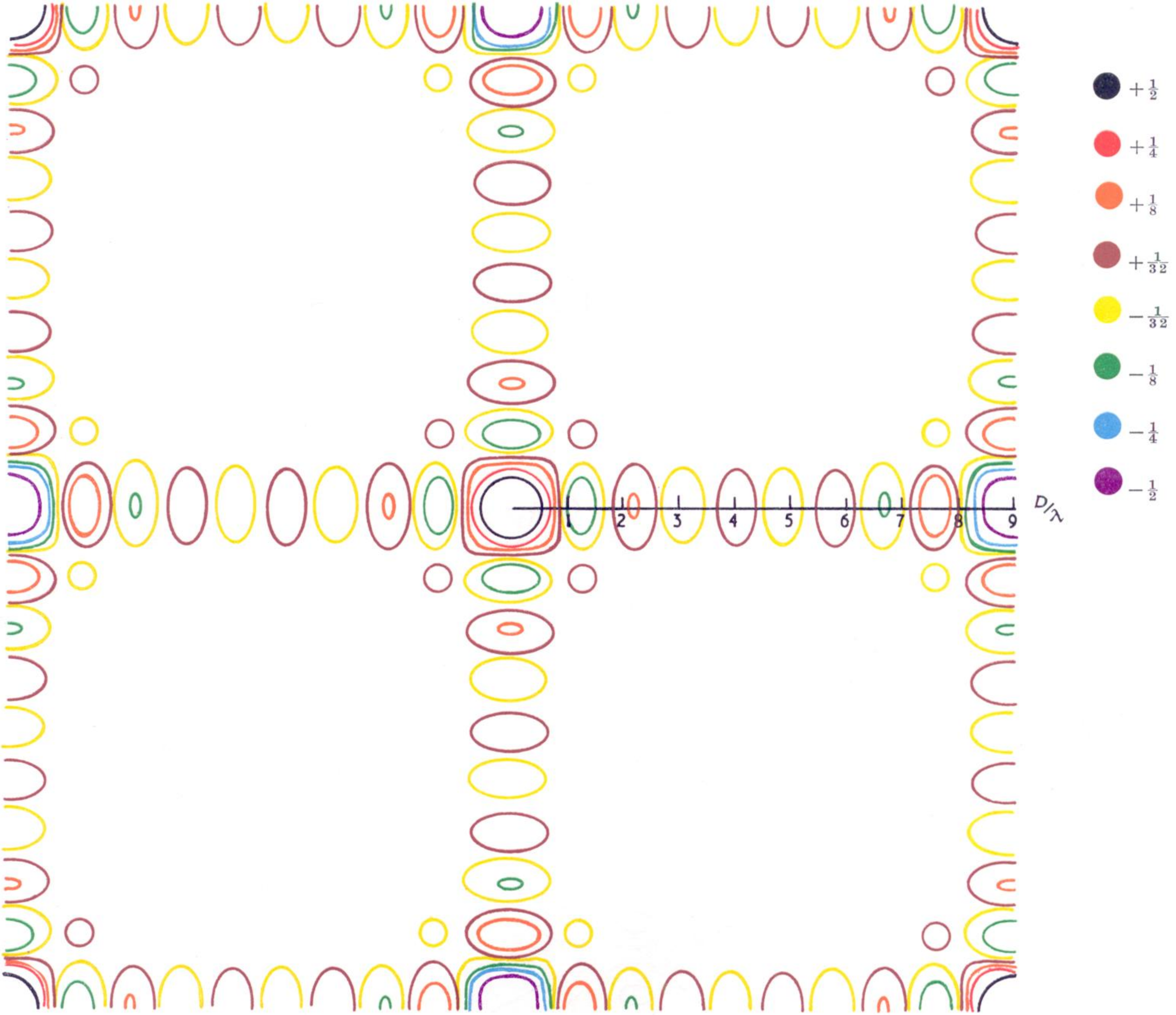

FIGURE 9. Correlator response of 20 element symmetrical cross array.

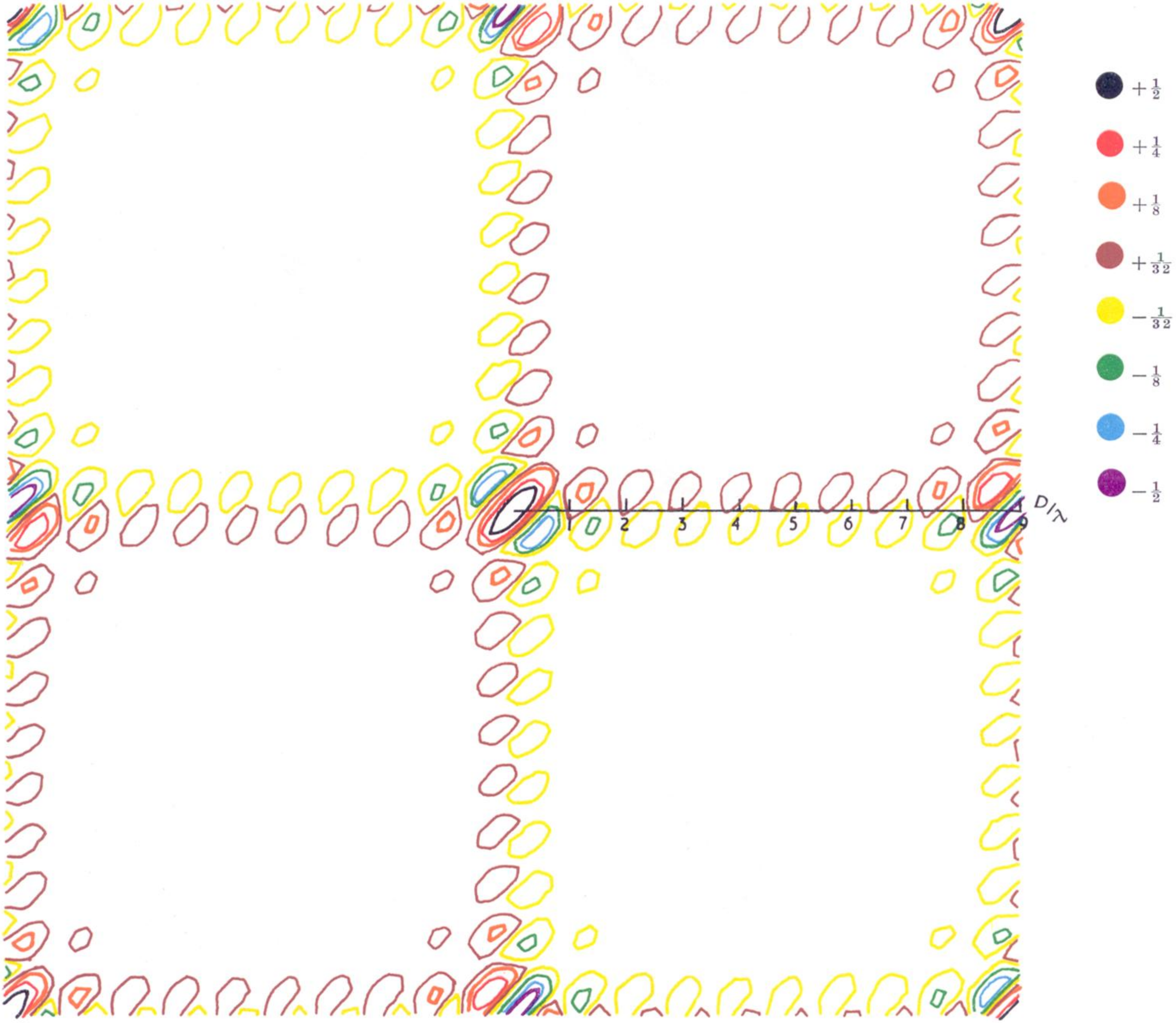

FIGURE 10. Correlator response of 20 element L-shaped array.

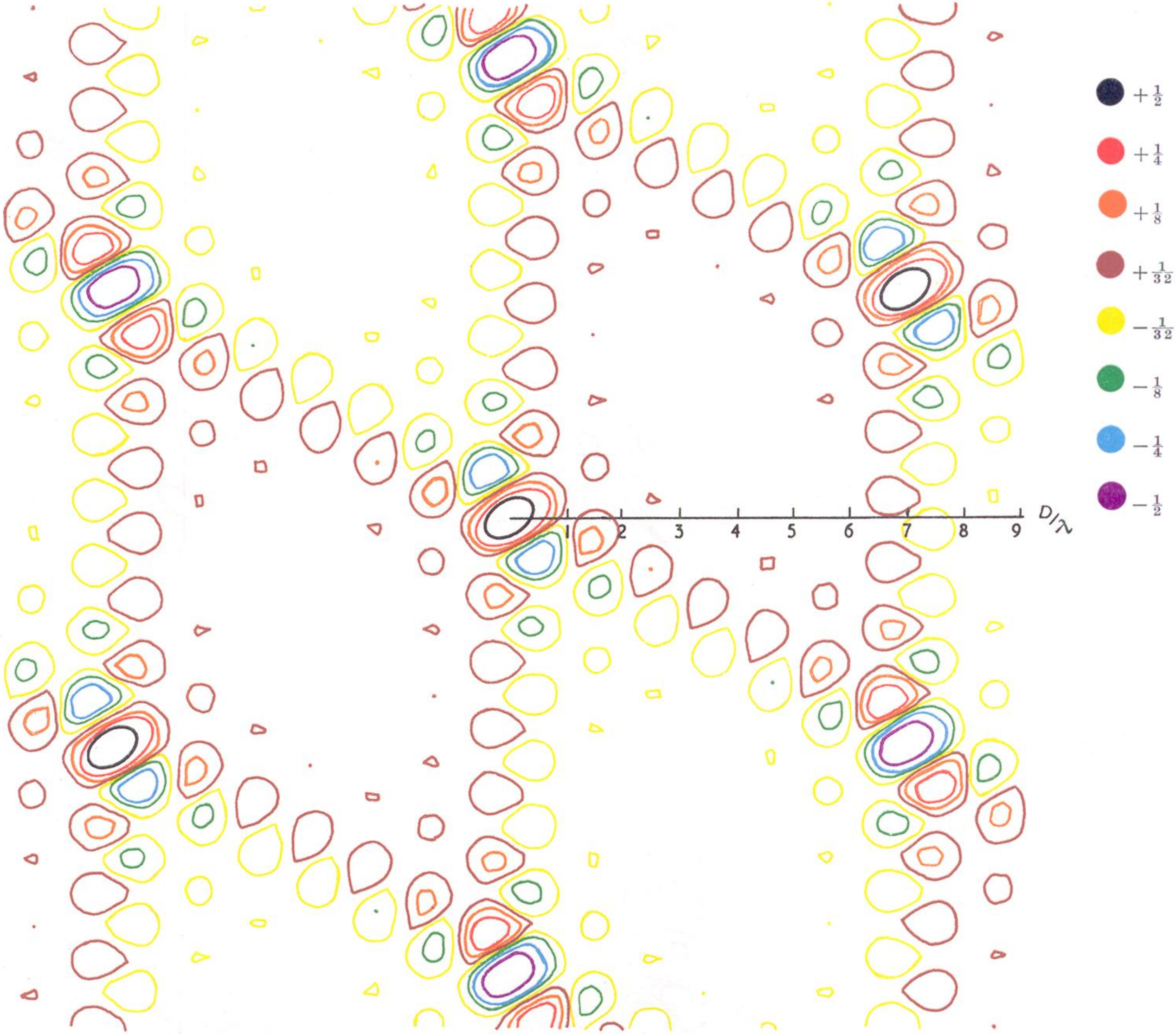

FIGURE 11. Correlator response of 14 element V-shaped array.

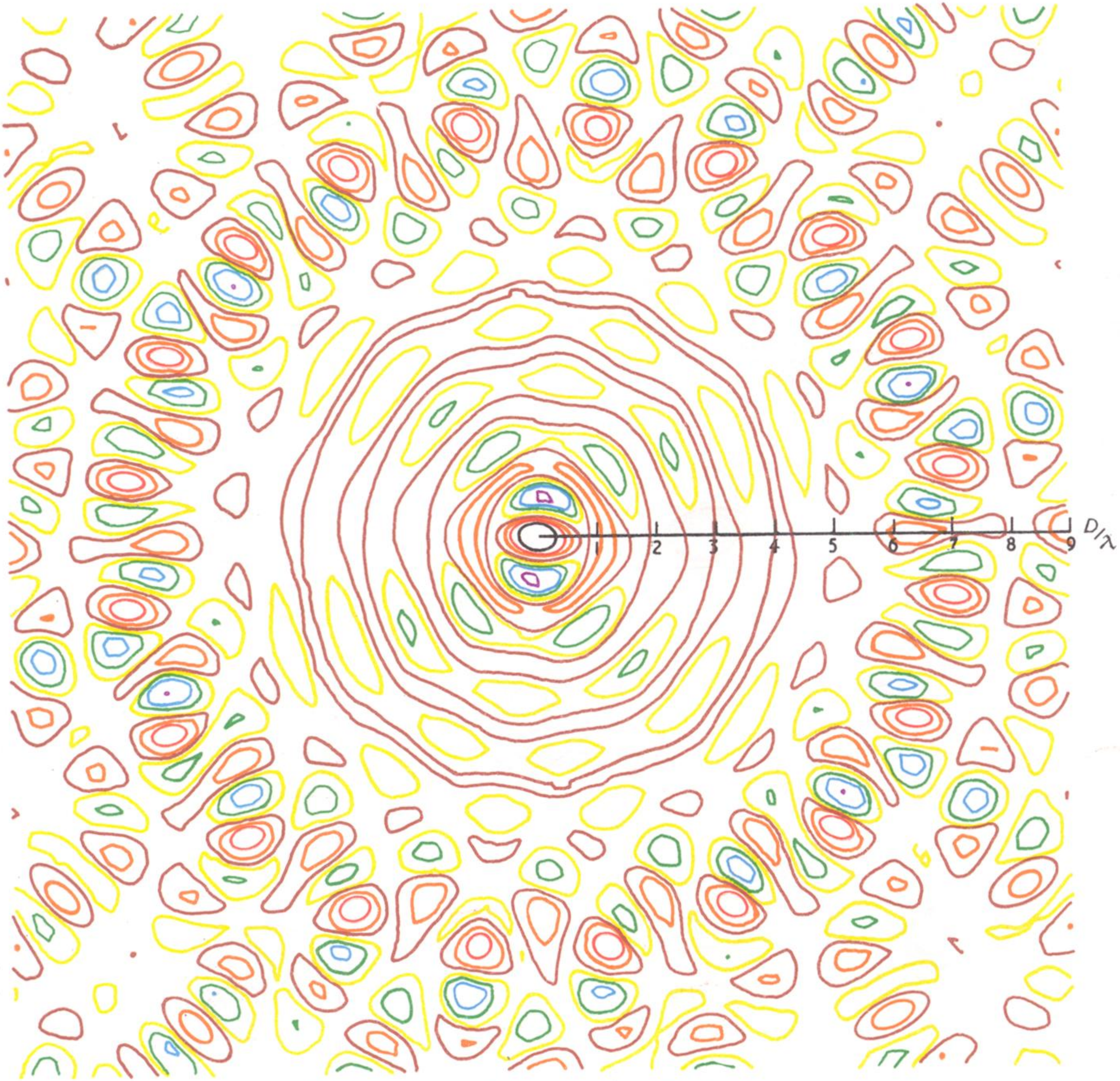

FIGURE 12. Correlator response of 20 element circular array.

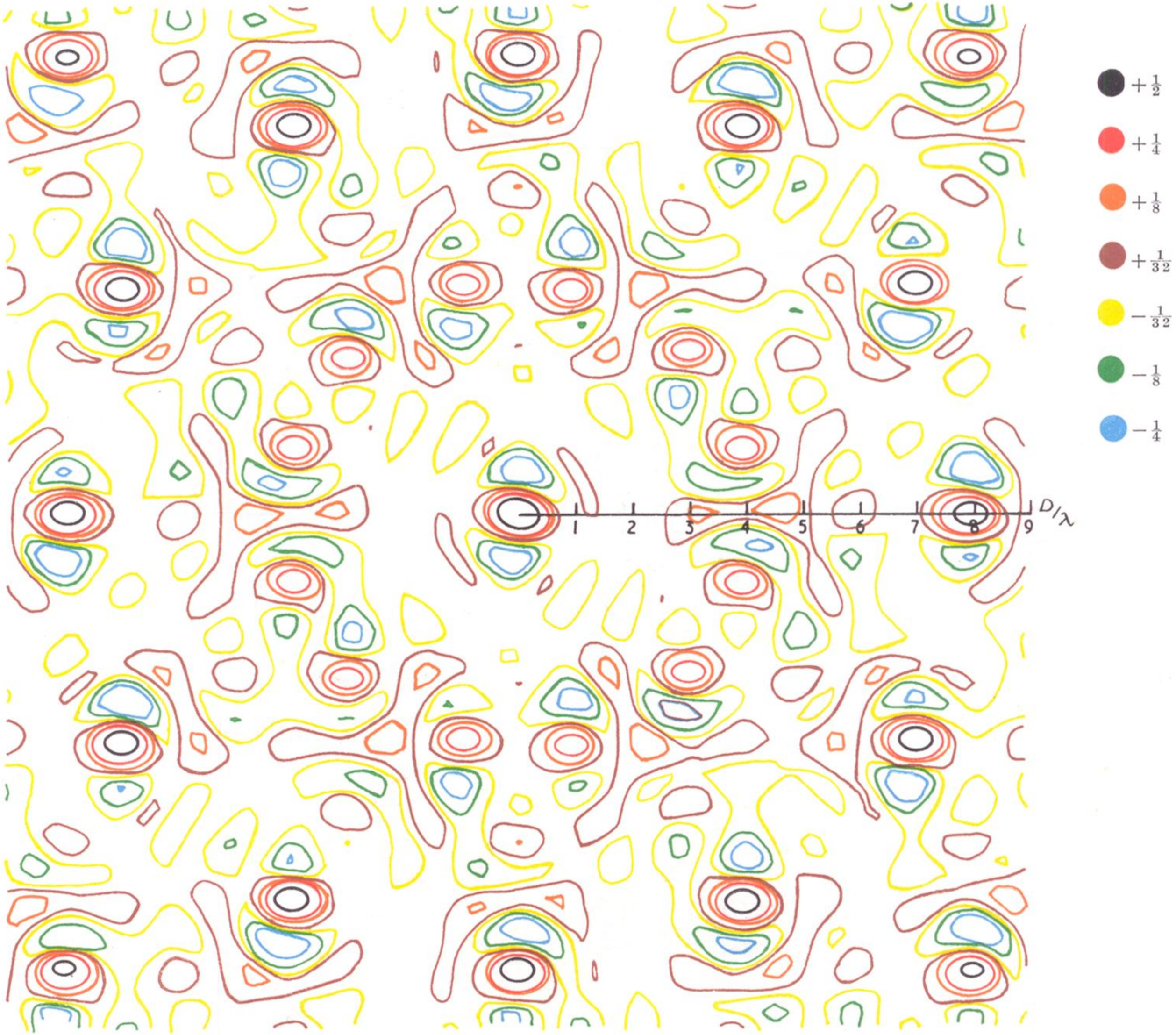

FIGURE 13. Correlator response of 18 element cluster.